DTIC
SELECTE
MAY 3 1 1994
S B D

AD-A279 768

Acrylic Plastic Spherical Pressure Hull for Continental Shelf Depths

94-16115

J. D. Stachiw

Technical Report 1606

March 1993

NRaD

UNITED STATES NAVY

ES

SUMMARY

Since the introduction in 1970 by the U.S. Navy of an acrylic plastic spherical hull for the NEMO submersible with a design depth of 1,000 feet, many other acrylic plastic submersibles have been built with the same, or greater, design depths. The maximum design depth reached so far by acrylic plastic submersibles is 3,300 feet (1,000 meters). Still, there exists an operational requirement for an acrylic plastic spherical hull design with a design depth of 8,000 feet that would provide scientists with panoramic visibility for exploration of most continental shelves around the world.

In response to this need, a program has been initiated that will provide the oceanographic community with a manned submersible with panoramic visibility to a design depth of 8,000 feet. The objective of the three phases of the program is to validate the design of the acrylic plastic pressure hull utilizing scale-model spheres with different diameters and t/D_i ratios.

This report summarizes (1) the criteria used in the design of the acrylic plastic hull with metallic hatches for depths to 8,000 feet, (2) the test plan for validation of the hull design, (3) the fabrication of scale models, (4) the testing of scale models under short-term, cyclic, and long-term pressurizations, and (5) then discusses the test results.

The selected spherical hull thickness of $t/D_i = 0.2$ appears to meet the design depth requirement for 8,000 feet. Its critical pressure of 16,000 psi provides the acrylic hull with: a safety factor >4 under short-term loading; capability to withstand 150-percent overpressure for >100 hours; and a cyclic fatigue life in excess of 1,000 dives with 4-hour's duration to design depth. The experimentally demonstrated structural performance of the acrylic spherical pressure hull meets the requirements of the American Society of Mechanical Engineers (ASME) PVHO-1 safety standard for NEMO-type windows with a design depth of 8,000 feet.

Nylon bearing gaskets around metallic hatches have been found to provide outstanding protection to the conical penetration in an acrylic hull against initiation and propagation of shear cracks during repeated dives to design depth.

iii

CONTENTS

FIGURES

TABLES

INTRODUCTION

Exploration of hydrospace requires the use of transparent structural materials to fabricate viewports in the pressure hulls of underwater vehicles through which the crew, or electro-optical systems, can observe hydrospace. To date, only three classes of materials have been utilized for this application: plastic, glass, and ceramic. Of these three materials, plastic has been found to be the most economical and readily available in large sizes and thicknesses.

The plastic which has been most widely used for this purpose is polymethyl methacrylate, or acrylic plastic, known as acrylic for short. Because of its excellent performance record in the field, acrylic has been accepted by ASME, American Bureau of Shipping, Det Norske Veritas, Lloyd's Register of Shipping, and others as the standard construction material for pressure-resistant structural components of pressure vessels for human occupancy (reference 1). Viewports with 4-inch diameters have been built to date for 20,000 psi service, and with 42-inch diameters for 1,500 psi service.

Acrylic has also been used for construction of spherical and cylindrical pressure vessels that serve as one-atmosphere cockpits on manned submersibles. Acrylic pressure hulls for submersibles represent an ideal engineering solution for the construction of such hulls. Acrylic pressure hulls are economical, light, corrosion resistant, non-magnetic, and transparent, providing the crew with a panoramic view of hydrospace. The first submersible incorporating an acrylic pressure hull was NEMO, with a design depth of 1,000 feet. Launched in 1970, it was operated successfully until 1980 as U.S. Navy DSV 4 (references 2 through 6).

Since then, several other submersibles have been built with acrylic pressure hulls: Johnson Sea-Link Numbers 1 and 2, Checkmate, Deep Sea Rover, and Seabus TI-45 (references 7 through 9). The design depth has steadily increased, and, presently, the record for the deepest diving acrylic submersible is held by Johnson Sea-Link with 3,300 feet (reference 10). Since the physical depth limit for acrylic pressure hulls has not been conclusively established, plans are underway in many quarters for submersibles with design depths in excess of 3,300 feet.

One of the organizations contemplating the construction of an acrylic submersible with increased depth capability is Harbor Branch Oceanographic Institution, HBOI. To satisfy the operational requirement for biological studies on the continental shelf around Florida, HBOI is proposing the construction of a submersible with an acrylic pressure hull capable of transporting a crew of three to a design depth of 8,000 feet (3,560 psi, or 2,438 meters). As the first step toward achieving this goal, HBOI has initiated a program to: study the factors impinging on the design of the acrylic hull for such a depth; select the smallest acceptable t/D_i ratio for the spherical hull; carry out an experimental design validation plan; procure scale-model pressure hull specimens; and evaluate experimentally their performance under short-term, cyclic, and long-term pressurization.

Because of abiding interest in transparent materials for underwater vehicles of potential use to the Navy, NRaD also has participated in this study.

STRUCTURAL CONSIDERATIONS IN PRESSURE HULL DESIGN

The design of a spherical acrylic pressure hull for service under external hydrostatic pressure poses a real challenge to its designer. It is a complex structural problem that requires detailed knowledge of this material, in particular, its response to ambient temperature, stress intensity, and duration of loading. The behavior of acrylic differs in many ways from metallic materials typically employed in the construction of underwater vehicle hulls, and unless this is understood and taken into account during design, catastrophic failure may ensue during its operational life.

The principal physical characteristics that differentiate the structural response of acrylic from metals are:

1. The magnitude of strain under stress is not only a function of *stress magnitude*, but also

of *ambient temperature* and *duration of load-ing.*

2. The rate of strain increase under constant stress (i.e., creep) varies *nonlinearly* with stress magnitude, temperature, and time.

3. The rate of strain decrease after unloading (i.e., relaxation) varies *nonlinearly* with temperature, magnitude of strain prior to unloading, and time.

4. The magnitude of permanent deformation varies *nonlinearly* with stress magnitude, temperature, and duration of sustained loading.

5. Implosion of the hull is initiated when the membrane compressive strain exceeds a certain threshold value. Elastic, plastic, and creep deformations contribute toward the magnitude of strain.

Because of these unusual physical characteristics, the spherical acrylic hull in a submersible may fail in more ways than a metallic hull. The known mechanisms of failure under external hydrostatic loading are:

1. *General elastic instability* (i.e., elastic buckling) due to elastic deformation of plastic under short-term loading (i.e., rapid dive) of a thin-walled sphere or cylinder to implosion.

2. *General plastic instability* (i.e., plastic buckling) due to plastic deformation (i.e., yielding) of a plastic under short-term loading (i.e., rapid dive) of a thick-walled sphere to implosion.

3. *General creep instability* due to excessive strain generated by long-term loading, i.e., submersible exceeding the duration of a planned dive due to entanglement with a wreck on the ocean floor.

4. *Local elastic, plastic, or creep instability* due to local deviations in circularity or sphericity, aggravated by nonuniform strain rates across the surface of the shell.

5. *Material fracture on the concave surface* of the sphere due to excessive tensile membrane stresses generated by the difference in relaxation rates across the wall thickness of the sphere following rapid depressurization of the hull after a long dive.

Thin acrylic spherical shells with t/D_i ratios less than 0.05 tend to fail primarily by general, or local, elastic instability, and for this reason, the design focuses on prevention of this type of failure. Medium-thick shells with t/D_i ratios in the 0.05 to 0.1 range are prone mostly to general, or local, plastic instabilities. Since both the thin- and medium-thick shells fail due to general or local instabilities, the design depth of these spheres is, by and large, based on analytically derived (reference 2) and empirically validated graphs relating implosion depth under short-term loading to t/D_i ratio at ambient room temperature.

The safe design depth is, as a rule, considered to be in the 25- to 50-percent range of the short-term implosion depth. To guarantee the users of the submersible at least a (1) cyclic fatigue life of 10,000 dives to design depth at 50°F ambient temperature and (2) static fatigue life of 40,000 hours at design depth of 50°F ambient temperature, the ASME PVHO-1 safety standard (reference 1) sets the design depth of acrylic components in pressure hulls at 25 percent of short-term implosion depth. The acrylic submersibles with spherical pressure hulls in the $0.04 \le t/D_i \le 0.09$ range built to date according to this standard have performed individually at least 1,000 dives without initiation of cracks on the concave surface. The successful performance of these submersibles indicates that the one-to-four (1:4) ratio of design to implosion depth recommended by the standard is a conservative design criterion for acrylic spheres with implosion depths $\le$10,000 feet. The 1:4 ratio of design to short-term implosion depth also provides an adequate safety margin for avoidance of general creep instability due to entrapment of the submersible at design depth (reference 2).

A different case presents itself for thick $(0.09 < t/D_i < 0.2)$ and very thick $(t/D_i \ge 2)$ spherical acrylic shells. Even though these spheres may also implode due to plastic, or creep, instability, the primary concern of the designer focuses on the potential for material fracture initiated by tensile strains during rapid depressurization of the sphere

from design depth. Pressure testing of thick spheres has shown that the magnitude of maximum tensile strain on the concave surface during depressurization is caused by the difference in strain relaxation rates across shell thickness. The magnitude of tensile strain is a function of the (1) sphere's t/D_i ratio, (2) magnitude of average membrane compressive stress generated by pressurization, (3) duration of external, sustained pressurization, and (4) number of repeat pressurizations (references 11 and 12).

The underlying reason for the presence of tensile strain on the concave surface of thick spheres during rapid depressurization is that the external and internal surfaces of a thick sphere creep at different rates (i.e., concave surfaces creep faster) during pressurization when subjected to compressive stresses of different magnitudes. Now, during depressurization, these surfaces also relax at different rates; the outside surface relaxes at a higher rate than the inside surface. The difference in strain relaxation rates across the wall thickness of the sphere generates stresses in the sphere; tensile on the concave surface, and compressive on the convex surface.

If the difference in relaxation rates across the wall thickness is large, the resulting tensile stress on the concave surface may exceed the tensile strength of the acrylic and initiate a crack on that surface which will proceed toward the exterior of the sphere. Depending on the rate of depressurization and the difference in relaxation rates between the exterior and interior surfaces, the crack may penetrate the whole wall thickness. Thick spheres, which were subjected to high compressive stresses and were depressurized rapidly, did disintegrate, as a rule, due to total penetration of the wall by radial cracks initiating on the interior surfaces.

When the average compressive membrane stress generated by external pressurization exceeded 25,000 psi, a thick sphere with a $t/D_i = 0.4$ ratio did, after a single pressurization of one hour's duration, disintegrate during depressurization when the external pressure decreased below 1,000 psi (reference 11). When the maximum compressive

membrane stress generated in another sphere during pressurization was 20,000 psi, 13 consecutive pressure cycles of 8 hour's duration were required to initiate a fracture on the concave surface. Another sphere, which was stressed during pressurizations to 11,000 psi, did not exhibit any internal cracks, even after 100 consecutive pressure cycles of 8 hours each. This would seem to indicate that if the maximum compressive membrane stress could be reduced by the designer to some low value, the cyclic fatigue life of the concave surface would increase beyond 1,000 pressure cycles of 8 hour's duration (i.e., 4 hours of sustained loading followed by 4 hours of relaxation at zero pressure).

Based on these tests, it appears that the average compressive membrane stress at design depth for spheres with $t/D_i = 0.4$ must be kept below 7,500 psi to ensure crack-free cyclic fatigue life for the sphere in excess of 1,000 dives. There is no experimental cyclic fatigue data for acrylic spheres with $0.1 < t/D_i < 0.4$. It can be postulated, however, with reasonable confidence that to provide a cyclic fatigue life in excess of 1,000 dives, the average compressive membrane stress at design depth should not exceed 7,500 psi, unless experimental data becomes available which shows that higher average compressive stress levels can be tolerated without lowering the cyclic fatigue life to less than 1,000 dives.

The presence of penetrations does not decrease the implosion pressure of acrylic spheres, providing that

1. The spacing between the edges of penetrations exceeds the radius of the larger of two adjoining penetrations (reference 13).

2. The beveled edge of the penetration lies on a conical surface of which the apex lies at the center of the spheres.

3. The penetration is sealed off with a tight-fitting hatch whose conical bearing surface matches that of the opening.

4. The membrane stiffness and compressive strength of the hatch are equal to, or exceed, those of the acrylic sphere (reference 2).

3

DESIGN OF THE SPHERICAL PRESSURE HULL FOR A DEPTH OF 8,000 FEET

The acrylic spherical pressure hull was designed on the basis of the following parameters:

1. *Implosion depth* under short-term pressurization must be equal to, or exceed, the design depth by a factor of *four.*

2. *The average compressive membrane stress* in the sphere must not exceed *7,500 psi* at design depth.

3. *The t/D_i ratio* selected for the sphere must represent the minimum value compatible with the other two parameters.

It was found that all three design parameters could be met by a sphere with $t/D_i = 0.2$. Empirically generated curves for hemispherical acrylic windows (reference 14) were predicting for $t/D_i = 0.2$ ratio an implosion at 15,660 psi, a pressure which exceeds the 14,241 implosion pressure requirement, based on the design pressure of 3,560 psi multiplied by a factor of four. The average compressive membrane stress at a design pressure of 3,560 psi was calculated to be 7,500 psi, meeting the 7,500 psi cyclic fatigue limit based on the pressure cycling of thick spheres (reference 11). The weight-to-displacement ratio of the sphere with $t/D_i = 0.2$ was estimated to be 0.616, a rather high value for a hull that serves as the main source of buoyancy for the submersible.

Access to the interior of the sphere was provided by conical penetrations developed and experimentally proven during the Navy's NEMO program (references 2, 3, and 6). The conical penetrations were sealed with removable aluminum hatches fabricated from 6061-T6 alloy. The conical acrylic bearing surfaces of penetrations were to be protected from scoring (by the relative movement between the hard metallic hatch and the soft acrylic) with plastic bearing gaskets. The 48-degree inclined angle of the penetration was selected to provide easy access to the interior of any full-sized sphere, even for the largest crew member.

EXPERIMENTAL VALIDATION OF SPHERE DESIGN

OBJECTIVE

Since the selected ratio of $t/D_i = 0.2$ was based to a large extent on the extrapolation of data from scale-model hemispheres with radically different t/D_i ratios tested in past programs, a new experimental program had to be established for the validation of the chosen t/D_i ratio. The experimental program was planned to answer the following questions about acrylic spheres with a ratio of $t/D_i = 0.2$:

1. Does the short-term implosion pressure actually exceed the specified implosion pressure of 14,241 psi?

2. Does the cyclic fatigue life of the sphere meet, or exceed, the specified 1,000 pressurizations to design pressure without crack initiation on the *concave surface of the sphere*?

3. How many pressurizations to design depth can the sphere withstand before shear cracks appear on the conical bearing surface of the penetration through the sphere?

4. Will the sphere withstand 1,000 pressurizations to design depth before the shear cracks on the conical acrylic bearing surface reach critical size (i.e., initiate catastrophic failure of the sphere)?

5. Which of the plastic bearing gasket materials are capable of surviving 1,000 pressure cycles to design depth without squeezing out, or disintegrating?

6. Which of the bearing gaskets provide the best protection against initiation of shear cracks on the conical acrylic bearing surface during application of 1,000 pressurizations to design depth?

APPROACH

To provide answers for these questions, a total of 13 scale-model spheres were designed and fabricated from acrylic castings with physical properties

meeting the specified values shown on tables 1 and 2.[1]

Model AA was tested to implosion and the recorded implosion pressure was compared with the specified critical pressure of 14,241 psi. If the model failed at lesser pressure, the t/D_i ratio was increased from 0.2 to some larger value.

Models BB and CC, after instrumentation with five strain gages each, were pressure cycled together from 0 to 3,560 psi at ambient room temperature. Appearance of cracks on spherical surfaces of the sphere in less than 1,000 pressure cycles required that the t/D_i ratio be increased from 0.2 to some larger, yet unspecified, value. Appearance of shear cracks on the conical acrylic bearing surface of penetrations in the sphere after some number of pressure cycles was expected, however, if they did not reach critical length before 1,000 cycles, it was considered acceptable.

The reason that the appearance of shear cracks on the conical acrylic bearing surface of penetrations *can be tolerated* before 1,000 cycles of 8 hour's duration are completed, while the appearance of cracks on spherical surfaces *is not acceptable*, is due to the fact that the cracked bearing surface of penetrations can be economically removed by machining and subsequently replaced by the bonding in of a conical acrylic ring. Such repair procedures are currently being performed routinely on operational spherical acrylic submersibles to extend their service lives.

The typical pressure cycle consisted of 4 hours of sustained pressure at 3,560 psi, followed by 4 hours of relaxation at 0 psi in a 65°F to 75°F ambient temperature range environment. An ambient temperature of 75°F was selected instead of the 40°F to 50°F temperature range existing at the 8,000 feet depth for two reasons: (1) it is easier to maintain the pressure vessel at this temperature for the duration of the cycling program, and (2) the

---

1. Figures and tables are placed at the end of the text.

test results generated at 75°F are considered conservative since the strains generated by cycling at that temperature are significantly higher than in the 40°F to 50°F temperature range.

The strains were recorded during the first, second, and each succeeding tenth pressure cycle, and the condition of all sphere components were inspected at the 180 and 450 cycles. Pressure cycling was not terminated prior to completion of 1,000 cycles unless cracks were observed on the spherical surfaces of both spheres. If any of the bearing gaskets on Models BB and CC permanently deformed or cracked, they were removed and replaced with polycarbonate plastic gaskets whose satisfactory performance in this application already has been established in previous test programs (references 8, 10, 14, and 15).

Models 1 through 8 were pressure cycled together in the same manner as Models BB and CC, but in a separate pressure vessel. Because of widely different t/D_i ratios ($01 \leq t/D_i \leq 0.225$), a few of the spheres imploded and some only cracked prior to completion of 1,000 cycles. Plotting the number of cycles at which individual spheres cracked and subsequently imploded, versus their t/D_i ratio, generated a family of cyclic fatigue curves for repeated pressurization to 3,560 psi. These empirically derived curves aided in determining the minimum t/D_i ratio, which would give the acrylic sphere a fatigue life of 1,000 cycles to 3,560 psi design depth without crack initiation on spherical surfaces, and 10,000 cycles without catastrophic failure. If the extrapolated t/D_i ratio was less than 0.2, the t/D_i ratio of the proposed acrylic submersible hull might be reduced to improve its weight-to-displacement ratio without reducing its specified fatigue life.

Models 6A and 6B with the same $t/D_i = 0.2$ as Model 6 were subjected separately to long-term pressurizations at 16,000 and 20,000 feet. These pressurizations demonstrated the ability of the spherical acrylic pressure hulls with 8,000 feet (3,560 psi) design depth to withstand 100- and 150-percent overpressurizations to which a submersible may be subjected accidentally during field operations.

SCALE-MODEL SPHERES

The process selected for fabrication of scale-model spheres was identical to the one developed jointly by Beasley, Lones, and Stachiw in 1970 for the fabrication of the spherical acrylic pressure hull NEMO Model 2000 that subsequently was incorporated into the Johnson Sea-Link submersible (reference 16). By using the same fabrication process for scale-model spheres that will be used for the full-scale, operational pressure hull, all the experimental data generated by the scale-model test specimens will be directly applicable to full-scale hulls. Furthermore, the physical properties of acrylic castings produced by this process meet, or exceed, the values specified for acrylic (tables 1 and 2) by the ASME (reference 1) and the American Bureau of Shipping (reference 17).

The scale-model spheres shown on table 3 were fabricated by casting a slurry of acrylic resin and fine acrylic powder in hemispherical molds, heating it in an autoclave, then machining the rough polymerized, hard, hemispherical, acrylic castings to final dimensions. They were subsequently bonded together with self-polymerizing acrylic cement. The scale-model spheres were annealed twice: prior to, and after, bonding. The quality of the bonded equatorial joints in Models AA and CC was excellent, while in Model BB it was barely acceptable. The joints in the 6-inch-diameter spheres (Models 1 through 8) were excellent, except for Models 6A, 6B, 7, and 8, which incorporated an undesirable quantity of voids. Still, the spheres were accepted for testing anyway, as attempts at recasting these joints failed to improve their quality due to inaccessibility of the spheres' interior to the fabricator's hands.

Model AA with an 18-inch outside diameter was the largest acrylic sphere in the test program (figures 1 through 3). Its design was typical of NEMO hulls built in previous programs. The sphere had a single penetration with conical bearing surfaces protected by a polycarbonate plastic gasket into which an aluminum plug hatch was fitted snugly (figures 4 through 7). The plastic gasket was sealed to the acrylic sphere by means of

room-temperature vulcanizing (RTV) silicon rubber; and the plug hatch was sealed to the plastic gasket by means of an O-ring. The reason for not using an O-ring seal between the plastic gasket and the acrylic bearing surface on the sphere is that the presence of an O-ring groove in the gasket in contact with acrylic has been found by past experience to act as a crack initiator in the conical acrylic bearing surface of the penetration in the sphere.

The construction of *Model BB* was similar to that of Model AA, except it was only 15 inches in diameter (figures 8 and 9). The only departure in design from Model AA was the incorporation of a removable plug hatch assembly (figures 10 through 15). The removable plug hatch assembly more closely resembled a functional hatch in a full-size acrylic sphere, than the fixed-plug hatch in Model AA.

Model CC was identical in size and construction to Model BB except for the number of penetrations in the sphere (figures 16 and 17). M⁻del CC had five penetrations instead of one to allc⁻ simultaneous evaluation of five different gasket-bearing materials under cyclic pressurization (figure 18). Two kinds of plug hatch assemblies were utilized in these penetrations. One of the penetrations was fitted with a removable plug hatch, identical to the one in Model BB (figures 10 through 14). This provided access to the interior for strain-gage instrumention. The other four penetrations were fitted with fixed plug hatches (figures 19 and 20) similar to the one in Model AA. All five penetrations used plastic gaskets of identical size (figure 13).

The materials chosen for evaluation as potential replacements for extruded polycarbonate plastic were selected on the basis of their ability to be cast in large sections economically (table 4). The search for a suitable replacement was motivated by the very high cost and unavailability of extruded polycarbonate in thick plates suitable for the machining of large bearing gaskets used around operational hatches in the proposed full-scale submersible hull with a design depth of 8,000 feet.

This constitutes a marked departure from past acrylic submersible construction programs where extruded polycarbonate plates were used exclusively as the construction material for bearing

gaskets around hatches. The idea behind the use of a polycarbonate gasket was that the shear stresses generated by contact between the metallic hatch and the plastic would not initiate cracks as readily in the tough polycarbonate as in the more brittle acrylic. Furthermore, a plastic gasket bearing against the acrylic sphere would not generate as high shearing stresses in the sphere as direct contact with metallic hatch would.

The successful performance of the extruded polycarbonate gasket in past programs (NEMO, Makakai, Sea-Link, and Checkmate) made it the prime candidate for the proposed submersible hull until a survey of plastic manufacturers brought out the fact that the cost of extruded polycarbonate plastic plates measuring 48 by 48 inches and 18 inches thick required for the machining of bearing gaskets represented about half the cost of the proposed pressure hull. The qualification of a castable, instead of an extrudable, plastic for this application would significantly decrease the cost and lead time for construction of any acrylic submersible with a design depth in excess of 3,000 feet.

One of the candidate materials serving as a bearing gasket in Model CC was a newly developed castable polycarbonate plastic with physical properties similar to those of extruded polycarbonate plastic. The other gasket materials in Model CC were cast epoxy, cast polyurethane, cast nylon, and cast acrylic. Bearing gaskets machined from 3-inch-thick extruded polycarbonate plastic were incorporated into Models AA and BB to serve as a standard of comparison for the other bearing gasket materials.

Models 1 through 8 were only 6 inches in diameter (figures 21 and 22). This size allowed all of them to be fitted inside a single pressure vessel for testing. In this manner, the pressure cycling of all models could be expedited while maintaining identical test conditions. The single penetrations in these models were *not equipped* with bearing gaskets as conical acrylic plugs were used instead of aluminum hatches (figure 23). Since there was no relative motion between the plugs and the penetrations, bearing gaskets were not required between

the conical mating surfaces of the plugs and the penetrations. Aluminum hatches were not used in these models as the objective of their construction was to *minimize* the presence, and thus the effect, of any discontinuities on the cyclic fatigue of spheres with different t/D_i ratios.

The aluminum plugs and hatches for Models AA, BB, and CC do not represent structurally optimized designs of metallic hatches and instrumentation bulkheads. The dimensions of these components were selected to give them the same strength as the acrylic sphere (i.e., fail at external pressure in the 14,000- to 15,000-psi range). This was done to prevent them from acting as potential initiators of buckling failure when the scale-model spheres were tested to implosion at completion of the pressure cycling program.

This will not be the case with operational hatches and feed-through bulkheads for the proposed full-size submersible. To reduce weight for this application, the hatches and bulkheads will be structurally optimized for the 3,560-psi design pressure with a safety factor of 2.5, based on the yield of material that is considered quite adequate for metallic components of submersibles. To reduce the weight further, cast titanium Ti-6Al-4Va might be substituted for the 6061-T6 aluminum alloy used in fabrication of hatches for the scale-model spheres.

TESTING OF SCALE-MODEL SPHERE AA

TEST SCHEDULE

Acrylic sphere AA was tested first, since the experimental confirmation of the predicted implosion depth for the proposed pressure hull with a $t/D_i = 0.2$ ratio would provide reassurance that the planned time-consuming pressure cycling of other scale models with the $t/D_i = 0.2$ ratio will conclude without cyclic fatigue failure.

Pressurization to implosion was preceded by pressure cycling of Model AA in the 0- to 6,000-psi range. The pressure cycling consisted of six pressure cycles

7

First: 0-1000-0 psi

Second: 0-2000-0 psi

Third: 0-3000-0 psi

Fourth: 0-4000-0 psi

Fifth: 0-5000-0 psi

Sixth: 0-6000-0 psi

Each pressure cycle consisted of pressurization at 650 psi/minute rate, sustained pressure loading of 60 minute's duration, depressurization at 650 psi/minute rate, and relaxation at 0 psi for a minimum of 60 minutes. Strains were read at 1,000 psi pressure, and 5-minute time intervals, respectively.

INSTRUMENTATION

Model AA was instrumented on the concave surface with four rectangular strain gage rosettes, type CEA-06-125WT-120 (figure 24). Gages 1 and 2 were located at the bottom pole of the sphere, while gages 3 and 4 were located at the top of the sphere near the edge of the penetration. Gages 1 and 2 were to provide information about the typical membrane compressive strain on the concave surface, while gages 3 and 4 were to provide peak strain readings on the concave surface near the hatch penetration.

TEST ARRANGEMENT

The test arrangement for Model AA consisted of attaching the sphere assembly to the pressure-vessel end closure with a pipe measuring 3/8 of an inch (figure 25). The pipe was threaded on both ends. One end was screwed into the threaded opening of an adaptor plug designed to fit the central penetration in the pressure-vessel end closure.

The instrumentation wires from the strain gages were fed from inside the sphere to the exterior of the pressure-vessel end closure through the interior of the pipe. This arrangement provided a dry and secure conduit for the instrumentation leads at any external pressure to which the sphere would be subjected during implosion testing.

TEST PROCEDURE

Testing was conducted inside an 18-inch-diameter pressure vessel rated at 20,000 psi. The pressurization was accomplished by means of an air-operated positive displacement pump with 20,000 psi capability. The ambient water temperature during testing of Model AA varied only plus-or-minus 1 degree from 65°F. Because of this small temperature variation, all the strains generated during the pressure testing of Model AA could be compared with each other directly without any adjustments for temperature variation.

During the final pressurization to implosion, considerable difficulties were encountered in trying to maintain the 650 psi/minute pressurization rate at pressures above 6,000 psi. The pressurization rate decreased steadily until 12,000 psi where it was only 100 psi/minute. To speed up the pressurization rate, a larger air hose was connected to the pump from the same compressor. As a result of this arrangement, the rate increased to 500 psi/minute. Unfortunately, the added air volume was not sufficient to maintain this pumping rate and it dropped to 100 psi/minute at 14,000 psi with the distinct possibility of decreasing to zero at 15,000 psi.

To remedy this situation, it was decided to connect a large, gasoline-engine driven compressor to the pump. Since the changeover from one compressor to another required approximately 1 hour, the pressure in the vessel was decreased to 4,000 psi to reduce static fatigue implosion or Model AA. After installation of the large portable compressor, the pump increased its pumping rate to 1,000 psi/minute and maintained this rate to 16,000 psi at which implosion took place with a loud noise.

FINDINGS

Pressure Cycling

The hoop and meridional strains recorded by gages 1 and 2 (at the pole of the lower hemisphere without penetration) did not differ from each other, indicating a uniform biaxial stress field on the concave surface of the sphere (figure 26). The meridional strain recorded by gage 3 on the concave surface at the penetration in the upper hemisphere

was, however, approximately 20 percent higher, and the hoop strain recorded by gage 4 at the same location was approximately 80 percent lower than the strains at gages 1 and 2.

This distribution of strains is considered typical for acrylic spheres with a conical penetration sealed by a metallic hatch. Testing of acrylic spheres with t/D_i ratios in the 0.04 to 0.09 range during the previous test programs has produced similar results (references 2, 3, 5, 6, and 14).

The basic difference between the effect of penetration on the magnitude of strains in the spheres with $0.04 \leq t/D_i \leq 0.09$ and Model AA with a t/D_i ratio of 0.2 is that the relative increase in strain magnitude at the penetration was larger for the thin spheres. Thus, for $t/D_i = 0.04$ the strain increase on the concave surface in meridional direction at the penetration was in excess of 50 percent, while for $t/D_i = 0.09$ the increase was only about 33 percent. Also, stiff hatch plugs generate higher strains at the penetrations than radially compliant hatch plugs.

The magnitude of membrane strains at the pole of the lower hemispheres increased linearly with pressure during pressurization in the first five pressure cycles (table 5); the strains became nonlinear during the sixth pressure cycle at pressures above 5,000 psi. This seemed to indicate that during short-term pressurization, the sphere with $t/D_i = 0.2$ compresses elastically in the 0- to 11,235-feet depth range.

The *creep rate* and *cumulative creep* increased exponentially with pressure. For example, at 1,000 psi sustained pressurization, the average *creep rate* during the *first five minutes* was approximately 10 microinches/inch/minute, while at 6,000 psi the rate became 330 microinches/inch/minute (figure 27). The *creep rate* decreased exponentially with time; after 60 minutes of sustained pressurization at 1,000 psi it became less than one microinch/inch/minute, and at 6,000 psi it became 35 microinches/inch/minute (figure 28).

As a result of the great variation in creep rates at different pressure loading, there was also a great variation in the magnitude of *cumulative creep* (figure 29). Thus, at the conclusion of one hour-

long sustained pressurization, the cumulative creep in the 1,000 psi cycle was only 100 microinches/inch, while in the 6,000 psi cycle, it was observed to be 5,100 microinches/inch (table 5).

The instantaneous strain, together with the large cumulative creep, resulted in an operationally significant decrease of the sphere's buoyancy (figure 30). The buoyancy of the 18-inch-diameter Model AA acrylic sphere decreased by approximately 7 percent after 60 minutes of sustained pressurization at 4,000 psi.

During relaxation periods between individual pressurization cycles, the acrylic attempted to return to its unstrained state. The 60-minute-long relaxation periods appeared to be of adequate duration for the compressive membrane strains to return almost to zero after 60-minute-long pressurization periods at 1,000, 2,000, 3,000, and 4,000 psi. After sustained pressurization at 5,000 psi, the 60-minute-long relaxation period generated tensile membrane strains on the concave surface (table 5). Tensile membrane strains again were observed after sustained pressurization to 6,000 psi, except that they were larger than during the relaxation period after sustained pressurization at 5,000 psi (80 versus 150 microinches/inch after 60 minutes of relaxation).

The appearance of tensile strains during a relaxation period indicates that some of the cumulative creep that took place on the concave surface during pressurization was in the nature of permanent compressive deformation. Since the cumulative creep on the convex surface during sustained pressurization is less due to lower membrane stresses, permanent compressive deformation also can be expected to be less on this surface than on the concave surface. As a result of this difference in magnitudes of residual compressive strains on these surfaces, at some time during the relaxation period the interior surface of the sphere may be placed in tension and the exterior surface in compression. The higher the pressure during sustained loading, the sooner the tensile strains will appear during the relaxation. If the pressure during sustained loading is high enough, fractures may appear on the concave surface immediately after, or even during, depressurization to zero.

9

The absence of tensile strains during the relaxation period after the 4,000 psi pressure cycle, and their appearance after the following pressure cycle to 5,000 psi indicated that permanent compressive deformation (i.e., yielding) will appear on the concave surface during 60-minute-long sustained pressure loading in 60°F ambient environment at some pressure level in the 4,000- to 5,000-psi range. At sustained pressure loadings in excess of 60 minute's duration, permanent compressive deformation may take place at pressure levels less than 4,000 psi. At low ambient temperatures encountered in deep ocean, on the other hand, the permanent compressive deformation may only appear at pressure in excess of 5,000 psi.

Implosion Testing

Implosion of Model AA took place at 16,000 psi in 65°F ambient temperature environment. Since the ambient temperature at design depth and beyond is in the 28°F to 34°F range, the actual implosion depth of the acrylic submersible would be in excess of 35,952 feet (16,000 psi x 2.247 feet/psi). The actual implosion depth can be fairly accurately predicted on the basis of data generated during the Navy's NEMO test program (reference 2). In that program, acrylic spheres with $t/D_i = 0.04$ were tested to implosion under different ambient temperatures, and the experimentally obtained implosion pressures were plotted versus ambient temperature. The relationship between critical pressure and ambient temperatures appeared to be linear in the 32°F to 110°F temperature range.

Utilizing that data, one can postulate that the implosion depth of the acrylic submersible with $t/D_i = 0.2$ ratio at 32°F under short-term loading will be approximately 25-percent greater. Using this information as the basis for predicting the short-term implosion depth, it is calculated to be 20,000 psi; well in excess of greatest ocean depth.

Data from the NEMO test program (reference 2) enables one also to predict with reasonable certainty the implosion depth under long-term

entrapment on the ocean floor. For entrapment of 150 hour's duration (typical duration of life support) the implosion depth is predicted to occur at 50 percent of short-term implosion depth. Thus, in order for an acrylic submersible with $t/D_i = 0.2$ ratio to implode during 150 hours of entrapment, or disablement on the ocean floor at 32°F ambient temperature, the depth of the ocean floor must exceed 20,000 feet.

The spherical sector hatch of 6061-T6 aluminum and bearing gasket of extruded polycarbonate plastic performed well in the 0- to 6,000-psi pressure range (0- to 13,482-feet depth range). Both the aluminum and polycarbonate plastic yielded during the short-term pressurization to 16,000 psi. There was extensive extrusion of the gasket into the sphere's interior and shear cracking on the hatch skirt. Based on this observation, it can be postulated that the structural performance of the aluminum hatch in Model AA matches that of the acrylic sphere, which also failed by yielding of material.

CONCLUSIONS

The short-term critical pressure of acrylic scale-model sphere AA with $t/D_i = 0.2$ *exceeds* the 14,240-psi short-term critical pressure requirement of the ASME PVHO-1 safety standard based on a 1:4 ratio between the 3,560-psi design depth and the implosion depth.

The return of all strains to zero after a 60-minute relaxation period at 0 psi following a 60-minute sustained pressurization at 4,000 psi indicates that there should be no accumulation of residual strains during repeated pressurizations to the design depth of 3,560 psi, provided that the relaxation periods equal, or exceed, the duration of individual pressurization periods and that the ambient temperature of the water is ≤ 65°F.

The presence of 48-degree conical penetrations plugged with aluminum closures increases the peak strains at the penetration by only 20 percent above membrane strains at the equator.

TESTING OF SCALE-MODEL SPHERES BB AND CC

TEST SCHEDULE

Acrylic models BB and CC were tested together in one of the pressure chambers located in HBOI's Deep Ocean Simulation Facility. The test schedule was to pressure cycle both acrylic spheres a minimum of 1,000 times to 3,550 psi at an ambient temperature of 75°F. The typical cycle consisted of pressure and relaxation periods, each of 4 hour's duration. Periodically, the chamber was opened and Models BB and CC visually inspected.

At the conclusion of cycles 180, 450, and 1,000, the pressure vessel was opened and the acrylic spheres visually inspected for the presence of cracks in the hulls and cracking or extrusion of the bearing gaskets. At the conclusion of the 450th and 1,000th cycle, the test models were disassembled and the condition of the acrylic hull bearing surfaces and bearing gaskets was noted and photographed. Some of the bearing gaskets were replaced during the inspection at the 180 and 435 pressure cycles because of extensive cracking. Since the equatorial bonded joint on Model BB had almost separated after 180 cycles because of a defective bond, Model BB was replaced with a new acrylic sphere with a properly bonded joint that performed satisfactorily for the remainder of the cycling program.

INSTRUMENTATION

Models BB and CC were instrumented with five rectangular 90° strain gage rosettes, type CEA-06-125WT-120 with a gage factor of 2.11, bonded to the interior of the acrylic sphere (figures 31 and 32). Placement, bonding, and wiring of gages inside Model BB was rather difficult as the small penetration allowed only a single hand to be inserted into its interior (figure 33). The even-numbered gages measured hoop strains and the odd-numbered gages measured axial strains. Model BB gages 1 and 2 and Model CC gages 5, 6, 9, and 10 were located near one of the penetrations to measure peak strains on the concave surface. The other rosettes were placed some

distance from the penetrations. On Model BB, gages 3 and 4 were one-third the distance from edge of penetration to equator; gages 5 and 6 were two-thirds the distance from edge of penetration to equator; gages 7 and 8 were 0.3 of an inch above equator; and gages 9 and 10 were at the pole of the lower hemisphere (figures 34 and 35). On Model CC, gages 7 and 8 were halfway between opening E and D; gages 3 and 4 were equidistant between openings A, B, and E; and gages 1 and 2 were at the pole of the lower hemisphere (figure 36).

TEST ARRANGEMENT

Considerable time and effort have been invested in HBOI's Deep Ocean Simulation Facility in preparation for pressure cycling of the model pilot spheres. The system has been designed to be automated and is nearly self sufficient. Two 4,500-psi pressure vessels have been installed in an insulated and air-conditioned block wall structure. An air-actuated high-pressure hydrostatic pump charges the two chambers. Chamber A (which contains the 15-inch-diameter spheres) and Chamber B (which contains the 6-inch-diameter spheres) have pressure rise-and-fall times which are offset by 2 hours. The result is eight separate and unique time periods that had to be taken into account during the system design and computer programming. Electronically actuated three-way solenoid valves control the flow of water to and from the chambers. These valves and most of their associated plumbing and wiring are located in the control panel. The pump and valves are operated by an Apple IIC minicomputer according to a realtime clock for constant pressure monitoring. In-line pressure transducers sense chamber pressures and send a linearly related analog voltage to an analog-to-digital converter. The computer reads chamber pressures and sends appropriate commands to the pump and valves via the binary out of the system.

The test arrangement for Models BB and CC consisted of attaching one end of a rigid pipe to the opening in the removable hatch and the other end to a penetration in the pressure vessel closure so as to provide venting during pressure testing (figure 37). The pipe was stiff enough to prevent its collapse under 3,560 psi external pressure during

pressure cycling. The instrumentation leads were fed through this pipe from the interior of the spheres to the strain recording equipment in the test laboratory.

TEST PROCEDURE

The typical pressure cycle for Models BB and CC consisted of pressurization at a 500-1,000 psi/minute rate, 4 hours of sustained pressure at 3,560 psi, depressurization at a 500-1,000 psi/minute rate, 4 hours of relaxation at 35 psi (city water pressure). Strain gages were wired to a strain gage conditioner that sensed strain as an analog voltage corresponding to the change in resistance occurring in each gage as it deforms with the material to which it is bonded. Addition of a multiplexer expanded the analog-to-digital capability of the system, thereby making it possible to incorporate the automated acquisition of strain data. The computer was programmed to record chamber pressures and strain gage readings (including the cycle number and time taken) via the printer at desired intervals. In addition, an uninterrupted power supply assured that data would not be lost during a power failure.

Ambient temperature of tap water used in the testing of Models BB and CC was 73°F ±2°, and maximum pressure was maintained at all times in the 3,400-3,600 psi range.

During cycles 1 through 5, water temperature and strains were read at 500-psi intervals during pressurization and depressurization and at 5-minute intervals during sustained loading and relaxation (tables 6 through 13, figures 38 through 45).

During cycles 6 through 1,000, water temperature and strains were read at the beginning and end of sustained loading and relaxation periods (i.e., four readings per pressure cycle).

The magnitude of permanent deformation at the conclusion of each relaxation period at gage locations 1 and 2, and 7 and 8 in Model BB, and 5 and 6, 9 and 10, and 1 and 2 in Model CC were plotted versus number of cycles. This allowed the test supervisor to predict initiation of a fracture in the acrylic hull.

In Model CC, the bonded joint bisected opening E. The type of inserts used in the five penetrations on this model were

A - cast nylon
B - cast polycarbonate
C - cast acrylic
D - cast epoxy
E - cast polyurethane

A removable hatch was located in opening C in this model.

FINDINGS

Strains on Interior Surfaces of Models BB and CC

The strain gages functioned properly only during the first five pressure cycles, so all the findings are based only on the data from these pressure cycles. Since the strains did not change significantly during performance of these cycles, it can be postulated with high confidence that the findings based on the data from the first five cycles apply also to all the other pressure cycles.

The short-term strains generated during *initial* pressurization of Models BB and CC increased linearly with pressure from 0 to 3,550 psi at all locations, except at the edges of some penetrations (figures 38 and 40). The strains remained linear also during pressurization in later pressure cycles (figures 39 and 41). There was no significant change in their magnitudes between individual cycles. The magnitude of short-term strains in Models BB and CC can be considered identical to Model AA when the 10°F difference in test temperatures is taken into account (75°F for Models BB and CC versus 65°F for Model AA).

The creep (time-dependent increase in strain under constant loading) was very low during the sustained pressure loading in the first pressure cycle (figures 42 and 44, table 7). The magnitude of cumulative creep varied from 1 to 10 percent depending on the location of the gages. There was no significant change in magnitude of creep between the first and fifth cycles (figures 43 and 45). All of the creep took place during the first

60 minutes of sustained loading. Extending the sustained loading phase of the pressure cycles beyond 240 minutes would not change the total strain reading at the conclusion of the sustained loading phase.

The residual strains recorded immediately after depressurization in the first pressure cycle were approximately the same magnitude as the cumulative creep at the conclusion of the 240-minute sustained pressure loading in the first pressure cycle (table 8). After a 240-minute relaxation period, the magnitude of residual strains was less than 100 microinches when one takes into account that relaxation pressure was 31 psig instead of 0 psig (table 9). The residual strains after depressurization from sustained pressure loading in the fifth cycle were higher than those in the first cycle. At the conclusion of the relaxation period, the difference in residual strains between the first and fifth cycles was, on the average, about 200 microinches/inch (tables 9 and 13).

Deterioration of Gasket and Surfaces on Model BB After 181 Cycles

Only the polycarbonate gasket in Model BB exhibited cracking of sufficient severity (figure 46) to require its removal and replacement with a new polycarbonate gasket. Only a single shear crack was observed on the conical acrylic bearing surface (figure 47). The shear crack was approximately 0.250 inch long and 0.125 inch deep. There was *extensive separation in the bonded equatorial joint* on the ID of the sphere, indicating improper quality of the bond. For this reason, Model BB was removed from further cycling until a new one was cast and bonded to replace the damaged one. The new Model BB sphere was equipped with a new extruded polycarbonate gasket prior to its placement into the pressure vessel for cycling.

Deterioration of Gaskets in Models BB and CC After 450 Cycles

Permanent deformation on Model CC was observed only on the plastic bearing gasket fabricated from cast polyurethane inserted between the metallic hatch and the acrylic sphere (figure 51).

Even though the extrusion of the polyurethane gasket into the interior of Model CC was significant (approximately 0.15 inch), the gasket was placed back into service for the remainder of pressure cycling.

Cracks were observed in polycarbonate, acrylic, and epoxy gaskets. The severity of cracking was greatest in epoxy (figure 48), followed by polycarbonate (figure 49), acrylic (figure 50), and polyurethane (figure 51) gaskets. Cracks were not detected in Nylon (figure 52). The polycarbonate gasket which served in Model BB from the 181st to 435th cycle exhibited only mild cracking (figure 53).

Deterioration of Surfaces on Models BB and CC After 450 Cycles

The condition of conical bearing surfaces around penetrations in Models BB and CC varied from one penetration to another, depending on the type of plastic gasket used in that penetration (table 14). Penetrations containing Nylon and polyurethane gaskets were free of cracks. Cracking was observed on bearing surfaces of penetrations containing epoxy, polycarbonate, and acrylic gaskets (figures 54 through 58). The cracks were oriented circumferentially around the penetration and were located within the first one third of the bearing surface width measured from the interior surface of the sphere.

The most severe cracking of conical bearing surfaces was observed in the penetration containing the epoxy gasket (figure 55). Cracks of lesser depth also were observed on bearing surfaces of penetrations containing acrylic (figure 54) and polycarbonate gaskets (figure 57). The bonded joint bisecting penetration E did not serve as a crack initiator on the conical bearing surface in contact with the polyurethane gasket (figure 58).

Neither the depth, nor the number of cracks precluded further testing of Models BB and CC, as past experience with scale-model and full-size NEMO-type spheres has shown that even very deep cracks (equal to wall thickness) do not initiate catastrophic failure (reference 5).

Neither crazing, nor cracking was observed on the concave and convex surfaces of Models BB and CC, indicating that the residual stresses on the surfaces of the models did not put those surfaces in sufficient tension to initiate fractures.

Deterioration of Gaskets in Models BB and CC After 1,000 Cycles

Permanent deformation was observed only on the plastic bearing gaskets fabricated from cast polyurethane (Composition Calthane #9 and #10). The polyurethane gasket (Calthane #10), which was in Model CC from the very beginning of the cycling program and was subjected to 1,000 cycles, extruded 0.3 inch past the edge of the penetration into the interior of the acrylic sphere (figure 59). The polyurethane gasket (Calthane #9), which was placed in service only after the 435th cycles as a replacement for the badly cracked epoxy gasket and was subjected to only 565 pressure cycles, extruded only 0.15 inch past the opening in the sphere (figure 60).

Cracks were observed in bearing gaskets fabricated from polycarbonate (figure 61), acrylic (figure 62) and polyurethane (figures 59 and 60). Since all gaskets, except Nylon and polyurethane Calthane #10, were placed in service during the inspection of Models BB and CC after the 435th cycles, all were subjected to only 565 pressure cycles. Observation here confirmed the finding made during the inspection after the 435th cycle; polycarbonate exhibits more extensive and deeper cracks than acrylic or polyurethane after only 500 pressure cycles. The shear cracks in the polyurethane Calthane #10 gasket after *1,000 pressure cycles* were less severe than those in the polycarbonate, epoxy, or acrylic gaskets after only *565* or *435 cycles.*

No cracks were found in the Nylon bearing gaskets from Model BB exposed to 565 pressure cycles (figure 63) and Model CC exposed to 1,000 pressure cycles (figure 64). Because of their excellent condition, Nylon bearing gaskets can be placed back into service after the 1,000 pressure cycle inspection.

Extrusions were observed on the inner surface of the gaskets where they contacted the O-ring

grooves on the aluminum hatches. The height of these extrusions was in the 0.005- to 0.01-inch range (figure 65). The Nylon gasket did not have an O-ring groove extrusion on its inner surface.

Based on the visual observation of all bearing gaskets during the inspections after the 435th and 1,000th pressure cycles, the gasket materials can be ranked on their ability to remain serviceable under cyclic pressure loading. When ranked on the basis of their durability under cyclic pressure loading, the preferred materials are

1. Nylon	MOST DURABLE
2. Acrylic	
3. Polyurethane	
4. Polycarbonate	
5. Epoxy	LEAST DURABLE

Deterioration of Surfaces on Models BB and CC After 1,000 Cycles

A thorough visual inspection of Models BB and CC was made at the conclusion of the pressure cycling program (figures 66 and 67). The inspection did not discover any crazing or cracking on spherical surfaces or separation of bonded equatorial bonds. Cracking, however, was observed on the bearing surfaces of some of the penetrations (figures 68 through 73).

The *most extensive* and *deepest cracking* was found in penetration D on Model CC served by an epoxy insert for the first 435 cycles and a polycarbonate insert for the following 565 cycles (figure 68).

There was a total *absence of cracks* in penetration E served by a polyurethane Calthane #10 insert for 1,000 cycles (figure 69). Also, surprisingly, the equatorial bonded joint which bisects penetration E did not initiate any cracks in the acrylic bearing surface. Penetrations A, B, and C in Model CC served by polycarbonate (figure 70), acrylic (figure 71), and Nylon (figure 72) inserts exhibited cracking in varying amounts. Only slight crazing was observed on the penetration in Model BB (placed in service after the 180th cycle) protected

14

by a Nylon insert (figure 73). The extent and severity of cracks in the penetrations of Model BB and CC are summarized in table 15.

Based on the observations, one can rank the performance of different gasket materials as suppressor of crack initiation and propagation in acrylic bearing surfaces during repeated pressure cycling. The ranking from most effective to least effective suppressor of crack formation in acrylic bearing surfaces at penetrations in sphere are

1. Polyurethane   MOST EFFECTIVE
2. Nylon
3. Polycarbonate
4. Acrylic
5. Epoxy   LEAST EFFECTIVE

CONCLUSIONS

1. Models BB and CC with $t/D_i = 0.2$ wall thickness and 48-degree conical penetrations sealed by conical aluminum hatches resting on plastic gaskets can be pressure cycled $\geq 1,000$ times to the design pressure of 3,560 psi at ambient temperature $\leq 75°F$ without potential catastrophic failure.

2. The cyclic fatigue life of acrylic spheres with metallic hatches in conical penetrations is determined by the formation of cracks on the bearing surfaces of the conical penetrations.

3. The use of plastic gaskets between the metallic hatches and the conical seats in an acrylic sphere can delay the initiation of cracks in the seat and the rate of their propagation.

4. Type 6 unfilled cast Nylon and Calthane #10 polyurethane plastic gaskets have been found to provide significantly better protection to the acrylic bearing surfaces in conical seats than gaskets fabricated from acrylic, epoxy, and polycarbonate.

5. The number, length, and depth of cracks in acrylic bearing surfaces on conical seats after 1,000 pressure cycles to design depth make the refinishing of these surfaces advisable.

6. Cracking was not observed on exterior and interior surfaces of the spheres, as well as in the equatorial joint between hemispheres, indicating the absence of tensile strains on these surfaces.

7. An equatorial joint bisecting a conical penetration in the sphere does not serve as a crack initiator in the conical seat.

8. The decrease of creep to zero on interior surfaces of Models BB and CC after 30 minutes of sustained pressurization at 3,560 psi indicates that the length of individual sustained pressurizations during pressure cycling can be extended beyond 4 hours without reducing the cyclic fatigue life of the spherical shell (i.e., intrinsic cyclic fatigue life).

TESTING OF SCALE-MODEL SPHERES 1 THROUGH 8

TEST SCHEDULE

Model numbers 1 through 8 also were pressure cycled together in a separate automated chamber at HBOI's Deep Ocean Simulation Facility connected through a series of servovalves to the same pressurization system that operated the larger chamber containing Models BB and CC.

The test schedule was to pressure cycle the 6-inch-diameter models 1 through 8 a minimum of 1,000 times to 3,560 psi at an ambient temperature of 75°F. The typical cycle consisted of pressure and relaxation periods, each of 4 hour's duration. Periodically, the chamber was opened and all 8 models were visually inspected for their condition. Inspection took place at the conclusion of 120, 180, 450, and 1,000 cycles.

In addition, models 6A and 6B, identical in all aspects to model 6, were subjected to long-term pressurization at 100 and 150 percent above design pressure (i.e., 7,120 and 9,000 psi, equivalent to 16,000 and 20,000 feet) to establish the magnitude of safety factor (SF) that the $t/D_i = 0.2$ pressure hull with 3,560-psi design depth possesses under overloads associated with potentially catastrophic plunges of the submersible to the bottom during at-sea operations.

INSTRUMENTATION

The scale-model spheres 1 through 8 were not instrumented for pressure cyclir j, as the objective of the tests was only to determine experimentally the onset of cracking and subsequent plastic instability. This was accomplished by periodic visual inspection of the spheres during the cyclic testing program.

Models 6A and 6B, slated for long-term pressure testing, were instrumented with a single strain gage rosette located on the interior surface of each sphere at its lower pole.

TEST ARRANGEMENT

All eight 6-inch-diameter scale-model spheres were enclosed in hard plastic shells and then stacked in a cylindrical rack designed to fit the interior of the chamber. This arrangement was to prevent sympathetic implosions when there was a failure of a single sphere. Implosions due to local plastic buckling were expected since the strains in the thinner spheres were definitely of a plastic nature.

Models 6A and 6B were tested individually, as the long-term pressurizations to which they were subjected were conducted at different pressure levels.

TEST PROCEDURE

The test procedure for the chamber containin j the 8 models was identical to the test procedure for the chamber containing Models BB and CC since both were operated by the same computer-controlled pressurization system at the HBOI Deep Ocean Simulation Facility.

The test procedure for Models 6A and 6B under long-term pressurization differed from the test procedure for pressure cycling models 1 through 8 at the HBOI Deep Ocean Simulation Facility. The long-term testing was conducted at the pressure testing facility of Stachiw Associates which was capable of generating the high pressures called for in these tests. The procedure consisted of cooling the pressure vessel down to 65°F, inserting the test model into the vessel (figure 74), hooking the

strain gage instrumentation cables for the test model up to the strain readout equipment, and tightening the end closure.

The subsequent testing consisted of raising the pressure at 1,000-psi per-minute rate to 7,200 psi for Model 6A, or 9,000 psi for Model 6B, and maintaining this pressure for >100 hours unless implosion occurred beforehand. Strains were read at 1,000 psi intervals during pressurization, at 1-hour intervals during sustained loading for 10 hours, at 1,000 psi during depressurization, and at 1-hour intervals during relaxation for 10 hours.

Cyclic Fatigue Buckling of Models 1 through 8 During First 450 Cycles

Model SNO1 with $t/D_i = 0.1$ failed by local buckling after withstanding 120 pressure cycles. This is an unusually good performance, as the membrane compressive stresses on the interior of Model SNO1 at 3,550 psi pressure were 12,675 psi. The local failure consisted of a conical fracture with an approximately 1.4-inch-diameter opening on the convex surface (figure 75). This is the same type of fracture observed previously on 15-inch-diameter scale-model NEMO spheres with $0.017 \leq t/D_i \leq 0.076$ subjected to long-term, or cyclic, pressure loadings.

Models SN02, 03, 04, 05, 06, 07, and 08 withstood 450 pressure cycles without any visible deterioration of spherical surfaces.

Cyclic Fatigue Buckling of Models 1 through 8 During Second 565 Cycles

Models SN02, 03, 04, 05, 06, 07, and 08 withstood a total of 1,000 pressure cycles of 4 hour's duration to 3,560 psi without any visible deterioration of spherical surfaces (figure 76). Based on their performance, it can be concluded that a t/D_i ratio of 0.125 (Model SN02) is adequate to prevent buckling under repeated pressurizations to 3,560 psi provided that the following conditions are met

1. Ambient temperature is $\leq 75°F$

2. Pressure loading $\leq 3,560$ psi

3. Duration of sustained pressurization ≤ 4 hours

4. Duration of relaxation at 0 psi is ≥ 4 hours

16

5. The hatch plug is fabricated from acrylic or other plastic with same physical properties as acrylic.

Under such conditions, acrylic spheres with $t/D_i \geq 0.125$ may be safely utilized as floats, or housings for oceanographic instruments. For containment of humans, a $t/D_i = 0.125$ is not considered adequate to provide acceptable safety margins for deviations from above conditions (i.e., accidental overpressure, duration of loading in excess of 4 hours, stress concentrations due to presence of metallic hatches, etc.).

Creep Buckling of Models 6A and 6B Under Long-Term Pressurization

Model 6A did not fail during sustained pressurization of 312 hour's duration at pressures that varied from 7,200 to 7,500 psi and at ambient temperatures that varied between 55°F to 65°F. The compressive strains measured by strain gages on the interior surface of the sphere during the test show (figures 77 through 84 and tables 14 through 17) that the creep rate on the interior surface of the sphere decreased from -515×10^{-6}/minute at the beginning of sustained pressurization to -33×10^{-6}/minute after 1 hour, -6.75×10^{-6}/minute after 10 hours, -0.77×10^{-6}/minute after 100 hours, and -0.01×10^{-6}/minute after 300 hours (figures 79 and 80).

The average magnitude of compressive strains during sustained pressurization was -23.590×10^{-6} immediately after pressurization to 7.200 psi, $-31,835 \times 10^{-6}$ after 1 hour, $-39,405 \times 10^{-6}$ after 10 hours, $-46,575 \times 10^{-6}$ after 100 hours, and $-48,895 \times 10^{-6}$ after 312 hours.

After depressurization to 0 psi, the relaxation rate decreased from $1,732 \times 10^{-6}$/minute at the beginning of relaxation to 72×10^{-6}/minute after 1 hour, to 4.2×10^{-6}/minute after 10 hours, and to 0.22×10^{-6} after 100 hours.

Relaxation continued with the compressive residual strains continously decreasing in magnitude until their character changed from negative to positive after approximately 217 hours. The positive strain continued to increase—when the relaxation period was terminated, the magnitude of positive

strains was $2,400 \times 10^{-6}$ and the relaxation rate was 0.1×10^{-6}/minute. Using this data, the tensile membrane stress on the inside of the sphere at the end of the relaxation period was calculated to be 1,600 psi.

Cracking was not observed on the conical bearing surface at the penetration, or any other spherical surface. Some delamination was observed, however, between the two bonded-plane equatorial surfaces on the hemispheres (figure 85). All delaminations originated on the interior circumference of the joint and propagated toward the exterior circumference of the joint. The presence of these delaminations confirmed the presence of tensile relaxation strains on the interior surface of the sphere recorded by electric-resistance strain gages. Furthermore, when Model 6A was subsequently cleaned with methyl alcohol, the concave surface crazed severely while the convex surface did not, demonstrating the presence of tensile stresses on the concave surface.

While the residual tensile stress of 1,600 psi magnitude was not high enough to fracture the hemispherical castings with 9,000 psi tensile strength, it was high enough to fracture the much weaker adhesive bonded joint. Joint delamination did not penetrate far enough to cause leakage through the joint or separation of the acrylic hemispheres while they were lifted out of the water.

In summary, it appears that an acrylic spherical pressure hull with $t/D_i = 0.2$ dimensions can safely withstand an accidental 100-percent overpressure for ≥ 312 hours in ≤ 60°F ambient environment, provided that the hatches are designed with an SF of ≥ 2 based on yielding of hatch material.

Model 6B did not fail during sustained pressurization of 144 hour's duration at pressures that varied from 8,800 to 9,300 psi and at ambient temperatures that varied from 55°F to 65°F. The compressive strain measured on the interior surface of the sphere (figures 86 through 93 and tables 18 through 21) increased with duration of loading significantly faster than during sustained pressurization of Model 6A to 7,200 psi. Its magnitude was $-31,897 \times 10^{-6}$ at the beginning of sustained pressurization, $-48,000 \times 10^{-6}$ after 1 hour, $-63,163 \times 10^{-6}$ after 10 hours, and $-82,900 \times 10^{-6}$ after

100 hours. The rate of creep decreased from -950×10^{-6}/minute at the beginning of sustained pressurization to -100×10^{-6}/minute after 1 hour, -15×10^{-6}/minute after 10 hours, -3.3×10^{-6}/minute after 100 hours, and -1.4×10^{-6}/minute after 144 hours.

During the short-term depressurization, the strains decreased instantaneously from $-86,807 \times 10^{-6}$ at 9,000 psi to $-66,547 \times 10^{-6}$ at 0 psi, followed by rapid positive creep which further decreased the residual compressive strain to $-53,707 \times 10^{-6}$ after 1 hour, $-43,949 \times 10^{-6}$ after 10 hours, and $-36,942 \times 10^{-6}$ after 100 hours. The relaxation rate decreased from $1,027 \times 10^{-6}$/minute imediately after depressurization to 73×10^{-6} after 1 hour, 14×10^{-6} after 10 hours, and 0.73×10^{-6} after 70 hours.

Cracking was not observed on the conical bearing surface of the penetration or any other spherical surface. Extensive delamination took place, however, in the joint between the two bonded hemispheres (figures 94 and 95). The width of separation between the edges of hemispheres varied from approximately 0.125 inch on the interior circumference to 0 inch on the exterior circumference (figure 96). Leakage to the interior of the sphere did not occur as the exterior edge of the joint around its circumference was still securely bonded (figure 96).

The delamination between edges of hemispheres was caused by the difference in magnitude of permanent deformations across the thickness of the sphere. The permanent compressive deformation caused by yielding of acrylic was greatest on the interior surface and least on the exterior surface *as predicted* by analytical calculations. Because of the large difference between compressive residual strains on the exterior and interior surfaces of each hemisphere, tensile strains are generated on the interior edge of the bond causing it to separate. If, by chance, the bond was stronger than the cast hemispheres, cracking originated on the interior surface of the hemispheres instead of in the joint.

Following visual inspection, tested Model 6B was disassembled by sawing through the 0.06-inch-wide strip of adhesive bond on the exterior surface of the joint that was still holding the hemispheres together. The two hemispheres were subsequently submerged in methyl alcohol to initiate crazing on surfaces where residual tensile stresses were present. After 30 minutes, the hemispheres were wiped dry and inspected for crazing.

Visual inspection of both hemispheres failed to detect crazing anywhere on the hemispheres. Absence of crazing demonstrated that tensile stresses were absent on both the concave and convex surfaces of the hemispheres.

The absence of residual tensile stresses on Model 6B, even though it experienced greater permanent deformation than Model 6A, can be explained by the fact that the almost total delamination of the equatorial joint during the relaxation phase of the test allowed the interior and exterior surfaces of the sphere to relax independently at different rates. If the 0.125-inch wide separation did not occur at the edge of the equatorial bond (figure 96), the tensile stresses on the concave surface of Model 6B would have caused it to craze and crack after wetting it with alcohol.

In summary, it appears that acrylic spherical pressure hulls with $t/D_i = 0.2$ dimensions can safely withstand an accidental 150-percent overpressure for ≥ 311 hours in $\leq 60°F$ ambient environment, provided that the hatches are designed with an SF of ≥ 2.5 based on yielding of hatch material.

CONCLUSIONS

1. The cyclic fatigue life of spheres with $t/D_i = 0.1$ under repeated pressurizations to 3,560 psi of 4 hour's duration is 120 cycles. The maximum membrane stresses in that sphere's interior surface under 3,560 psi external pressure are $-12,675$ psi. When the 120-cycle fatigue life of scale-model sphere model 1 with $t/D_i = 0.1$ is extrapolated to scale-model sphere model 6 with $t/D_i = 0.2$, its cyclic fatigue life is predicted to exceed 10,000 pressure cycles at 3,560 psi design pressure.

2. The thinnest acrylic sphere capable of withstanding 1,000 pressurizations of 4 hour's

duration to 3,560 psi is model 2 with $t/D_i = 0.125$. The maximum membrane stresses on the interior surface of that sphere under 3,560 psi external pressure are −10,985 psi. The weight-to-displacement ratio of model 2 is 0.57.

3. Total absence of shear cracks on the conical seats in models 2 through 8 after 1,000 pressurizations to 3,560 psi indicated that the conical bearing surfaces in contact with acrylic plugs do not require refinishing after 1,000 cycles like the conical seats in Models BB and CC in contact with metallic hatches. Thus, in applications where the acrylic sphere may serve as a pressure-resistant housing for electro-optics, the use of an acrylic hatch plate may extend the intervals between refinishings of conical bearing surfaces on spheres beyond 1,000 cycles.

4. Acrylic spheres with $t/D_i = 0.2$ will not implode or leak when accidentally submerged to a depth of 20,250 feet (6,164 meters; 9,000 psi) for 144 hours, provided that the hatch plates are designed with a 2.5 SF based on yielding. The residual mebrane strains on the interior of the sphere after sustained overpressurization to 9,000 psi are in the range of $-34,000 \times 10^{-6}$ to $-37,000 \times 10^{-6}$. There is almost complete delamination of the bonded equatorial joint.

5. Accidental submersion of acrylic spheres with $t/D_i = 0.2$ to a depth of 16,178 feet (4,931 meters; 7,200 psi) for 314 hours does not result in residual compressive membrane strains. After repair of the partially delaminated bonded joint, the sphere may be returned to service without reduction in design depth.

6. When the strains generated by sustained pressure loading are plotted on log-log coordinates, a straight line can be drawn through the data points (figure 97). This plot is a useful tool for extrapolating time-dependent strains beyond experimentally generated short-term strain data. Thus, to predict strains on an acrylic sphere for any duration of sustained loading at any pressure, one needs

only to pressurize the sphere to the desired pressure, read the strains during the first 10 hours, plot the results on log-log coordinates, and connect the data points with a straight line. With the aid of this linear graph, one can predict strains for any length of sustained loading, providing that local buckling does not initiate at some other location on the sphere.

7. Acrylic Models 6A and 6B with $t/D_i = 0.2$ will never cease to creep when subjected to external pressure loading $\geq 7,200$ psi at 60°F (figure 97). This is not the case when subjected to sustained pressure loading at design pressure of 3,560 psi.

DISCUSSION

MODELS BB AND CC

Strains ⋅ ⋅ the interior of Models BB and CC did not appear to increase progressively with each pressu⋅⋅ cycle. This indicates that the creep experienced during the sustained pressure loading phase of each cycle was recovered during the following relaxation phase of each cycle. Since the creep ceased approximately 60 minutes after application of sustained loading, it can be postulated with absolute certainty that extending the sustained loading phase beyond 240 minutes would not increase the magnitude of total (short-term plus creep) strain above the values observed during the pressure cycling with 240-minute sustained loading and relaxation phases.

Cracking of bearing gaskets under cyclic application of bearing stresses does not appear to be a function of their compressive or tensile strength, but of their compressive deformation (ASTM-D-621) under sustained load and/or tensile elongation (ASTM-D-638) at fracture. Plastics with high compressive deformation under sustained load and tensile elongation at fracture (i.e., Nylon and polyurethane) exhibit fewer, and less severe, cracks than plastics with *low* compressive deformation under sustained load and low tensile elongation at fracture (for example, epoxy, polycarbonate, and acrylic).

Extrusion of bearing gaskets is also a function of compressive deformation under sustained load, but only if the material's deformation is not recoverable during relaxation. Thus, for example, a polyurethane gasket extrudes significantly more than a Nylon gasket after repeated load applications, even though the 24-hour compressive deformation of Nylon is higher than that of polyurethane. The reason for it lies in the fact that the deformation of Nylon, under sustained compressive loading of 8,420 psi between the metallic hatch and the interior edge of the acrylic sphere, is recoverable during the relaxation phase of the pressure cycle while that of polyurethane is not (i.e., the creep generated by each cycle is cumulative).

Formation of cracks in acrylic bearing surfaces under cyclic application of bearing stresses is *fostered* by bearing gaskets fabricated from a hard, brittle plastic characterized by low elongation at tensile fracture (ASTM-D-638 at 75°F and 0.2 inch/minute test rates) and low deformation under sustained compressive loadings (ASTM-D-621 at 75°F, 4,000 psi loading for 24 hours). As example of such a plastic can serve hard, brittle epoxy plastic.

The formation of cracks in acrylic bearing surfaces under cyclic application of bearing stress is *prevented/retarded* by bearing gaskets fabricated from a compliant, tough plastic characterized by high elongation at tensile fracture, and extensive deformation under sustained compressive loading. As example of such a plastic can serve compliant, tough, cast Nylon Type 6/12, or specially formulated, cast polyurethane Calthane 5520/2300 composition.

Selection of optimum gasket material should be based on two criteria: (1) the cyclic fatigue life of the gasket prior to replacement due to excessive cracking and/or extrusion, and (2) the gasket's effect on suppressing the formation of shear cracks in conical bearing surfaces around penetrations in the acrylic sphere. Ideally, the material from which the bearing gasket is fabricated should provide the gasket with infinite cyclic fatigue life. At the same time, the material should prevent the formation of shear cracks in the acrylic bearing

surfaces for an infinite number of pressurizations to design pressure.

Theoretically, a penetration in the acrylic sphere protected by a bearing gasket from an ideal material will never require refinishing, and the gasket will never have to be replaced. Unfortunately, such a material has not yet been discovered and for this reason, a tradeoff has to be made between frequent replacement of bearing gaskets and infrequent refinishing of the conical bearing surface around the penetration. Since the cost of refinishing the conical bearing surfaces around penetrations in the operational pressure hull of a submersible is approximately an order of magnitude higher than the replacement of bearing gaskets in two penetrations, it is more cost effective to replace the bearing gasket two to three times rather than to refinish the bearing surfaces once (figure 98).

The reasons for it are that the replacement of bearing gaskets can be performed by the operators of the submersibles at their facility, while refinishing requires shipping of the hull to the plastic fabricator for machining and bonding of acrylic bearing rings, followed by hydrostatic proof testing at a deep-ocean simulation laboratory. In addition, replacement of the bearing gaskets removes the submersible from service for about a week, while the refinishing of the bearing surfaces on penetrations requires more than 8 weeks.

Based on this line of reasoning, the optimum gasket material was polyurethane of Calthane #10 formulation. Calthane #10 gasket material is a mix of Calthane 5520 and Calthane 2300 formulations in 7:1.25 ratio. Formulation Calthane 5520 is made up of components A and B in 2.75:1 ratio, and formulation Calthane 2300 is made of components A and B in 2:3 ratio. The gasket cast from this material prevented initiation of cracks in the acrylic bearing surface of the penetration during 1,000 pressure cycles to design depth. It was the *only* gasket material of the five tested (polycarbonate, polyurethane, acrylic, epoxy, and Nylon) to accomplish that. In the process of doing so, it underwent permanent deformation resulting in significant extrusion (0.300 inch) past the edge of the penetration.

20

Such a large extrusion is unacceptable in an operational hull (approximately 1.5 inches, based on linear scaling of extrusions in scale-model spheres). For this reason, the gasket would have to be replaced often, the replacement schedule being a function of maximum depth to which the dives were performed. If all the dives were to design depth, the polyurethane gasket would have to be replaced at 200-dive intervals (i.e., annually).

If, on the other hand, the goal of the pressure hull maintenance program is to strike a balance between the replacement of gaskets and the refinishing of bearing surfaces in penetrations, Nylon is the optimum gasket material. Nylon *never* requires replacement since it doesn't crack or extrude, even after 1,000 sustained pressurizations of 4 hour's duration to design pressure.

At the same time, its performance as a compliant interface between the metallic hatch and the acrylic hull, although not as effective as polyurethane, surpasses that of acrylic, epoxy, and polycarbonate gaskets. The conical bearing surfaces of an acrylic hull protected by Nylon gaskets exhibit fewer and shallower cracks than surfaces protected by acrylic, epoxy, or polycarbonate gaskets. Because of their shallow depth, even after 1,000 pressure cycles to design pressure, the refinishing of bearing surfaces around penetrations protected by Nylon gaskets does not have to take place before the acrylic sphere has accumulated *at least* 1,000 pressure cycles to design depth. Since most dives performed by a submersible are not to design depth, the rate of crack growth may be low enough to allow larger intervals than 1,000 dives between the refinishings of the bearing surfaces around penetrations in the acrylic sphere.

Selection Criteria for an Acceptable Bearing Gasket

Although Nylon 6/12 and polyurethane of Calthane #10 composition appear to satisfy the requirements of an acceptable bearing gasket for metallic hatches in acrylic spheres, there are many other plastics that may perform better in this application because of a more fortuitous combination of physical properties. To ensure that the application of

yet-untested materials for fabrication of bearing gaskets does not result in premature cracking of the bearing surfaces on the acrylic sphere, or, in a potentially worse situation, premature catastrophic failure of the gasket resulting in flooding of the sphere interior, there is a tentative specification to be met by any material considered for potential service in bearing gaskets (table 16).

This specification is based on the physical properties of gaskets whose performance was experimentally proven in this test program to be acceptable for service in acrylic spheres with operational capability to a depth of 8,000 feet (2,438 meters). If bearing gaskets are fabricated from a plastic meeting the physical properties shown in table 16, its performance should equal, or exceed, that of the Nylon or polyurethane gaskets experimentally evaluated in Models BB and CC.

ACRYLIC MODEL SPHERES 1 THROUGH 8

Cyclic fatigue life of acrylic spheres under 4-hour-long pressure cycles to 3,560 psi (8,000 feet) has exceeded original expectations. Model 1 with $t/D_i = 0.1$, pressure cycled at approximately 50 percent of its short-term critical pressure, survived 120 cycles prior to failure by local plastic creep buckling. Model 1 with $t/D_i = 0.125$, pressure cycled at approximately 40 percent of its short-term critical pressure, survived 1,000 pressure cycles without any visual signs of damage to its surfaces. Using a linear extrapolation on a log-log plot, the cyclic fatigue life of model 6 with $t/D_i = 0.2$, pressure cycled at approximately 20 percent of its short-term critical pressure, is predicted to exceed 100,000 cycles. This exceeds the ASME PVHO-1 requirement for a cyclic fatigue life of 10,000 dives to design depth, each of 4 hour's duration.

Since models 1 through 8 do not incorporate metallic hatches in their penetrations, the cyclic fatigue life is dependent solely on the creep buckling of the acrylic shell which is only a function of the sphere's t/D_i ratio and the physical properties of the acrylic casting. This is not the case with NEMO-type spheres incorporating stiffness discontinuities at the interfaces between the rigid metallic hatches and soft plastic shell.

Because of this stiffness discontinuity, tensile stresses generated on the surface of the conical penetration in the acrylic sphere result in cracks that propagate at right angles to the conical seat. These cracks, when they exceed acceptable magnitude, necessitate refinishing of the bearing surfaces on the conical penetrations. Thus, while the intrinsic cyclic fatigue life of an acrylic sphere may exceed 10,000 cycles, the refinishing of bearing surfaces at penetrations will have to be performed frequently (typically at 1,000 cycle intervals) for the sphere to retain its intrinsic cyclic fatigue life.

Static Fatigue Life of the acrylic spheres with different t/D_i ratios has not been established in this testing program as it is not considered to be of particular interest to operators of NEMO-type pressure hulls that will be primarily subjected to cyclic, rather than static fatigue. Still, there are two potential operational scenarios where static fatigue resulting in plastic creep buckling is the primary cause of failure. These scenarios are (1) the submersible being trapped, or disabled at design depth (i.e., 8,000 feet) in excess of typical 4-hour dive duration before returning to the surface, and (2) the submersible sinking out of control and coming to rest on the ocean floor at a depth that exceeds the design depth by 100 or maybe even 150 percent.

There is no concern with the first scenario since the static fatigue life of acrylic model 6 with $t/D_i = 0.2$ and Models BB and CC at 3,560 psi (8,000 feet) is infinite. This is based on the observation that the strains recorded on the interior of Models BB and CC during sustained pressure loading at 3,560 psi stopped to increase after approximately 30 minutes (i.e., it ceased to creep). Without continuing creep, plastic creep buckling cannot take place, regardless of how long sustained loading is maintained.

The case is quite different for the second scenario, as the relationship between static fatigue life and magnitude of overpressure has not been considered for experimental determination in this program because of the large number of scale models and the testing time required. Still, the sustained pressurizations of models 6A and 6B at 100- and 150-percent overpressure provide the information

on the minimum value of static fatigue life that the crew can expect at these depths. Since models 6A and 6B individually withstood under-sustained pressurization for 311 hours at 100-percent overpressure and 144 hours at 150-percent overpressure, one can conclude with a high degree of certainty that full-size acrylic spherical hulls with $t/D_i = 0.2$ *will not* implode under the same magnitude of overpressure in a shorter time period than the scale models. In addition, the inspection of strains recorded on model 6A under 7,120 psi sustained pressurization leads one to believe that the static fatigue life of a spherical pressure hull with $t/D_i = 0.2$ significantly exceeds 300 hours at that pressure.

One can postulate with a high degree of certainty, therefore, that the occupants of a NEMO 8,000 pressure hull have a safety margin of at least 300 hours at 100-percent overpressure (16,000 feet depth), and 100 hours at 150-percent overpressure (20,000 feet depth) before the hull will implode by plastic creep buckling.

CONCLUSIONS

1. Acrylic spherical pressure hulls with $t/D_i = 0.2$ wall thickness and conical penetrations sealed with conical aluminum hatches resting on plastic gaskets can be safely operated to design depth of 8,000 feet at $\leq 75°F$ ambient temperature.

2. The implosion pressure of 16,000 psi at 75°F ambient temperature of an acrylic sphere with $t/D_i = 0.2$ provides the pressure hull for a design depth of 8,000 feet with an SF of 4.5 under short-term loading. This exceeds the minimum critical-pressure/design-pressure ratio of 4 required by the ASME PVHO-1 Safety Standard 1993 Edition for NEMO-type windows.

3. The concave and convex surfaces of acrylic spheres with $t/D_i = 0.2$ remain free of cracks after 1,000 dives to design depth of 8,000 feet, indicating that the cumulative residual strain generated by pressure cycling does not exceed the tensile strain limit of acrylic. For this reason, the cyclic fatigue life

22

of the acrylic shell itself can be predicted with confidence to exceed 10,000 cycles.

4. The cyclic fatigue life of the whole pressure hull assembly is determined not only by cyclic fatigue life of the acrylic shell, but also by the formation and growth rate of shear cracks on the conical bearing surfaces around hatch penetrations sealed with conical aluminum hatches resting on plastic bearing gaskets.

5. The spherical acrylic pressure hull with $t/D_i = 0.2$ incorporating single, or multiple, 48-degree conical hatch penetrations can safely withstand a minimum of 1,000 pressurizations of 4 hour's duration to design depth of 8,000 feet at 75°F ambient temperature, even though cracks will appear on the conical bearing surfaces around penetrations after several hundred dives to design depth.

6. The use of Type-6 unfilled Nylon and Cal-thane #10 polyurethane gaskets between the metallic hatches and acrylic bearing surfaces around penetrations delays the initiation and, subsequently, the propagation of cracks in acrylic. The use of gaskets fabricated from epoxy, acrylic, or polycarbonate plastics has been found to be less satisfactory, although acceptable.

7. Experience with past NEMO-model 3,000 pressure hulls in Johnson Sea-Link submersibles 1 and 2 has shown that cracked acrylic bearing surfaces around penetrations in the sphere can be satisfactorily repaired by machining out the fractured material and replacing it with an acrylic ring that, after bonding to the sphere with acrylic adhesive,

matches the concave and convex surfaces of the sphere.

8. The cyclic fatigue life of spherical acrylic pressure hulls with $t/D_i = 0.2$ is not decreased by the presence of multiple penetrations with $\leq$ 48-degree spherical conical angle sealed with aluminum hatches, provided that the separation between the edges of penetrations is $\geq$ 0.73 radians.

9. The cyclic fatigue life of an acrylic sphere with $t/D_i = 0.2$, whose conical penetration is closed by an acrylic conical plug, exceeds the cyclic fatigue life of acrylic spheres with metallic hatches due to the absence of shear cracks on conical seats even after 1,000 cycles.

10. For unmanned applications, where the dive duration is $\leq$ 4 hours to a design depth of 8,000 feet the wall thickness of the sphere may be reduced from $t/D_i = 0.2$ to some lesser value in the $0.125 < t/D_i < 0.2$ range, provided that the hatch plate is fabricated from acrylic.

11. The acrylic spheres with $t/D_i = 0.2$ have a static fatigue life in excess of 300 hours at depths of 16,000 feet (4,878 meters) and 100 hours at depths of 20,000 feet (6,097 meters) in sea water at 75°F (24°C) ambient temperature. This provides a proven safety net for an uncontrolled descent of the submersible to the bottom of the ocean in almost every location in the world.[2]

---

2. 60 percent of all ocean-bottom area is less than 16,000 feet (4,878 meters) deep, and 98 percent of all ocean bottom area is less than 20,000 feet (6,097 meters) deep.

RECOMMENDATIONS

1. The shell thickness of a spherical pressure hull for manned service to a depth of 8,000 feet must be ≥ 0.2 Di in order to meet the requirements of the ASME PVHO-1 safety standard for NEMO windows.

2. The bearing gaskets between conical metallic hatch plates and the conical seats in the acrylic sphere should be fabricated from plastics meeting the requirements of table 15 to minimize the number and size of cyclic fatigue shear cracks in the conical acrylic seats. Unfilled Type 6 Nylon and Calthane #10 polyurethane meet this requirement.

3. The conical seats in acrylic spheres should not be refinished prior to having accumulated 1,000 cycles unless the average depth of the shear cracks exceeds $0.016D_o$.

4. The hatch and penetration plates for spherical acrylic hulls with $t/D_i = 0.2$ should be designed with an SF of ≥ 2.5 based on the yielding of plate material even though this is not a requirement of the ASME PVHO-1 safety standard. Only with hatch plates designed for a design depth of 8,000 feet on the basis of an SF of 2.5 can the acrylic sphere withstand an accidental sustained overpressurization to 9,000 psi for at least 100 hours.

GLOSSARY

ASME	American Society of Mechanical Engineers	Institution	
		ID	inner diameter
Compressive Strain	compression of surface	L	length
		NOSC	Naval Ocean Systems Center
Creep	time dependent strain rate under constant stress; i.e., inches/inch/minute	OD	outside diameter
Cumulative Creep	total time-dependent strain generated by constant stress during a specified time interval	Residual Strain	permanent surface deformation remaining after removal of external loading
		RTV	room temperature vulcanizing
DOSF	Deep Ocean Simulation Facility	SF	safety factor
Extrusion	permanent deformation of shape	Strain	surface extension or compression measured in units of length per single unit of length; i.e., inches/inch, or mm/mm
HBOI	Harbor Branch Oceanographic		

REFERENCES

1. ASME PVHO-1, "Safety Standard for Pressure Vessels for Human Occupancy," The American Society of Mechanical Engineers, 1993 Edition.

2. Stachiw, J. D. 1970. "Development of a Spherical Acrylic Plastic Pressure Hull for Hydrospace Applications," Naval Civil Engineering Laboratory, TR R-676; (AD 707363).

3. Stachiw, J. D., and K. L. Mack. 1970. "The Spherical Acrylic Pressure Hull for Hydrospace Application; Part 2. Experimental Stress Evaluation of Prototype NEMO Capsule," Naval Civil Engineering Laboratory, Technical Note N-1113, (Oct) (AD 715772).

4. Ottsen, H. 1970. "The Spherical Acrylic Pressure Hull for Hydrospace Application; part 3. Comparison of Experimental and Analytical Stress Evaluations for Prototype NEMO Capsule," Naval Civil Engineering laboratory, Technical Note N-1094, (Mar) (AD 709914).

5. Stachiw, J. D. 1970. "The Spherical Acrylic Pressure Hull for Hydrospace Application; Part 4. Cyclic Fatigue of NEMO Capsule #3," Naval Civil Engineering Laboratory, Technical Note N-1134, (Oct) (AD 715345).

6. Stachiw, J. D. 1971. "Spherical Acrylic Pressure Hulls for Undersea Exploration," American Society of Mechanical Engineers, Journal of Engineering for Industry, Vol. 93, No. 2 (May).

7. Kelsey, R. A. and R. B. Dolan. 1970. "Johnson Sea-Link, the First Deep Diving Welded Aluminum Submersible," ASME Paper 70-WA/UnT-6.

8. Maison, J. R. and J. D. Stachiw. 1971. "Acrylic Pressure Hull for Johnson-Sea-Link Submersible," ASME Paper No. 71-WA/UnT-6.

9. Murphy, D. and W. Mazzone. 1972. "Transparent Hull Submersible MAKAKAI," ASME Paper 72-WA/OCT-8, (Dec).

10. Stachiw, J. D. 1976. "NEMO Type Acrylic Plastic Spherical Hull for Manned Operation to 3,000 feet Depth," ASME Transactions/Journal of Engineering for Industry, Vol. 98, No. 2.

11. Stachiw, J. D. and B. Beasley. 1970. "Precision Casting Process for Acrylic Plastic spherical Windows in High Pressure Service," ASME Paper 74-WA/OCT.

12. Stachiw, J. D., A. Clark, and C. B. Brenn. 1987. "Acrylic Plastic Spherical Pressure Hull for 2439 m Design Depth; Phase I," ASME Transactions/Journal of Energy Resources Technology, Vol 109, (Mar).

13. Stachiw, J. D. and R. B. Dolan. 1978. "Spherical Acrylic Pressure Hulls with Multiple Penetrations," ASME Transactions/Journal of Engineering for Industry, Vol. 100, No. 2.

14. Stachiw, J. D. 1969. "Critical Pressure of Spherical Shell Acrylic Windows Under Short-Term Pressure Loading," ASME Transactions/Journal of Engineering for Industry, Vol. 91, No. 3.

15. Stachiw, J. D., R. B. Dolan, and D. L. Clayton. 1981."Polycarbonate Plastic Inserts for Spherical Acrylic Plastic shells under Hydrostatic Loading," ASME Transactions/journal of Engineering for Industry, Vol 103, No. 1.

16. Stachiw, J. D. and J. J. Lones. 1977. "Development of Economical Casting Process for NEMO Type Acrylic Submersible Hulls," ASME Transactions/Journal of Engineering for Industry, Vol 99, No. 2.

17. "Rules for Building and Classing; Underwater Vehicles, Systems, and Hyperbaric Facilities," American Bureau of Shipping, 1990.

Figure 1. The 18-inch OD x 12.85-inch ID hemispheres for Model AA were slush cast from acrylic plastic in a metallic mold assembly.

Figure 2. The upper hemisphere of Model AA with a conical 48-degree penetration, the aluminum plug hatch, and the associated plastic bearing gasket.

Figure 3. Components of the hatch assembly for Model AA shown in their future relationship during mounting.
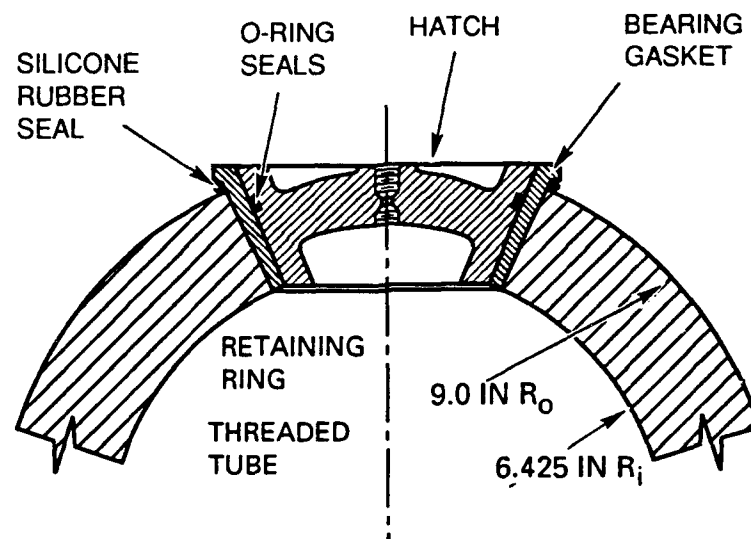
Figure 4. Fixed-hatch assembly for Model AA.
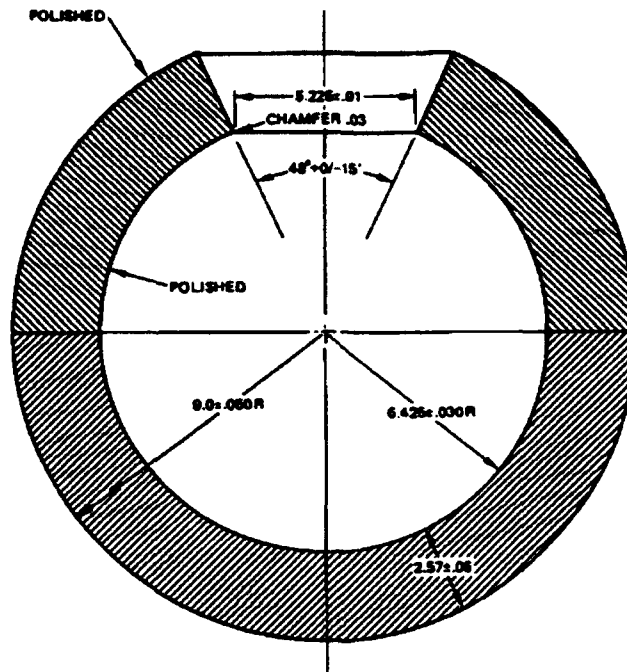
Figure 5. Dimensions of Model AA acrylic sphere.
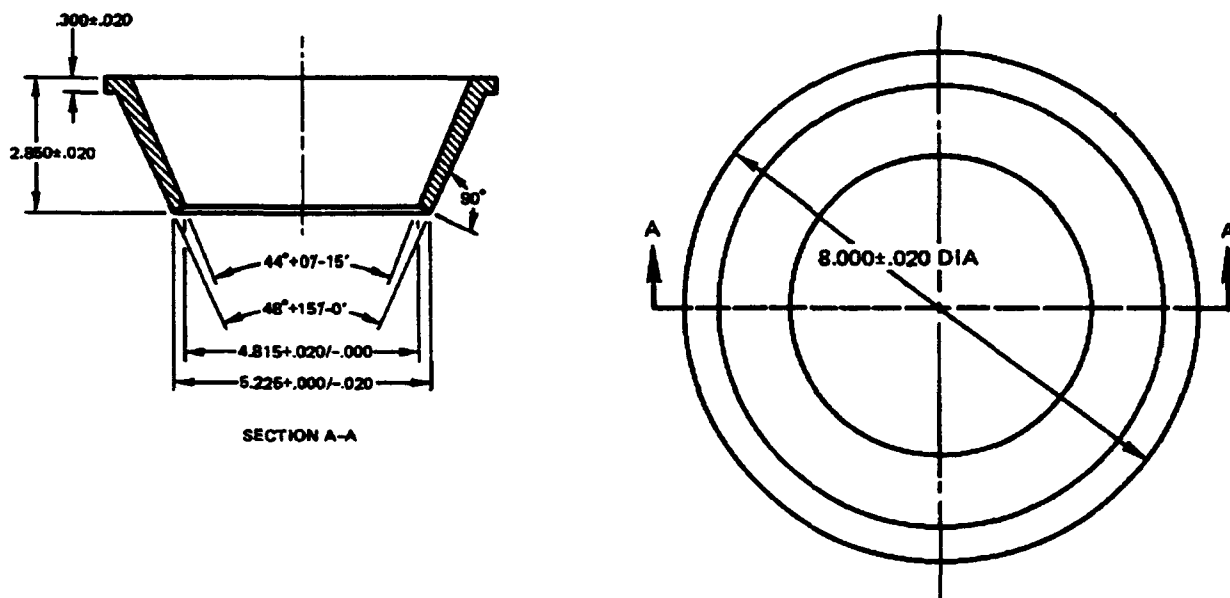
Figure 6. polycarbonate bearing gasket for Model AA.
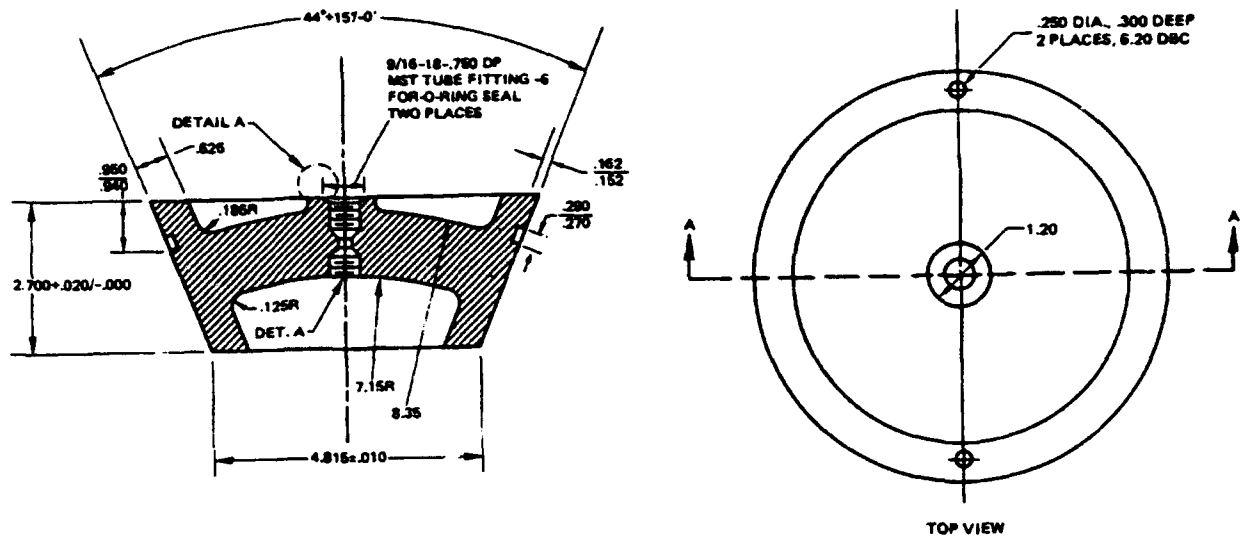
Figure 7. Aluminum 7075-T6 alloy hatch plate for Model AA.

Figure 8. The 15-inch OD x 10.7 ID Model BB acrylic sphere with single penetration.
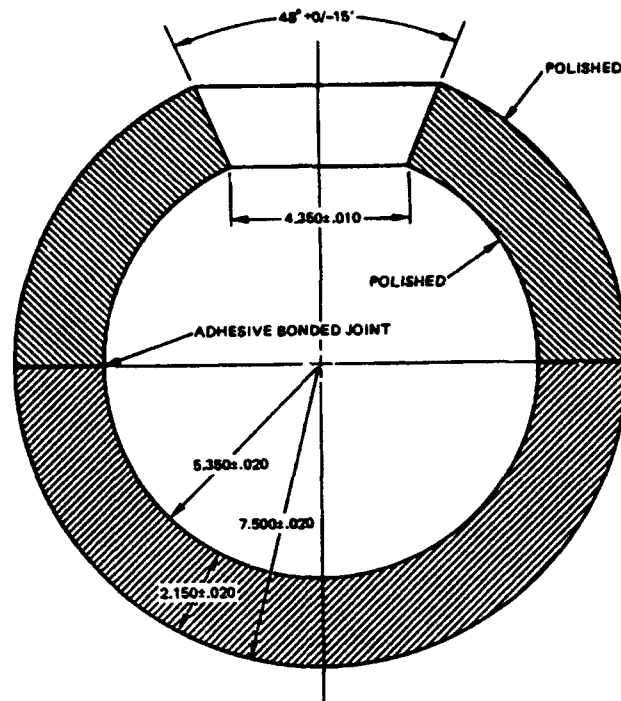
Figure 9. Dimensions of Model BB acrylic sphere.
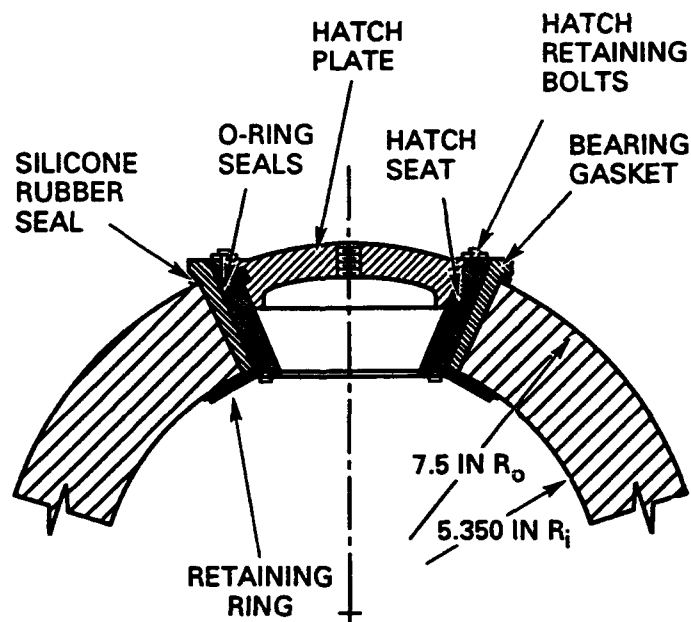
Figure 10. Removable hatch assembly for Model BB.

31
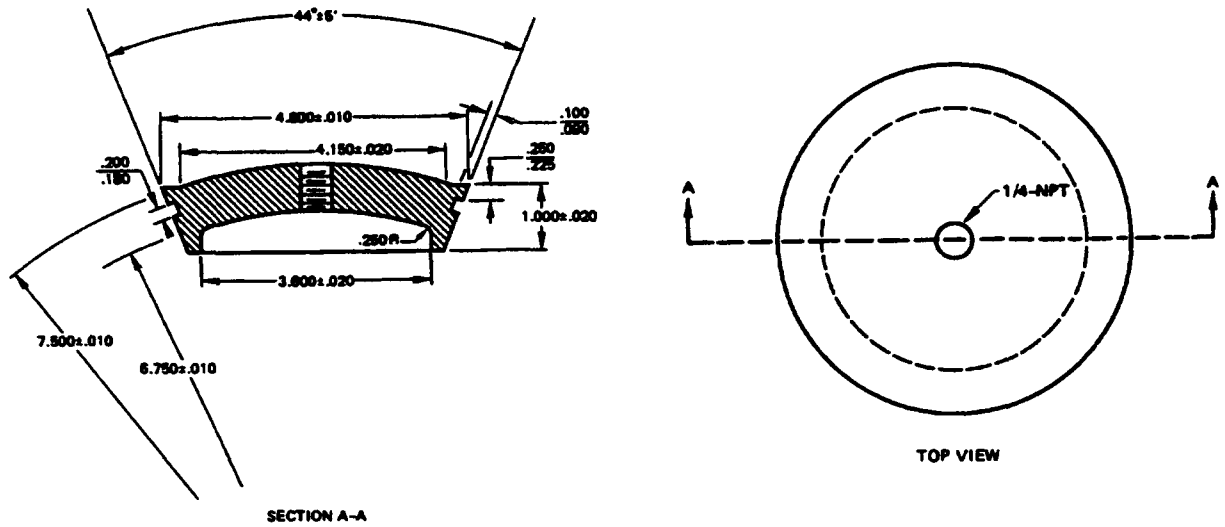
Figure 11. Removable aluminum 6061-T6 alloy hatch plate for Models BB and CC.
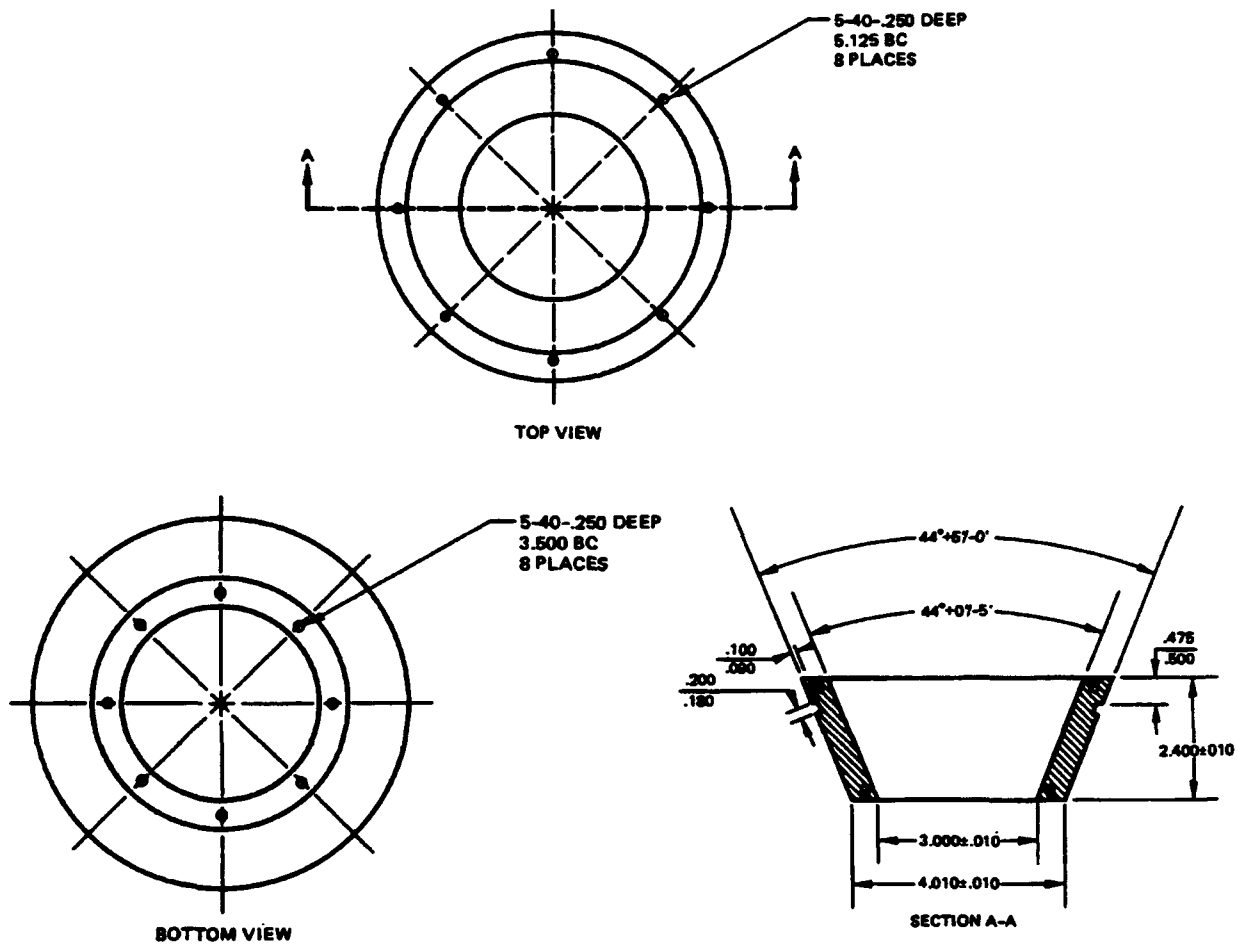
Figure 12. Aluminum 6061-T6 alloy hatch seat for removable hatches on Models BB and CC.

.275±.020

2.400±.020

90°

44°+0'/-15'

48°+15'/-0'

4.000+.020/-.000

4.350+.000/-.020

SECTION A-A

A — A

6.750±.020

TOP VIEW
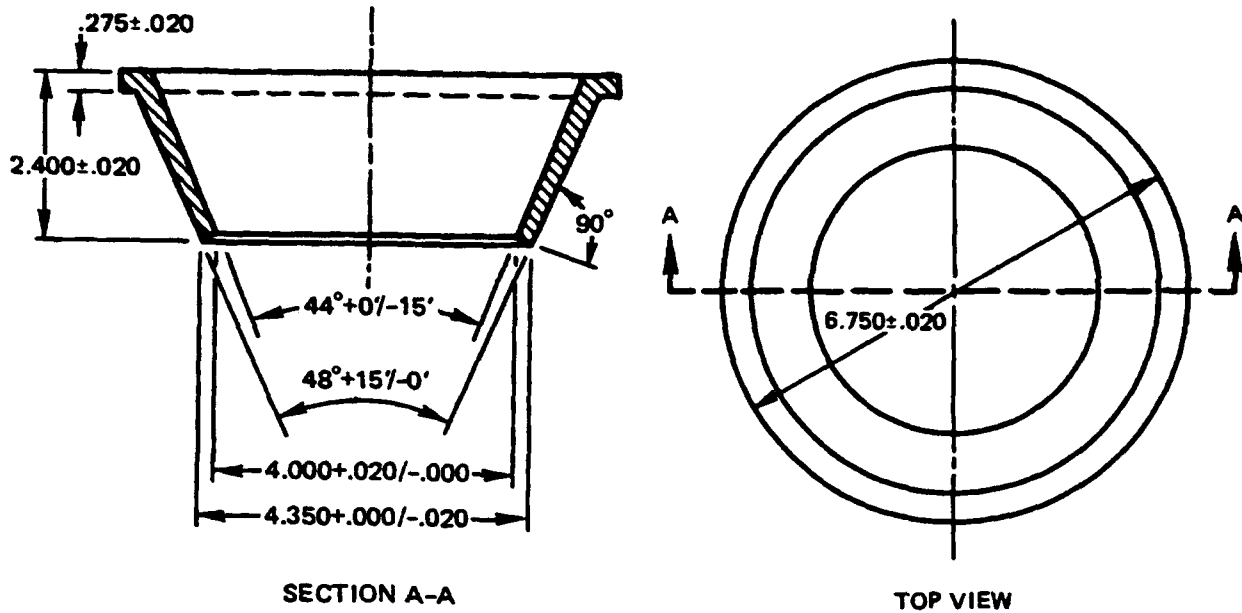
Figure 13. Plastic bearing gasket for Models BB and CC.

DRILL .1406
3.500 BC
8 PLACES

A — A

.06 SLIT

MATERIAL: 6061-T6 ALUMINUM

TOP VIEW

5.770
5.750

4.010
3.990

3.010
2.900

.070
.050

.130
.120

12° ± 30'

SECTION A-A
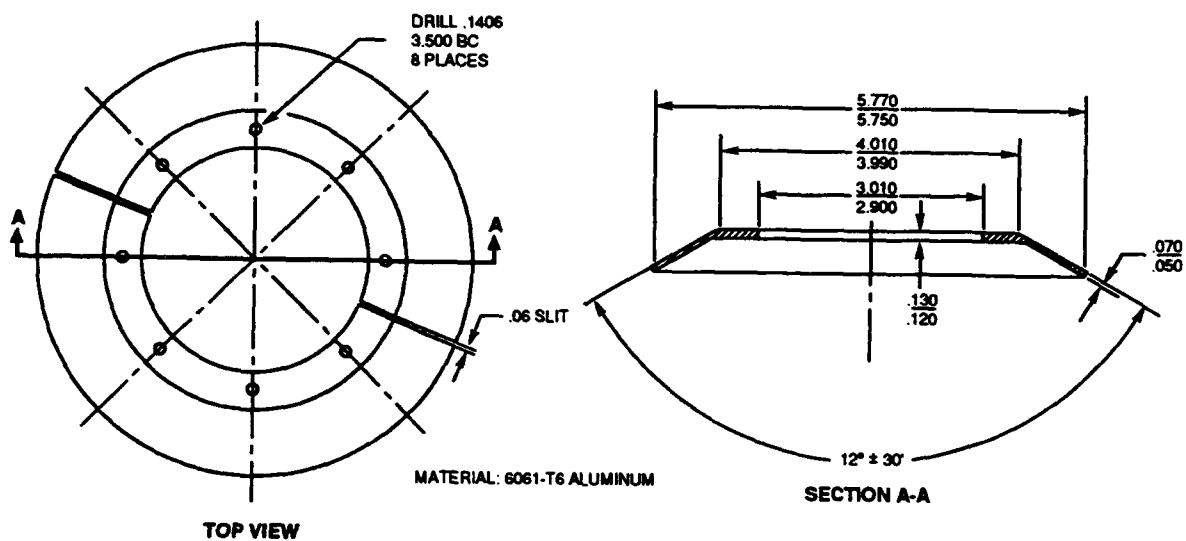
Figure 14. Hatch seat retainer for removable hatches in Models BB and CC.

33
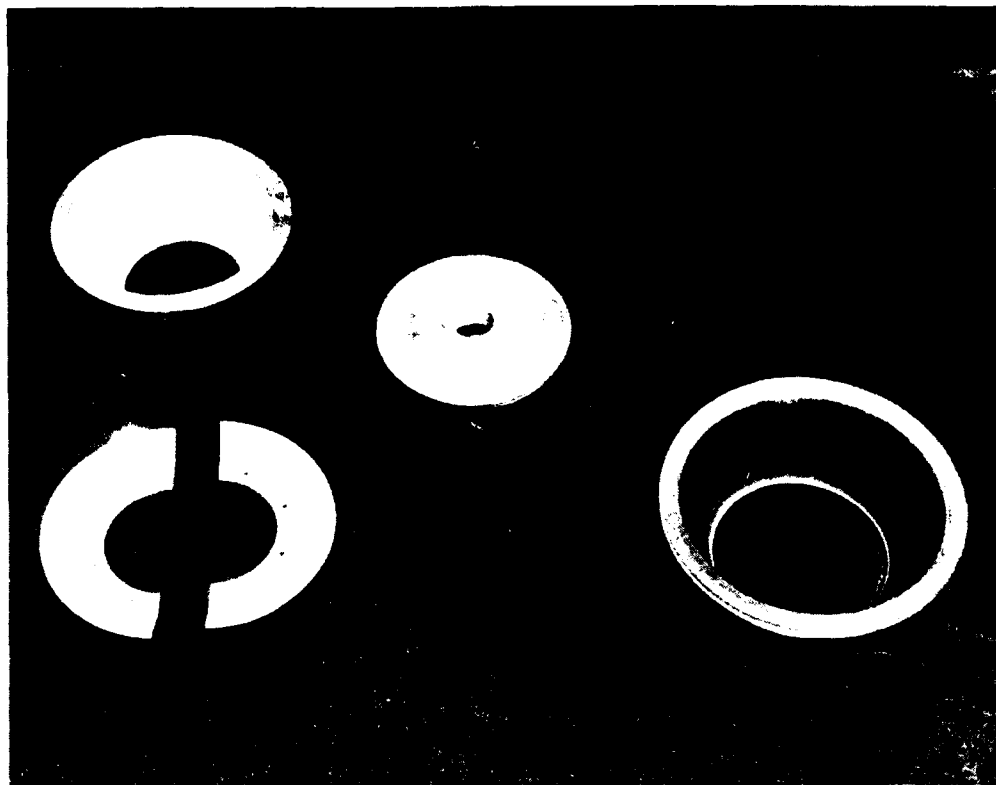
Figure 15. Components of the removable hatch assemblies for Models BB and CC.

Figure 16. The 15-inch OD x 10.7-inch ID Model CC acrylic sphere with five penetrations.
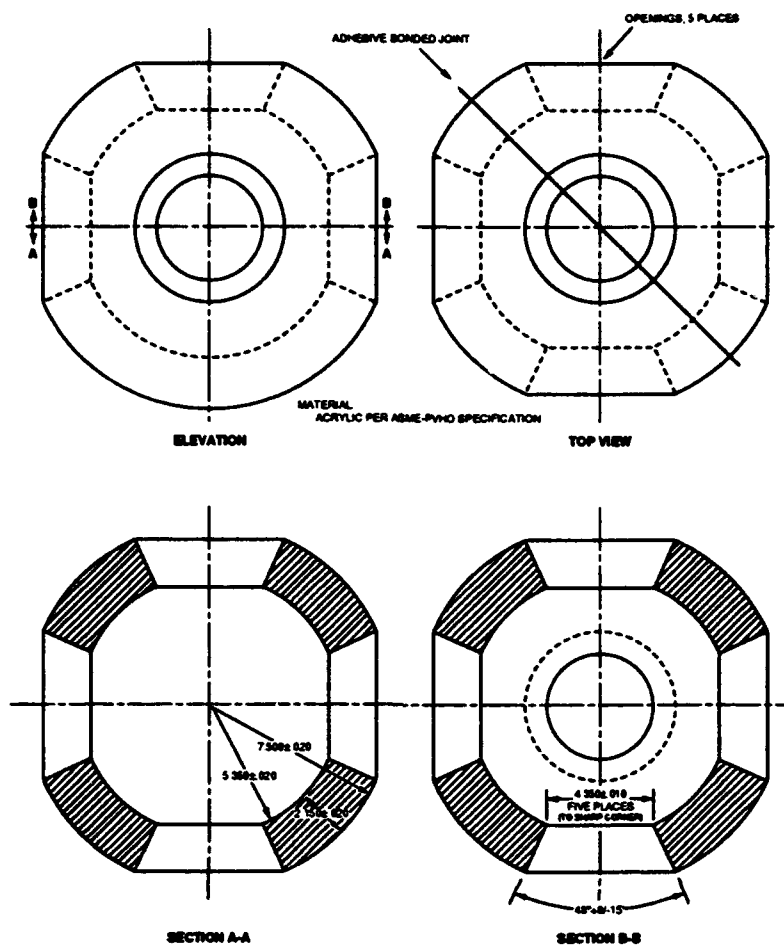
Figure 17. Dimensions of Model CC acrylic sphere.
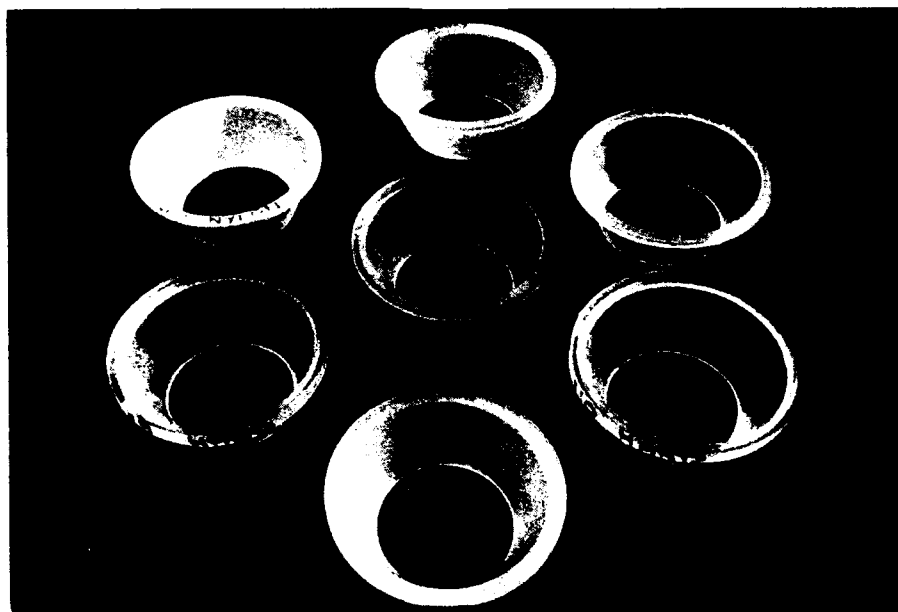
Figure 18. Bearing gaskets from different plastic materials for evaluation in Model CC: acrylic, epoxy, Nylon, polycarbonate, polyurethane.

35
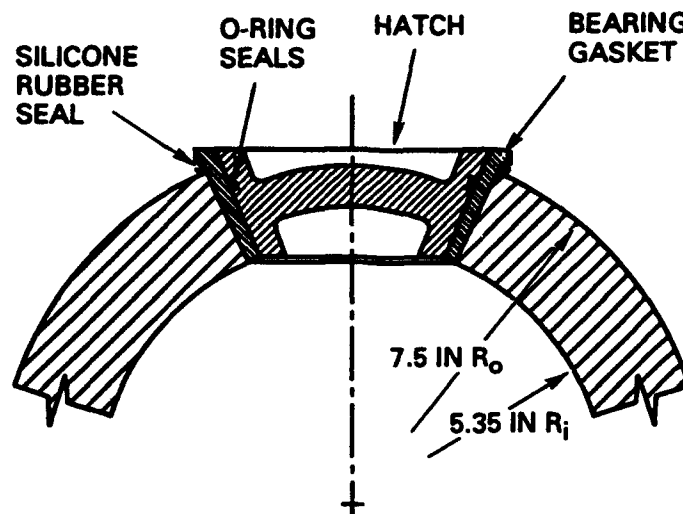
Figure 19. Fixed-plug hatch assembly for Model CC.

TOP VIEW
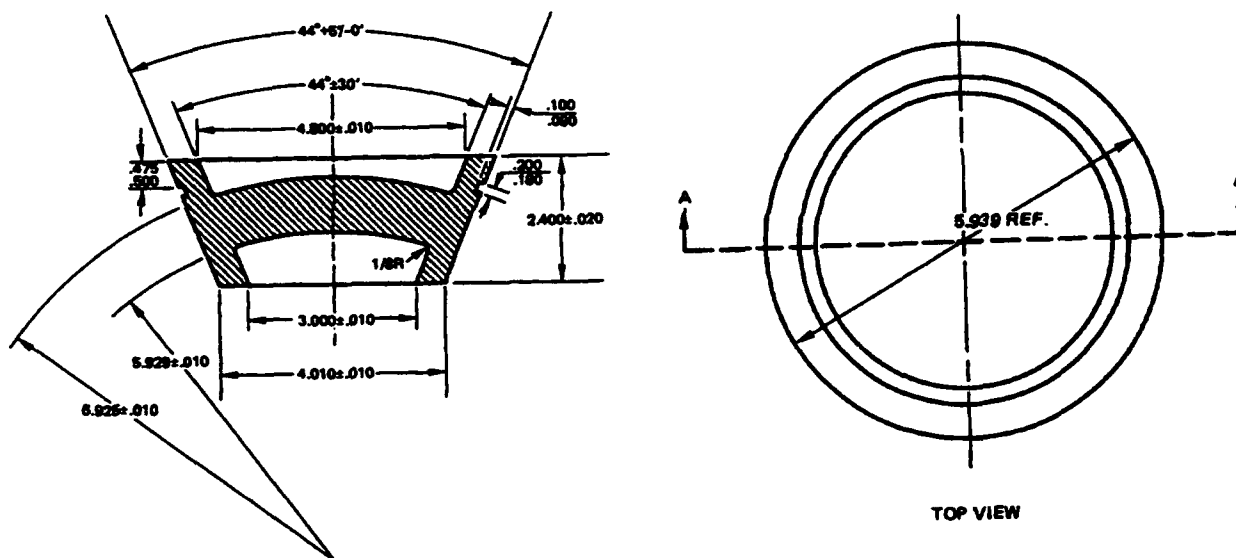
Figure 20. Aluminum 6061-T6 alloy hatch plate for Model CC.

Figure 21. Typical 6-inch-diameter acrylic sphere and acrylic plug hatch for models 1 through 8.
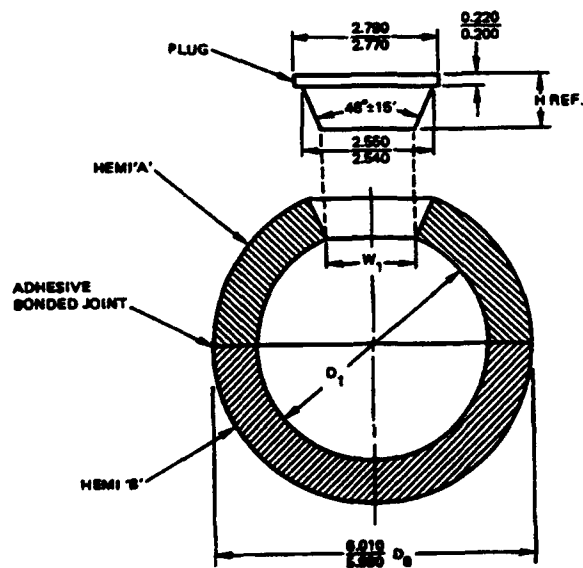
TABLE OF DIMENSIONS

SPECIMENS	T/D_1	T	D_1	W_1	H
SPHERE° 1	0.100	0.500	5.000	2.033	0.771
SPHERE° 2	0.125	0.600	4.800	1.952	0.862
SPHERE° 3	0.149	0.690	4.620	1.879	0.945
SPHERE° 4	0.175	0.780	4.440	1.806	1.027
SPHERE° 5	0.191	0.830	4.340	1.765	1.072
SPHERE° 6	0.200	0.860	4.280	1.740	1.100
SPHERE° 7	0.210	0.890	4.220	1.716	1.127
SPHERE° 8	0.225	0.930	4.140	1.683	1.164

Figure 22. Dimensions of models 1 through 8.
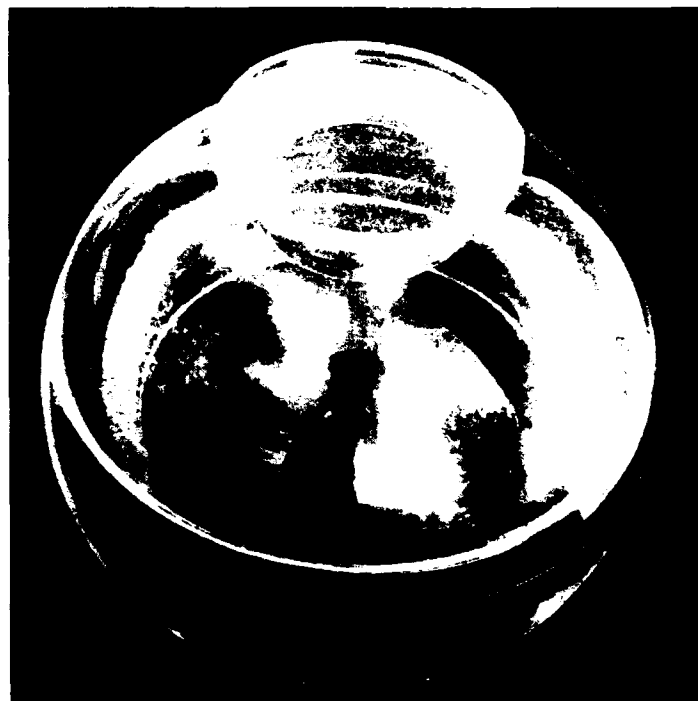
Figure 23. Typical 6-inch-diameter acrylic sphere for models 1 through 8 with an acrylic plug hatch inserted into the conical penetration.

Figure 24. The 18-inch-diameter Model AA after instrumentation with strain gages.
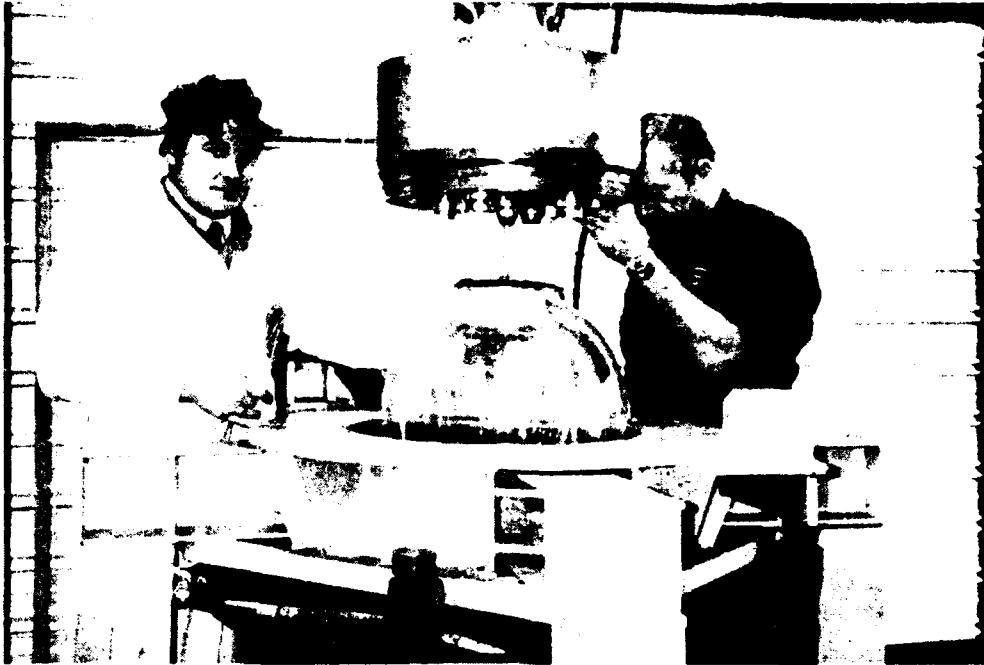
Figure 25. Model AA during placement into the pressure vessel for hydrostatic testing at the Naval Civil Engineering Laboratory Deep Ocean Simulation Facility. Note the pipe connecting the hatch plate to the vessel end closure. The pipe vents the interior of the acrylic sphere and also serves as a pressure-tight conduit for instrumentation wires.
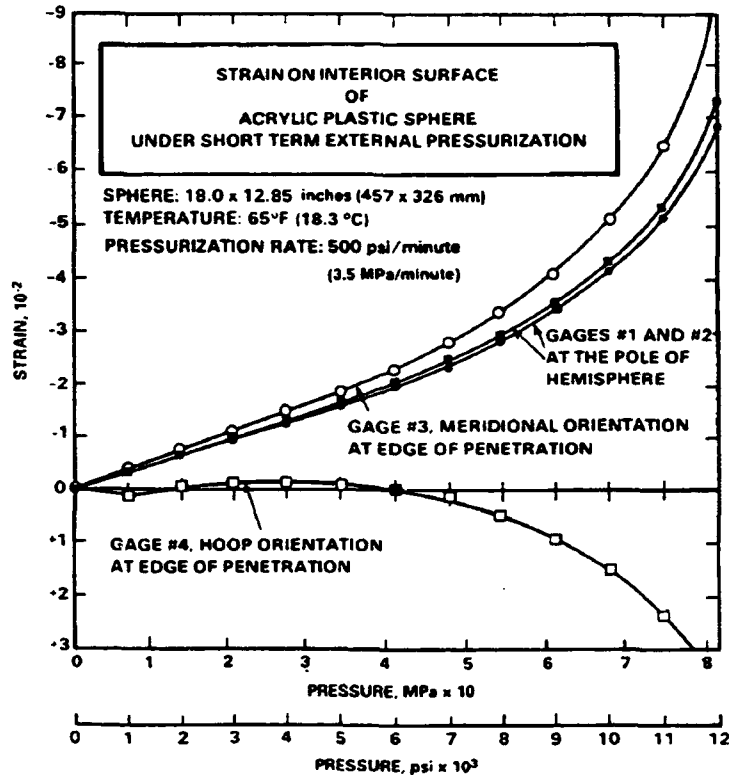
Figure 26. Compressive strain on the interior of Model AA during short-term pressurization.

39
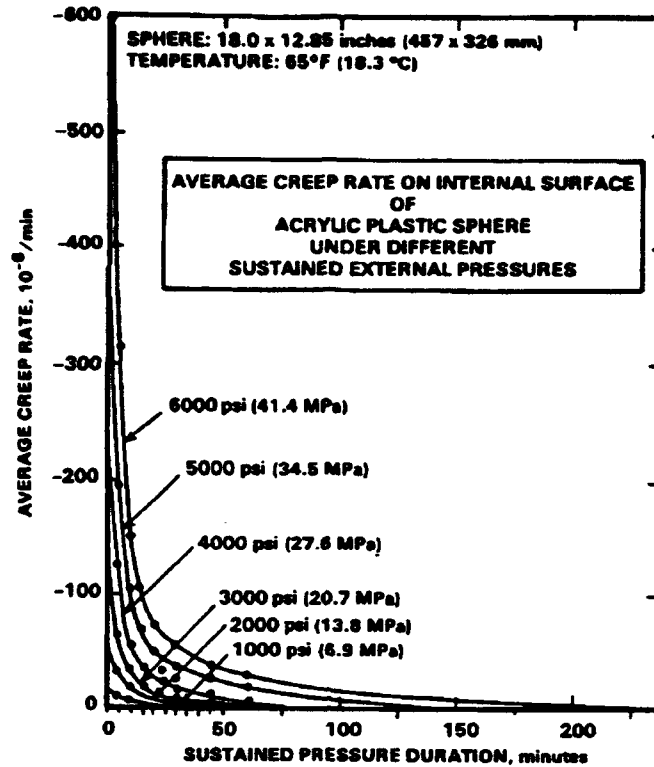
Figure 27. Average creep rate on the interior surface of Model AA as a function of sustained loading at different pressure levels.
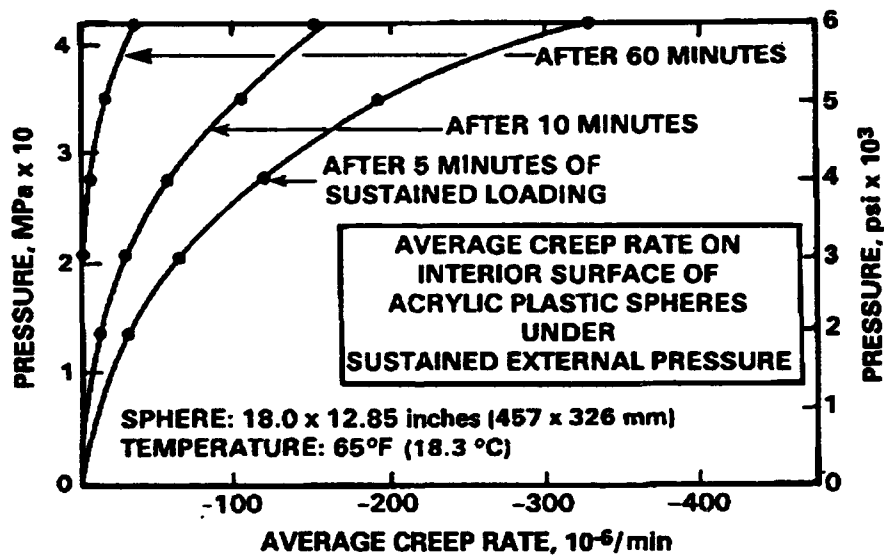
Figure 28. Average creep rate on the interior surface of Model AA as a function of pressure and time measured at various time intervals during sustained loading.

40
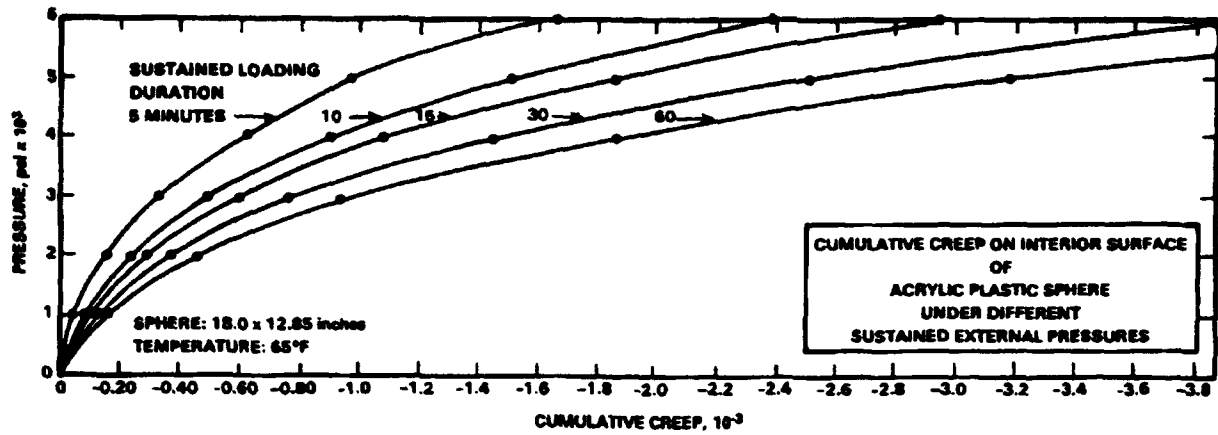
Figure 29. Cumulative creep on the interior surface of Model AA as a function of pressure and sustained loading duration.
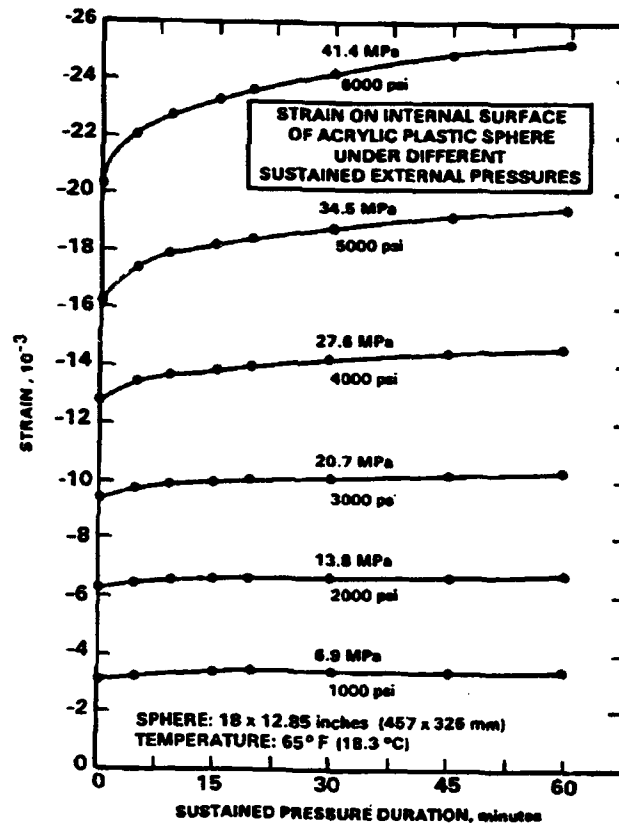
Figure 30. Total strain (short-term strain plus cumulative creep) on the interior surface of Model AA as a function of sustained pressure and duration of loading.

41
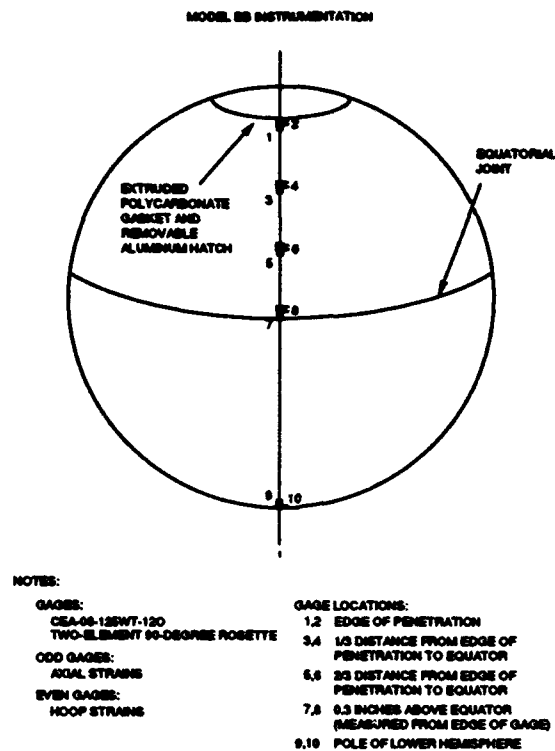
Figure 31. Location of strain gages on the interior surface
of Model BB.
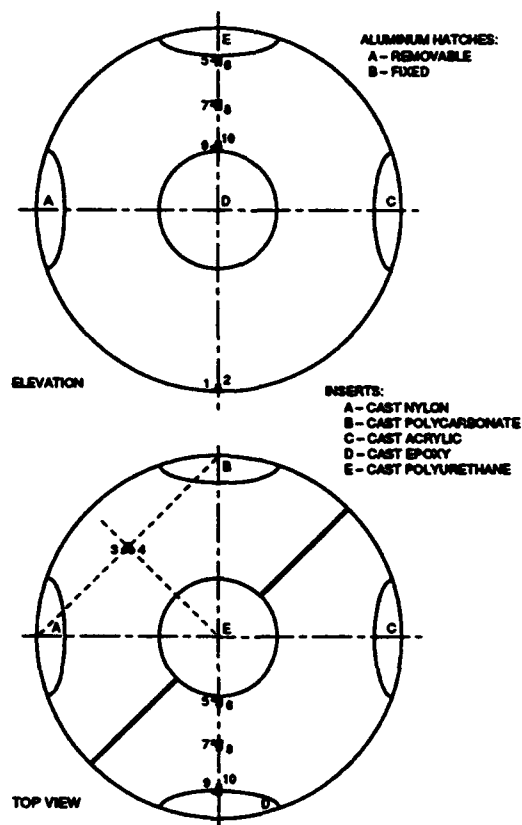
Figure 32. Location of strain gages on the interior
surface of Model CC.

Figure 33. Bonding of strain gages to the interior of Model BB.

Figure 34. Model BB after instrumentation with strain gages.
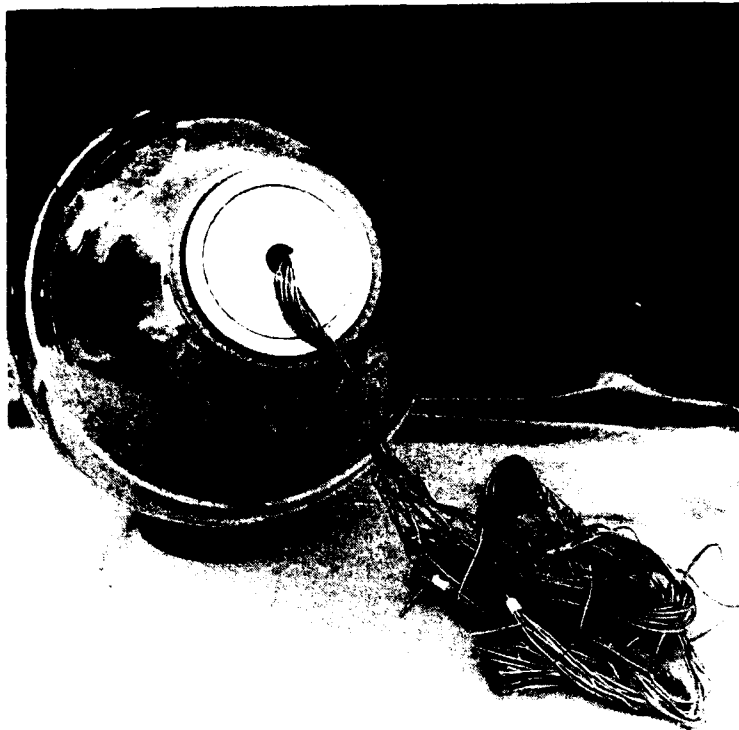
Figure 35. Instrumented Model BB after installation of removable hatch.

Figure 36. Instrumented Model CC after installation of a single removable and four fixed hatches.

Figure 37. Test arrangement for Models BB and CC inside the pressure vessel of HBOI Deep Ocean Simulation Facility. Note the tubing between the hatch place on Model BB and the vessel end closure for venting of the sphere's interior.
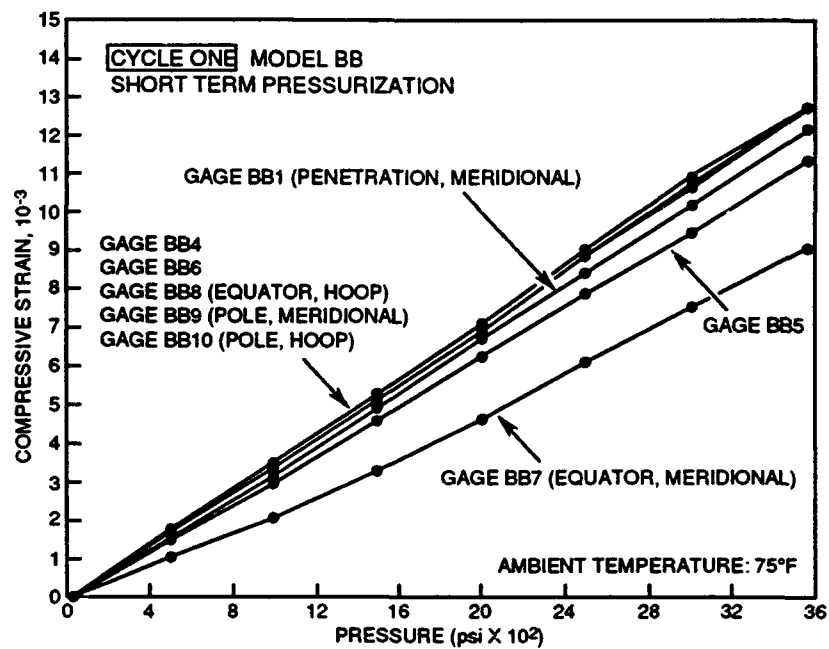
Figure 38. Strains during short-term pressurization; Cycle 1, Model BB.

45
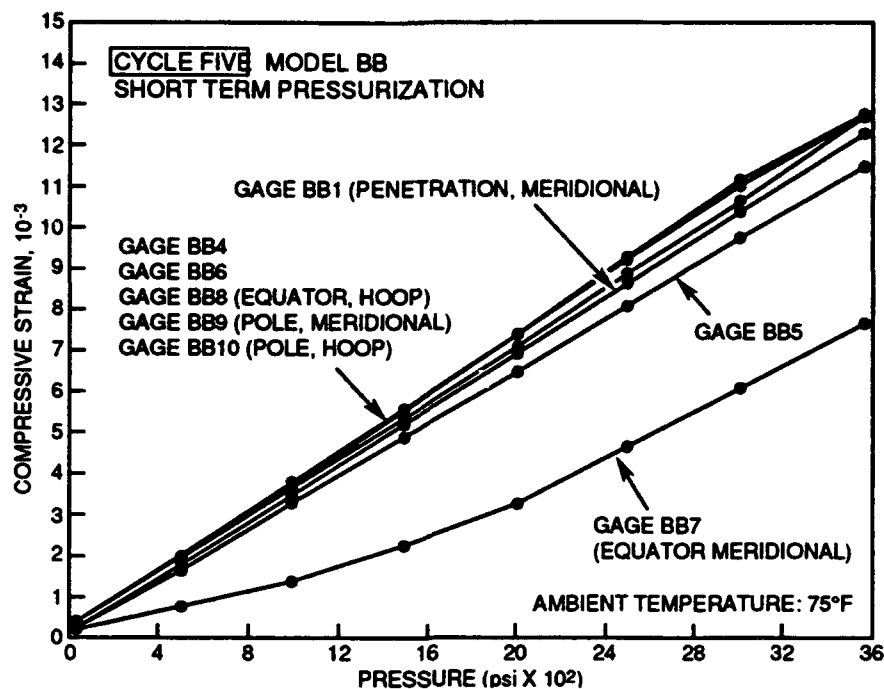
Figure 39. Strains during short-term pressurization; Cycle 5, Model BB.
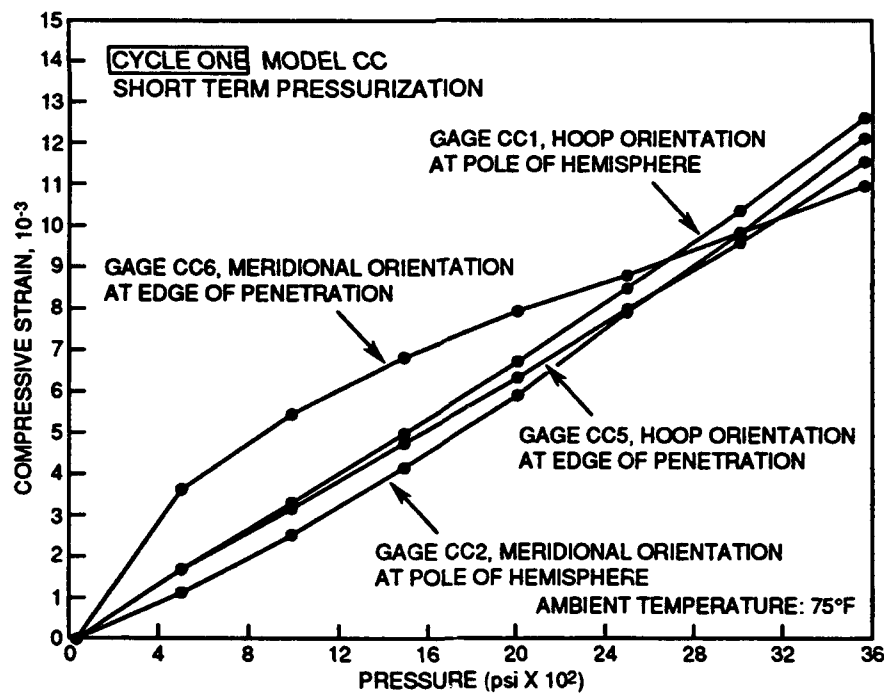
Figure 40. Strains during short-term pressurization; Cycle 1, Model CC.
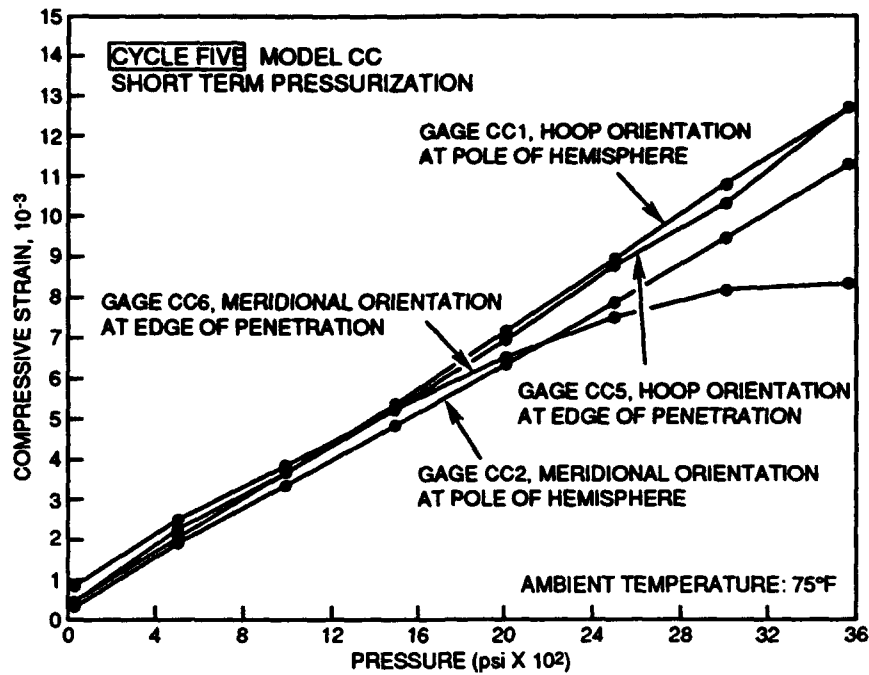
Figure 41. Strains during short-term pressurization; Cycle 5, Model CC.
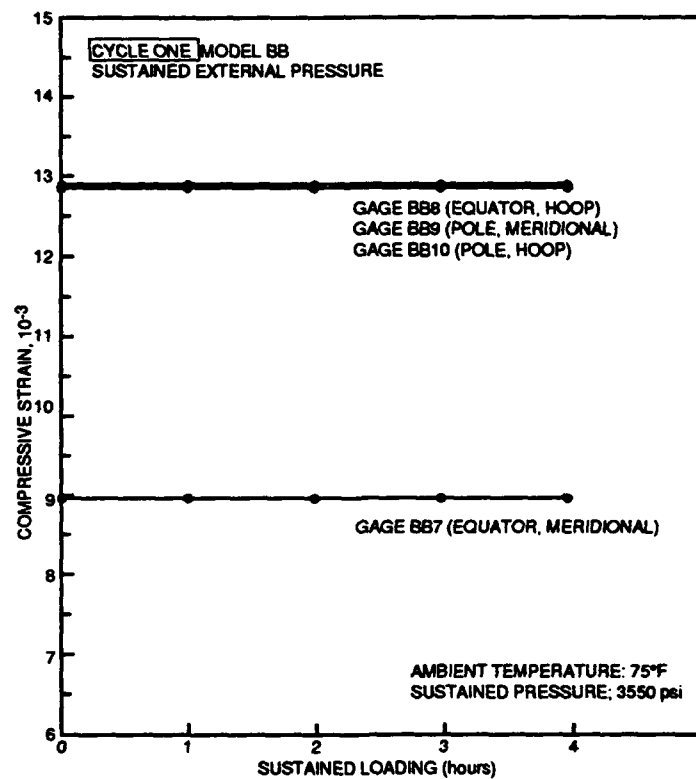
Figure 42. Strains during sustained pressurization; Cycle 1, Model BB.
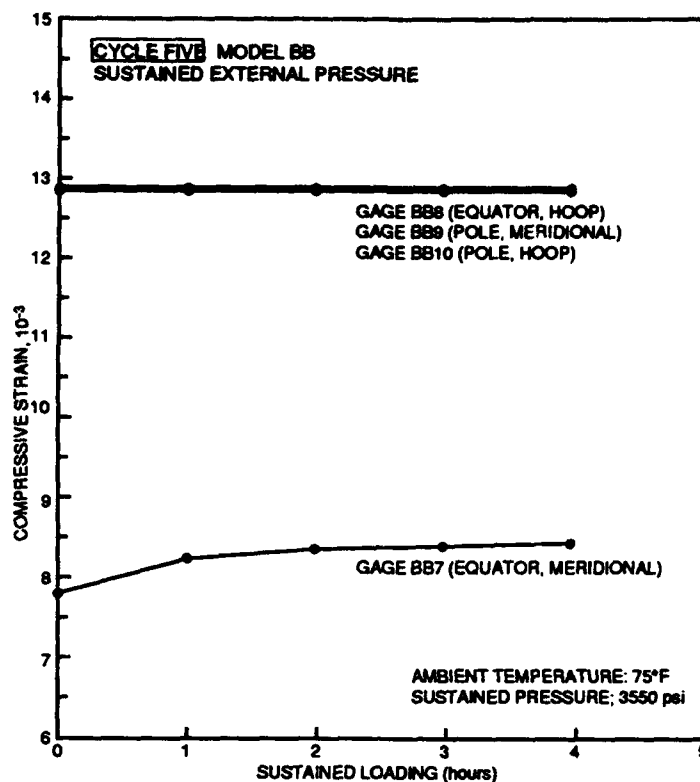
Figure 43. Strains during sustained pressurization; Cycle 5, Model BB.
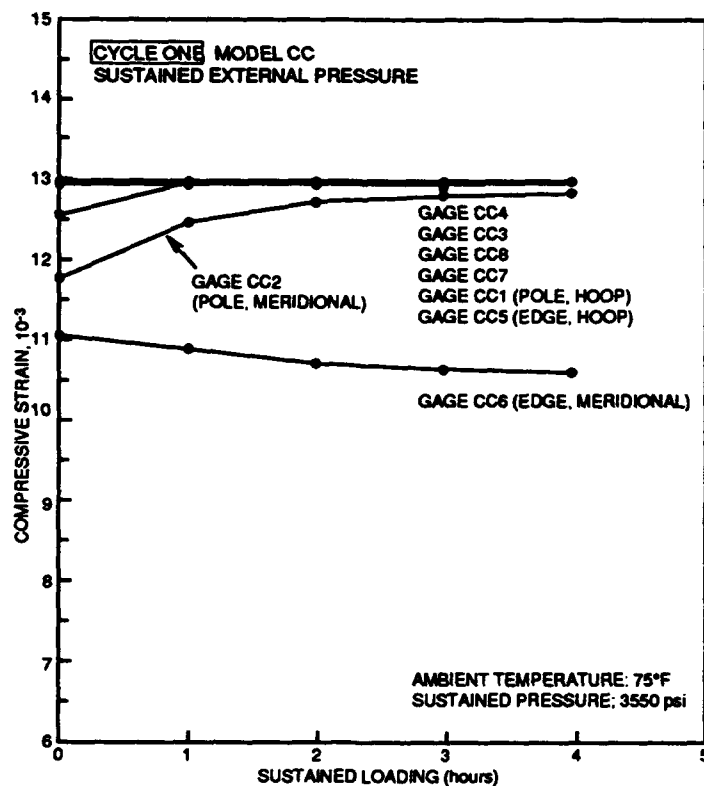
Figure 44. Strains during sustained pressurization; Cycle 1, Model CC.
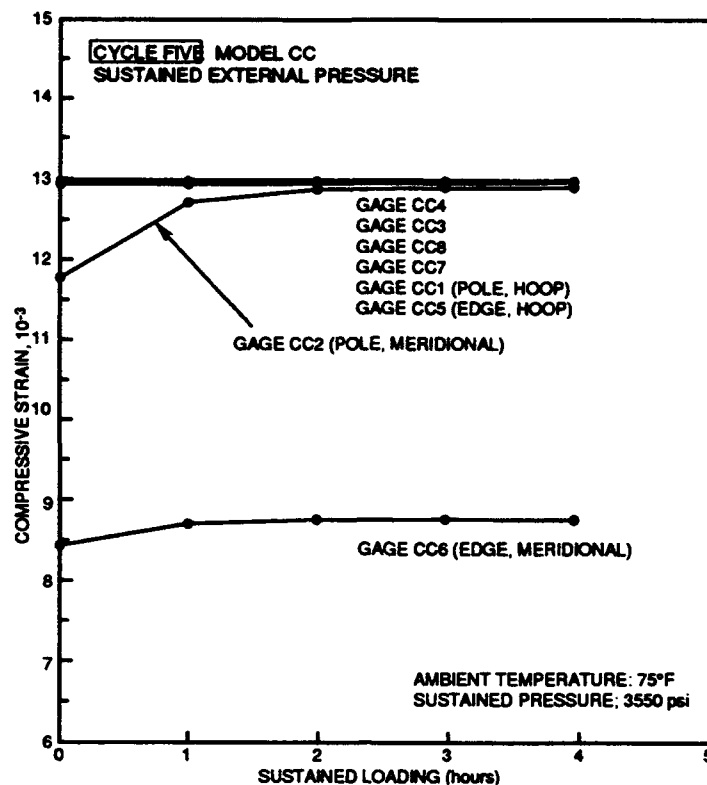
Figure 45. Strains during sustained pressurization; Cycle 5, Model CC.
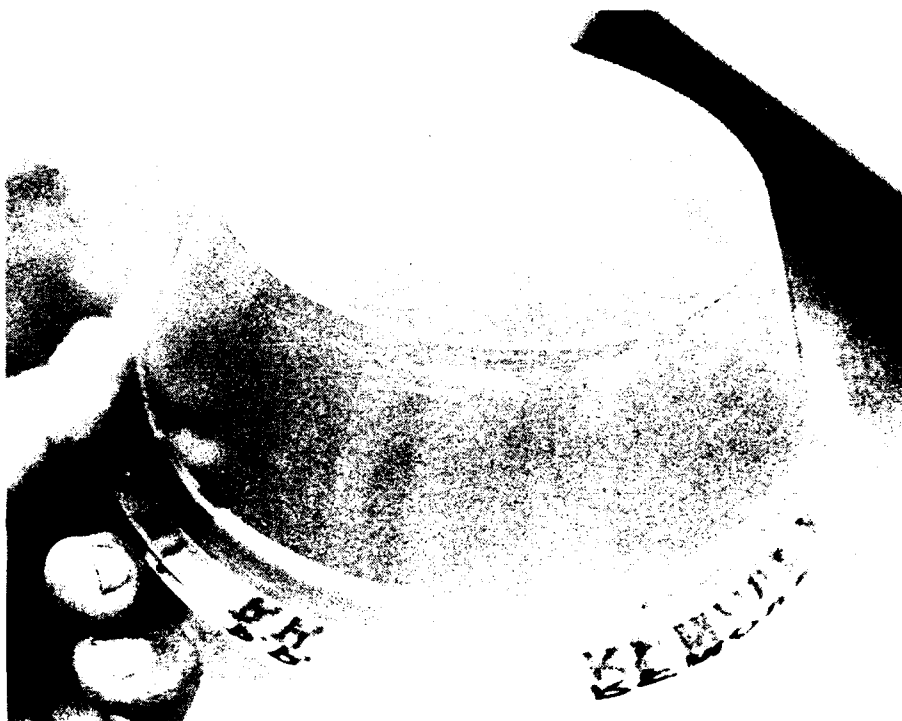
Figure 46. Polycarbonate bearing gasket from Model BB after 180 pressure cycles. Note the deep circumferential crack at location corresponding to O-ring groove in the hatch ring.

49

Figure 47. Penetration in Model BB after 180 pressure cycles. Note the single shear crack on the bearing surface. Subsequent to inspection, Model BB was taken out of service because of bond separation in the equatorial joint. A brand-new acrylic sphere replaced the one with a separated joint and was subsequently inspected at the 435th and 1,000th cycles.

Figure 48. Cast epoxy bearing gasket from Model CC after 435 pressure cycles.
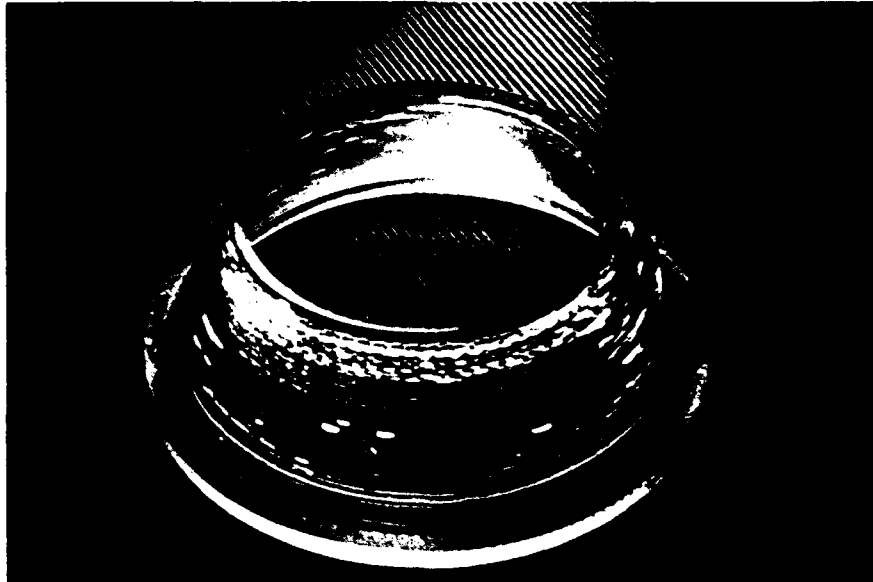
Figure 49. Cast polycarbonate bearing gasket from Model CC after 435 pressure cycles.
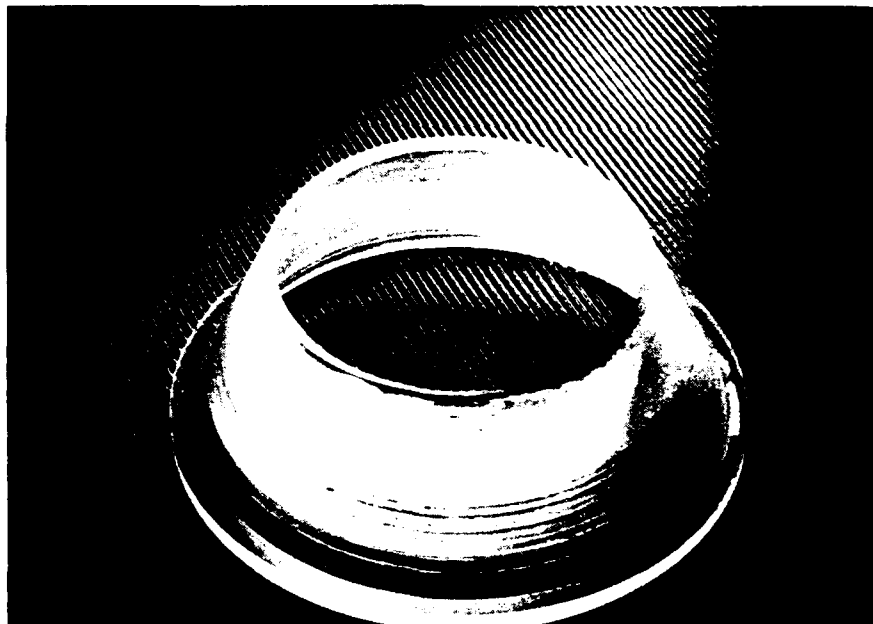
Figure 50. Cast acrylic bearing gasket from Model CC after 435 pressure cycles.

Figure 51. Cast polyurethane bearing gasket from Model CC after 435 pressure cycles.

Figure 52. Cast nylon bearing gasket from Model CC after 435 pressure cycles.

Figure 53. Extruded polycarbonate bearing gasket from Model BB. The gasket was installed at the 180th cycle and removed at the 435th pressure cycle.

Figure 54. Penetration C in Model CC after removal of cast acrylic bearing gasket upon completion of 435 pressure cycles.

Figure 55. Penetration D in Model CC after removal of cast epoxy bearing gasket upon completion of 435 pressure cycles.

Figure 56. Penetration A in Model CC after removal of cast nylon bearing gasket upon completion of 435 pressure cycles.
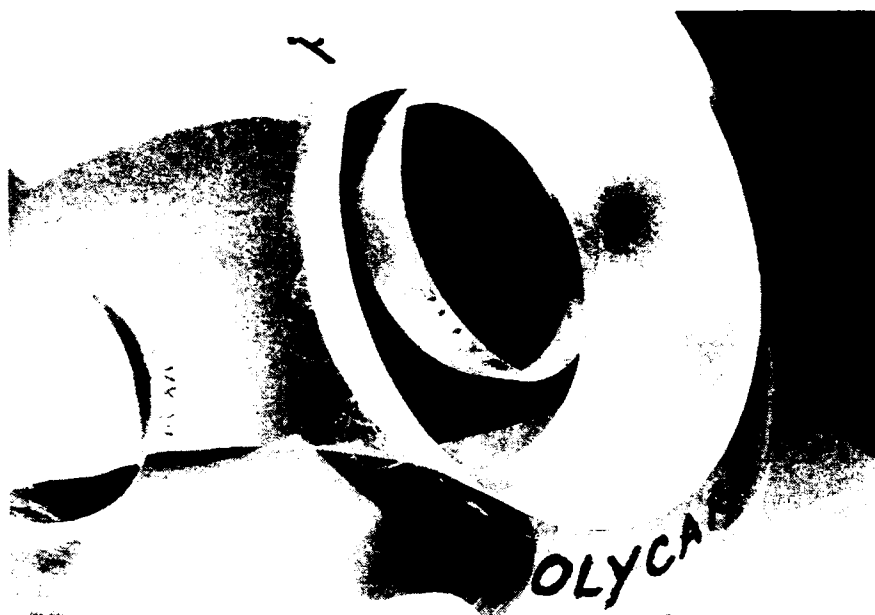
Figure 57. Penetration B in Model CC after removal of cast polycarbonate gasket upon completion of 435 pressure cycles.

Figure 58. Penetration E in Model CC after removal of cast polyurethane gasket upon completion of 435 pressure cycles.
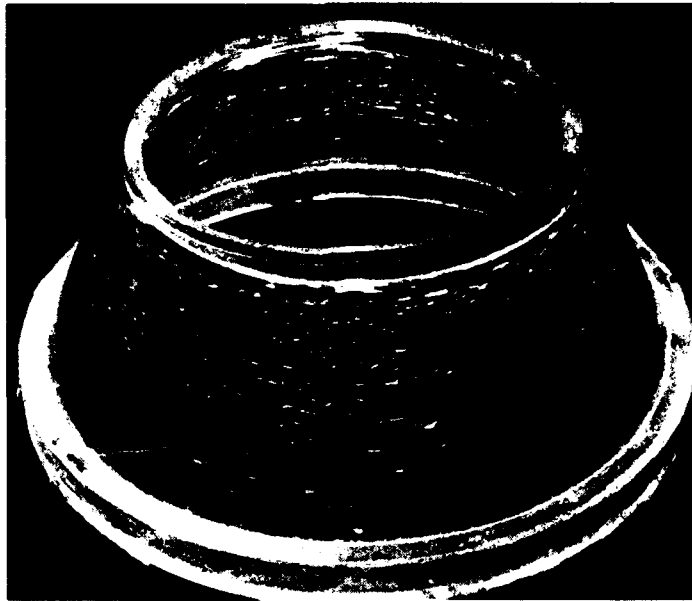
Figure 59. Cast polyurethane bearing gasket from penetration E
in Model CC after a total of 1,000 pressure cycles.
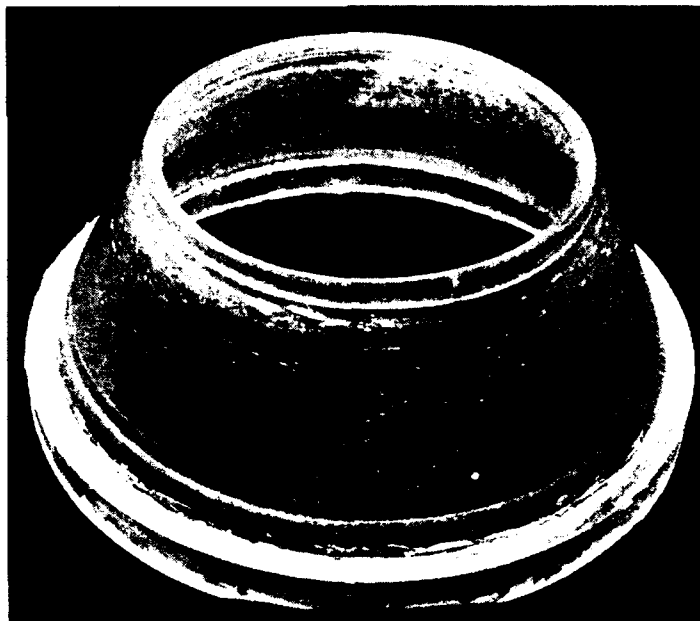
Figure 60. Cast Polyurethane bearing gasket from
penetration B in Model CC after total of 565 pressure cycles
(installed at 435th and removed at 1,000th cycle).
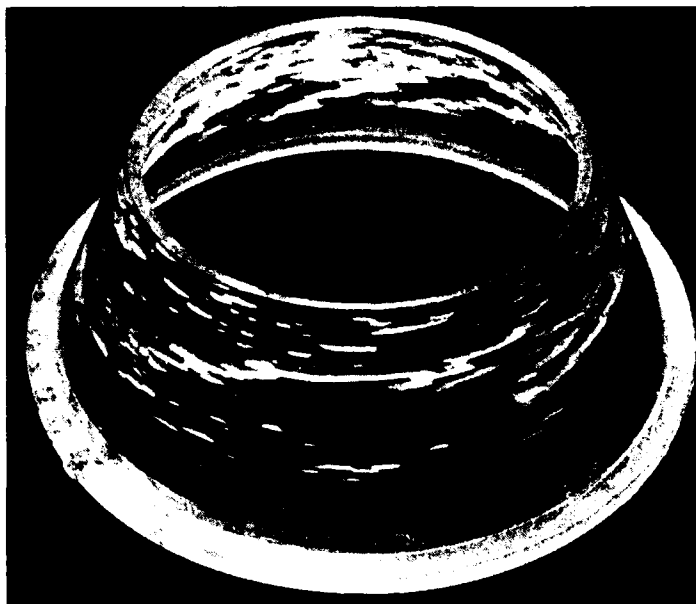
Figure 61. Cast polycarbonate bearing gasket from penetration
D in Model CC after a total of 565 pressure cycles (installed at
435th and removed at 1,000th cycle).
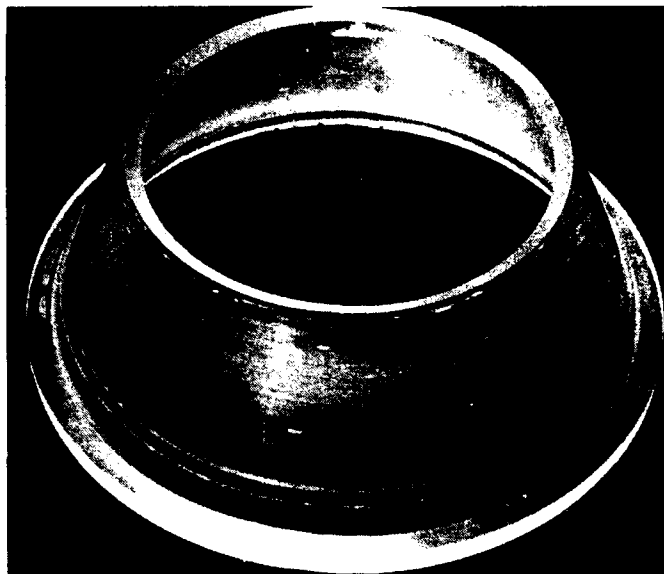
Figure 62. Cast acrylic bearing gasket from penetration C in
Model CC after a total of 565 pressure cycles (installed at
435th and removed at 1,000th cycle).

57
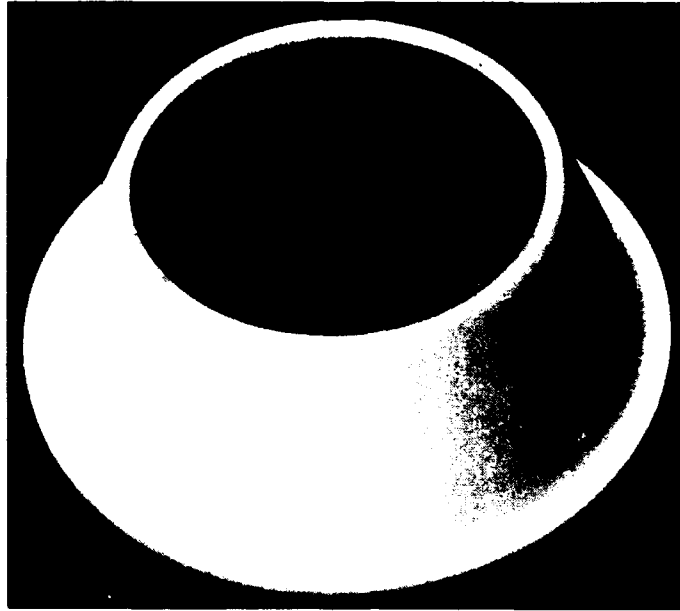
Figure 63. <u>Cast nylon</u> bearing gasket from penetration A in Model CC after a total of 1,000 pressure cycles.
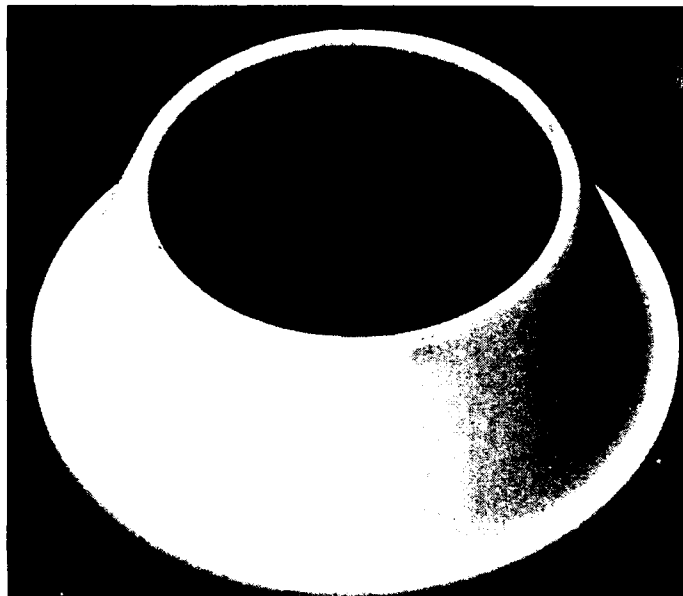
Figure 64. <u>Cast nylon</u> bearing gasket from penetration in Model BB after a total of 565 pressure cycles (installed at 435th and removed at 1,000th cycle).

Figure 65. Extruded circumferential land on the interior conical surface of <u>cast polycarbonate</u> bearing gasket contacting the O-ring groove in the metallic hatch plate. Photographed after 500 pressure cycles.

Figure 66. Visual inspection of Model CC after 1,000 pressure cycles performed by Dr. Stachiw at HBOI.

59

Figure 67. Visual inspection of Model BB after 1,000 pressure cycles.
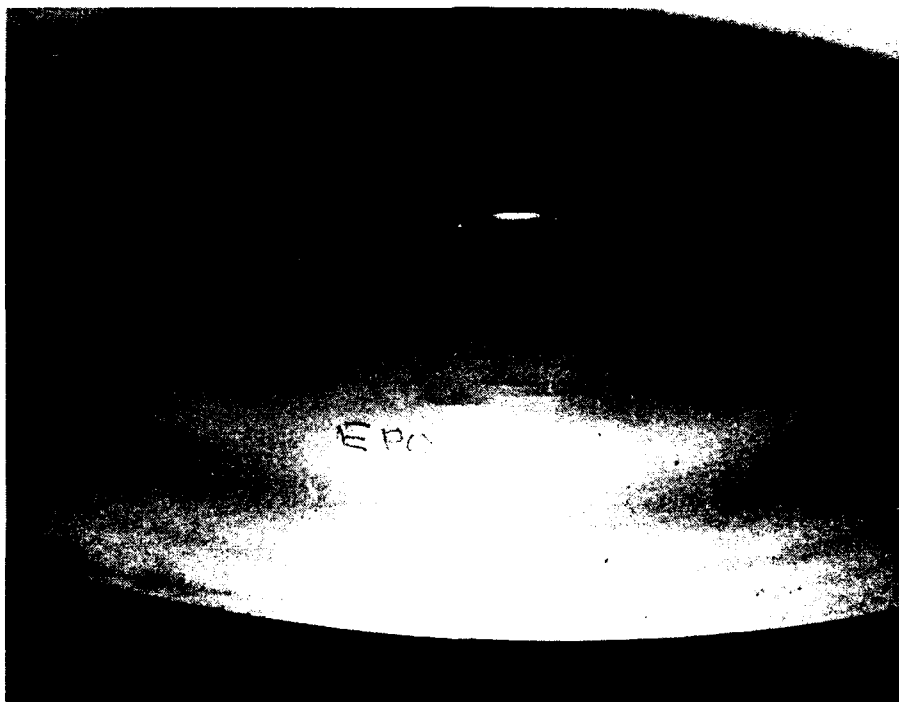
Figure 68. Penetration D in Model CC after 1,000 pressure cycles (435 cycles with cast epoxy and 565 cycles with cast polycarbonate bearing gaskets.
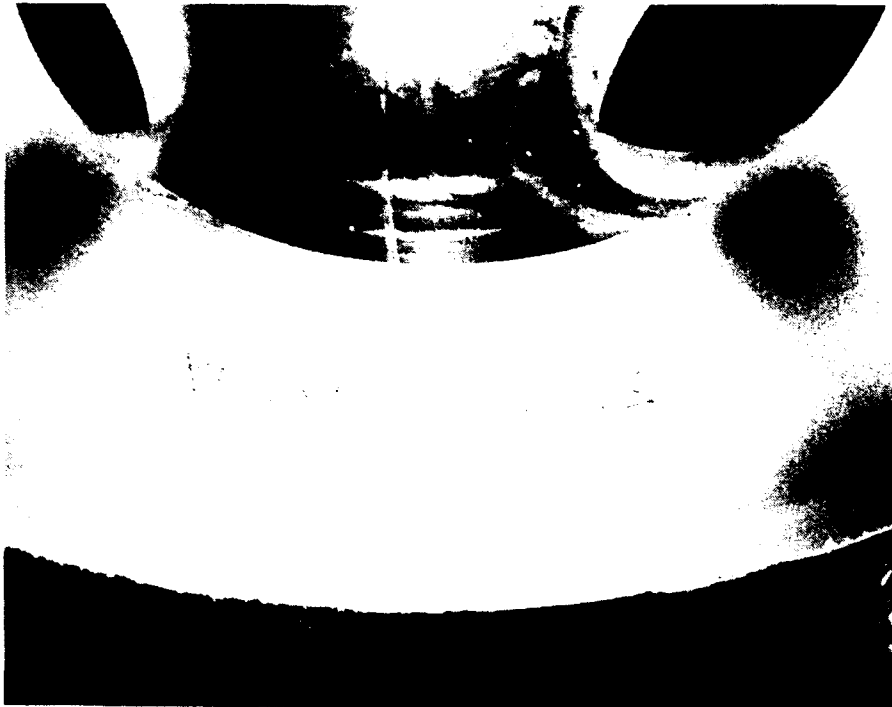
Figure 69. Penetration E in Model CC after 1,000 pressure cycles with cast polyurethane bearing gasket.

Figure 70. Penetration B in Model CC after 1,000 pressure cycles (435 cycles with cast polycarbonate and ' '5 cycles with cast polyurethane bearing gaskets.

Figure 71. Penetration C in Model CC after 1,000 pressure cycles with acrylic
bearing gasket.
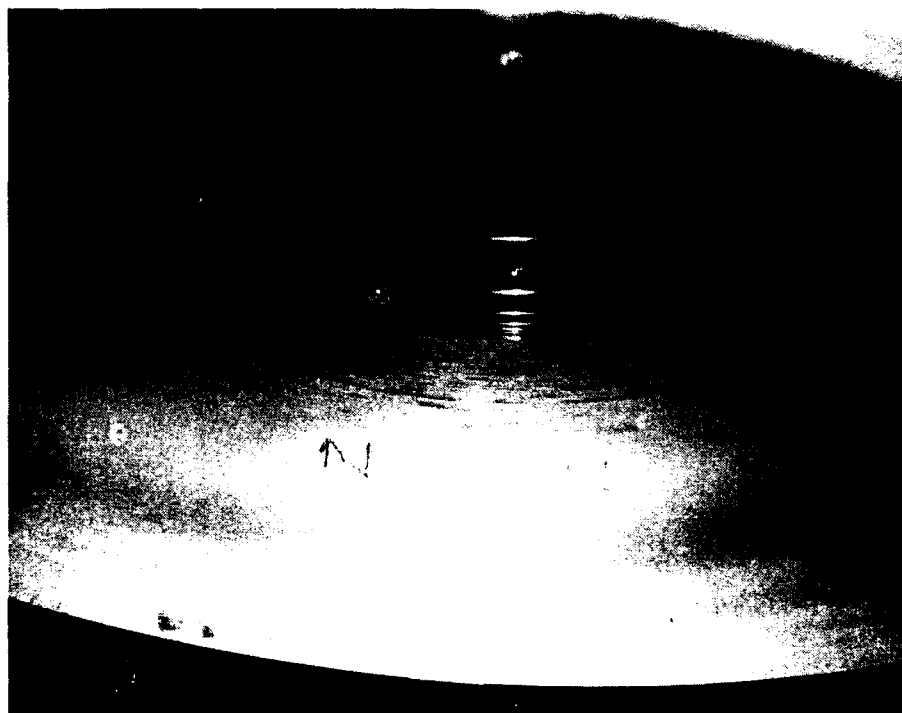
Figure 72. Penetration A in Model CC after 1,000 pressure cycles with cast nylon
bearing gasket.

Figure 73. Penetration in Model BB after 1,000 pressure cycles (435 cycles with polycarbonate and 565 cycles with nylon bearing gasket.
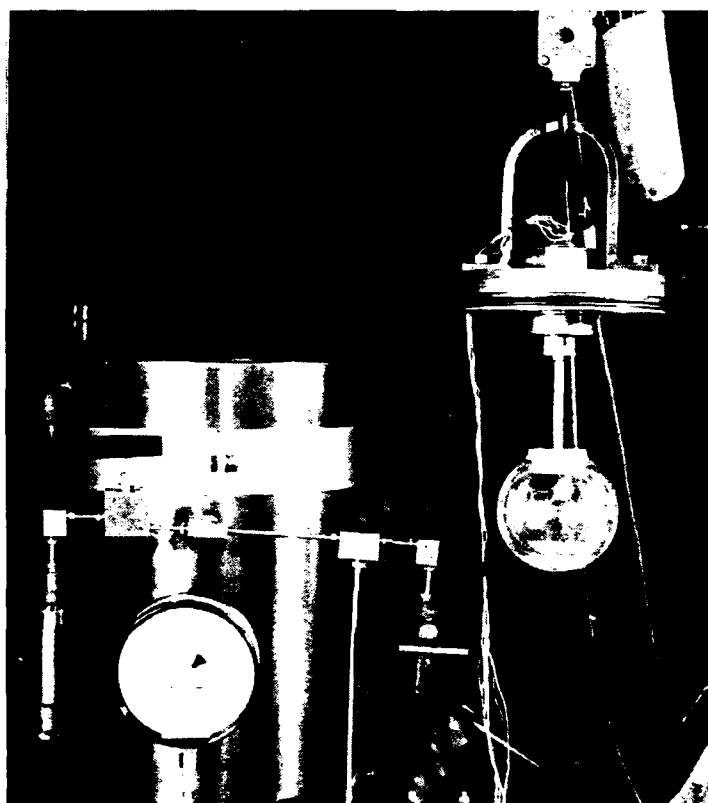
Figure 74. Test arrangement for long-term pressure testing of Models 6A and 6B.

63
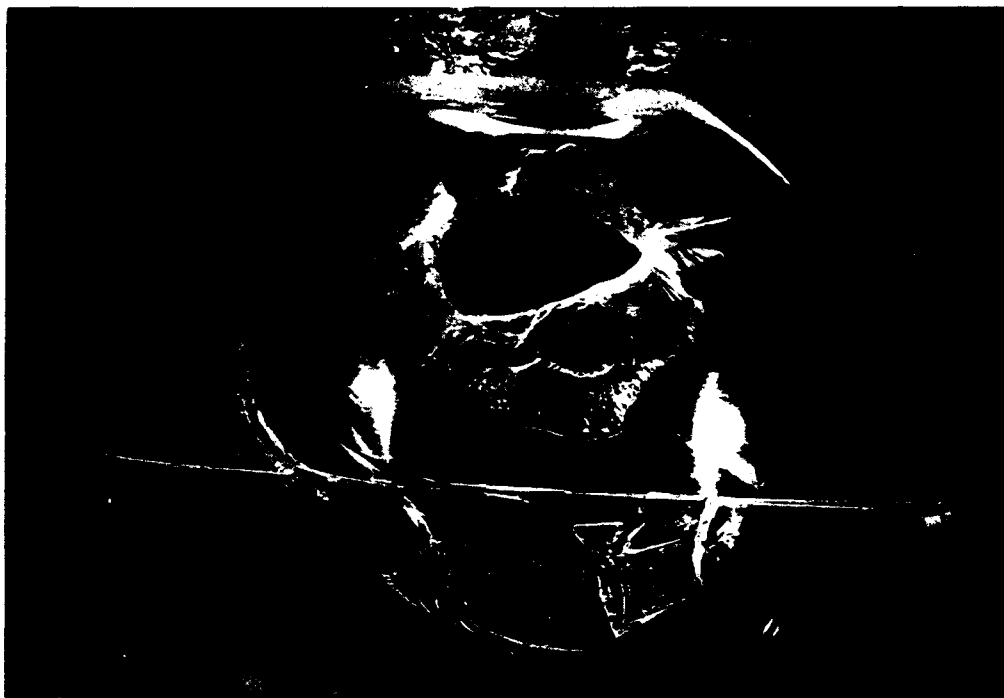
Figure 75. Local plastic buckling of Model 1 following 120 pressure cycles to 3,560 psi at 75° F.
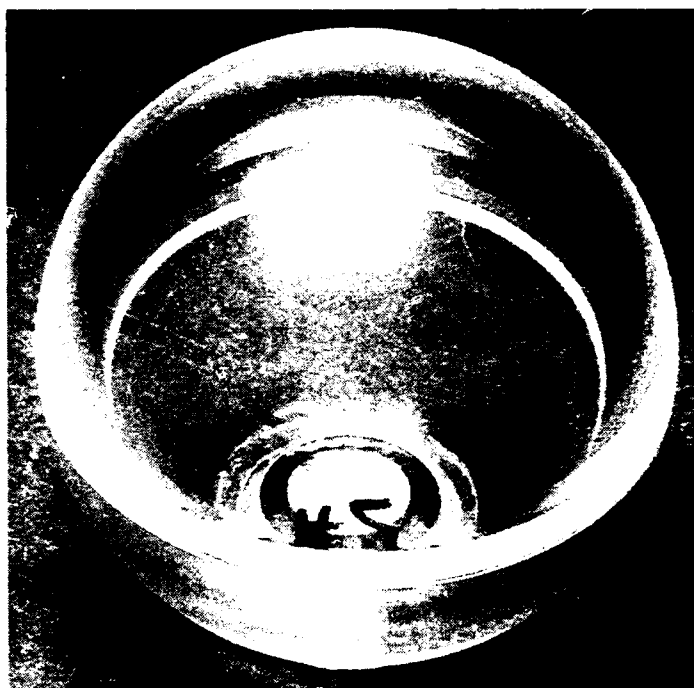
Figure 76. Model 2 after 1,000 pressure cycles to 3,560 psi at 75° F. Models 3,4,5,6,7, and 8 also did not show any cracking.
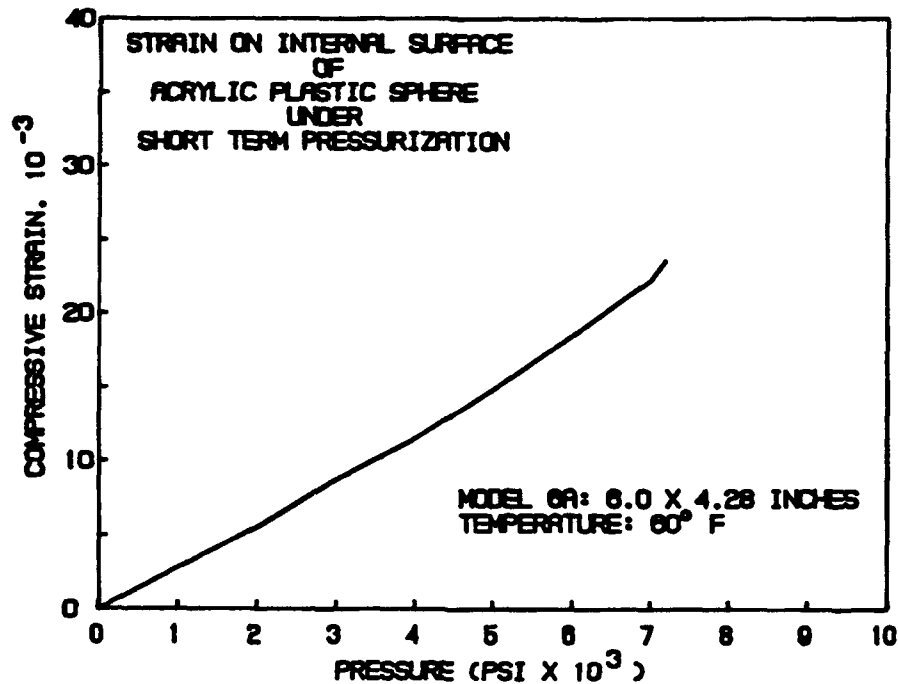
Figure 77. Strain on the interior surface of Model 6A during short-term pressurization to 7,200 psi.
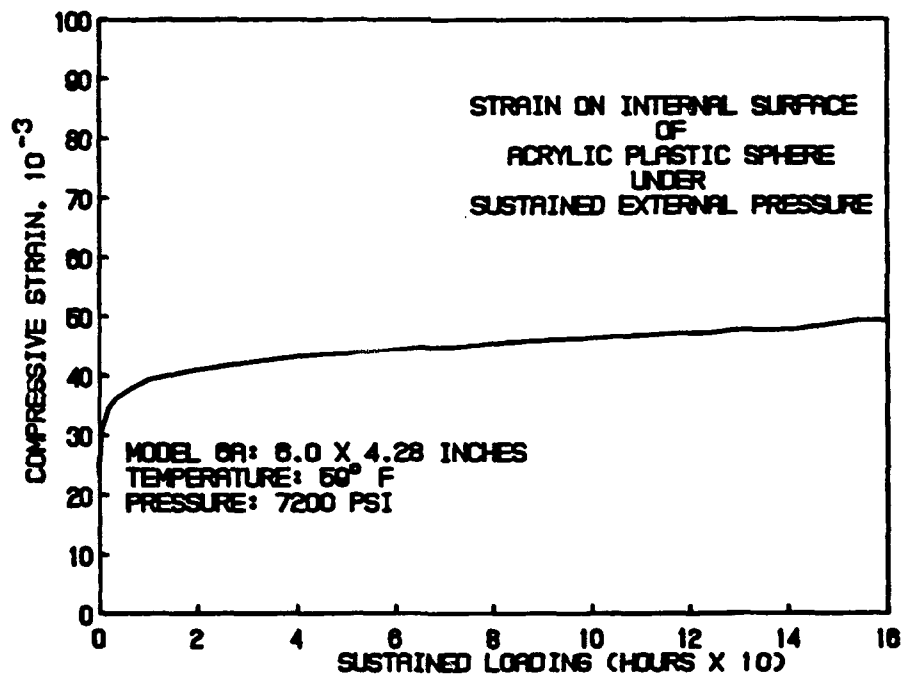
Figure 78. Strain on the interior surface of Model 6A during sustained pressure loading at 7,200 psi.
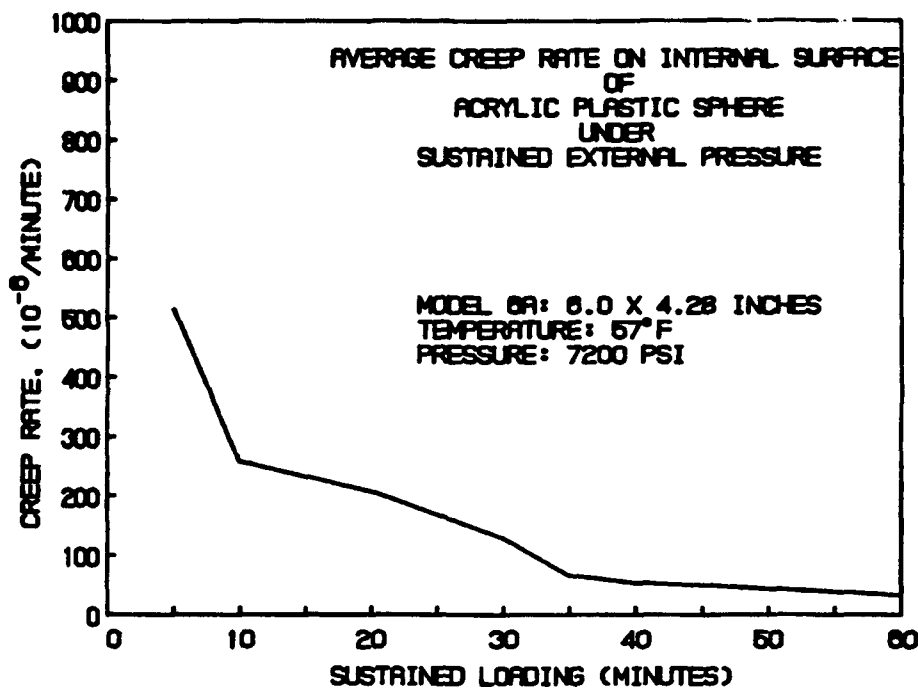
Figure 79. Creep rate on the interior surface of Model 6A during sustained pressure loading at 7,200 psi; 0 to 1 hour's duration interval.
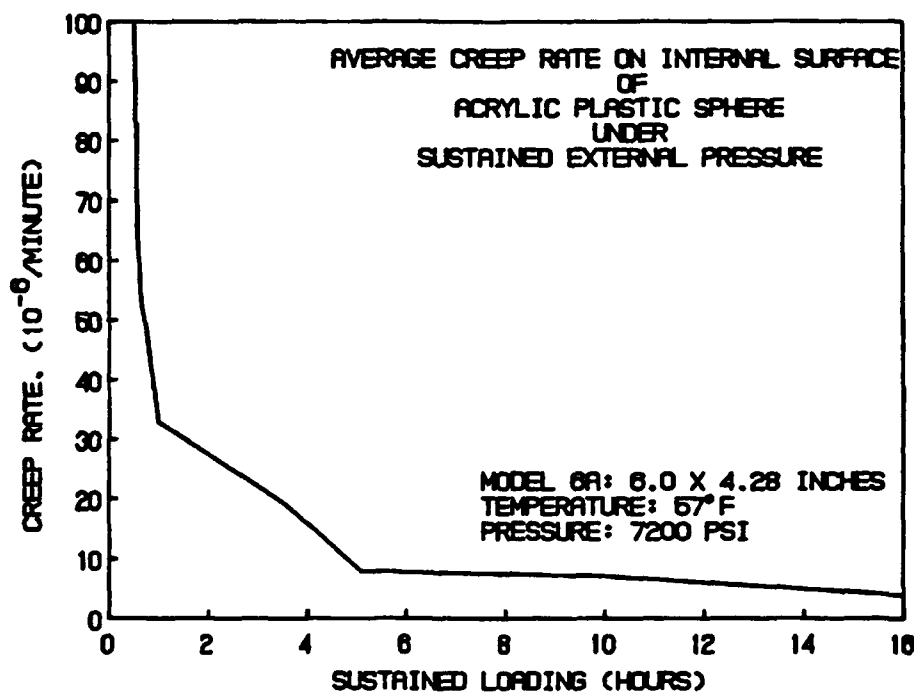
Figure 80. Creep rate on the interior surface of Model 6A during pressure sustained loading at 7,200 psi; 0 to 16 hour's duration interval.
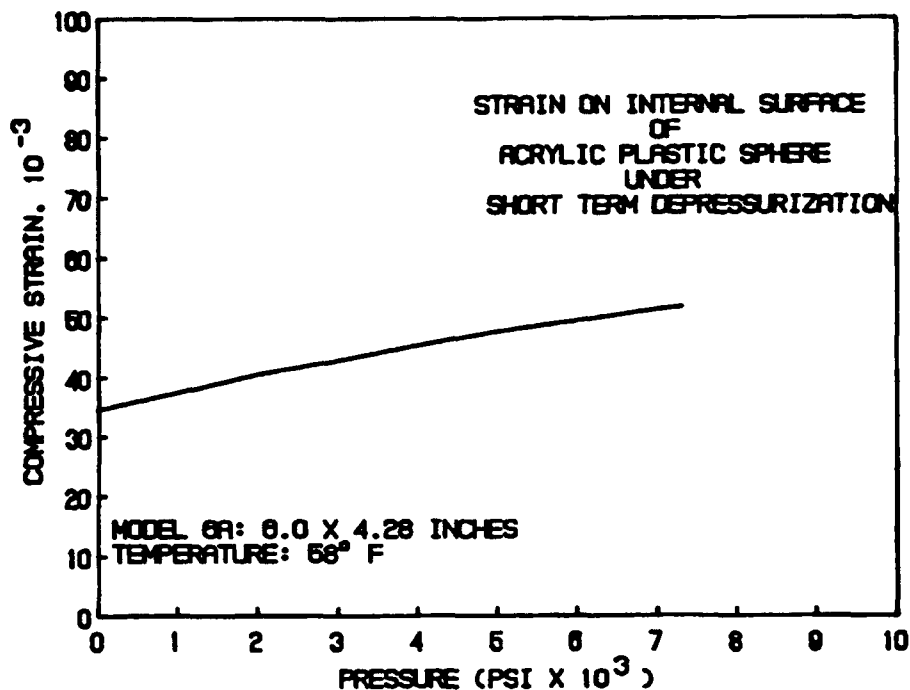
Figure 81. Strain on the interior surface of Model 6A during depressurization after 312 hours of sustained pressure loading to 7,200 psi.
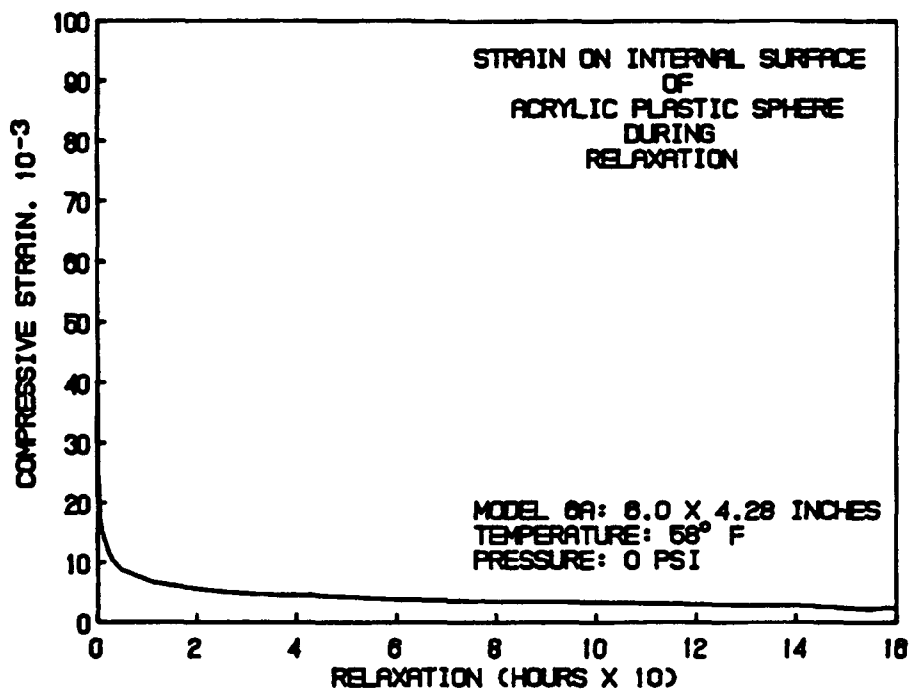
Figure 82. Strain on the interior surface of Model 6A during relaxation after 312 hours of sustained pressure loading at 7,200 psi.
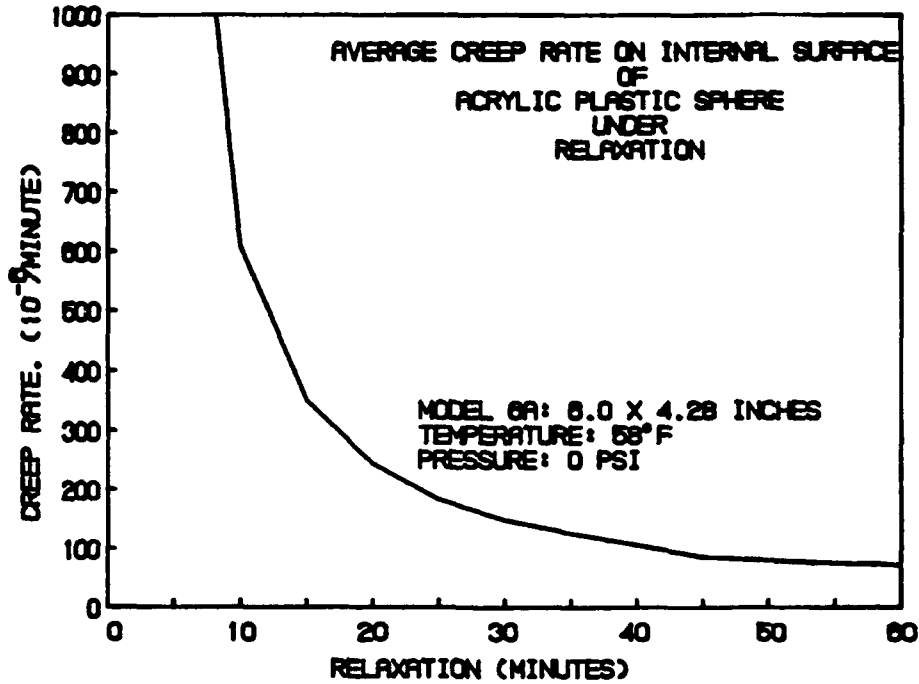
Figure 83. Creep rate on the interior surface of Model 6A during relaxation after 312 hours of sustained pressure loading at 7,200 psi; 0 to 1 hour's duration interval.
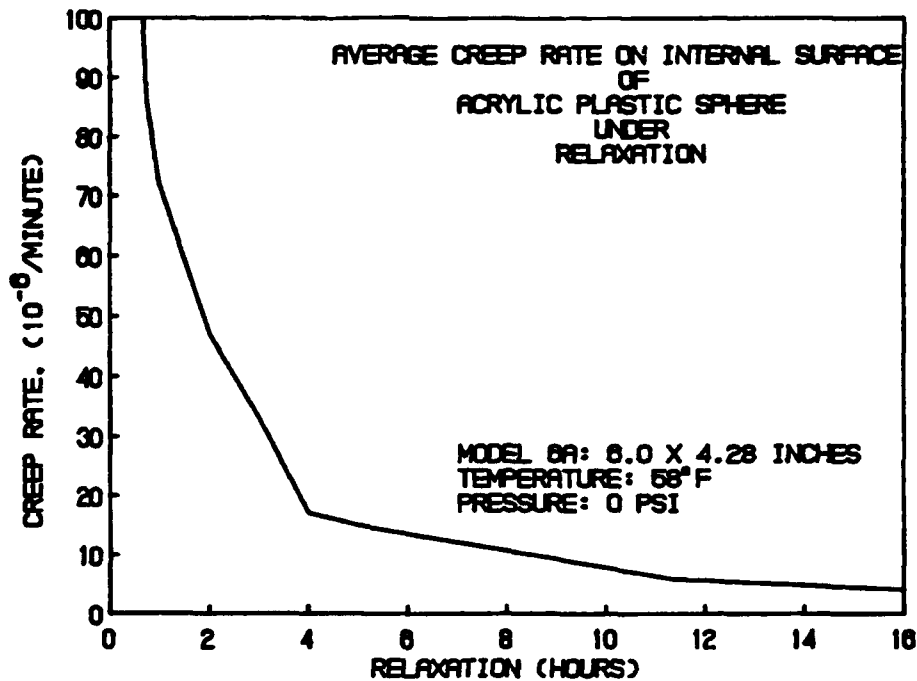
Figure 84. Creep rate on the interior surface of Model 6A during relaxation after 312 hours of sustained pressure loading at 7,200 psi; 0 to 16 hour's duration interval.

68

DELAMINATION AT RELAXATION

VOIDS IN ADHESIVE BOND INTRODUCED DURING BONDING
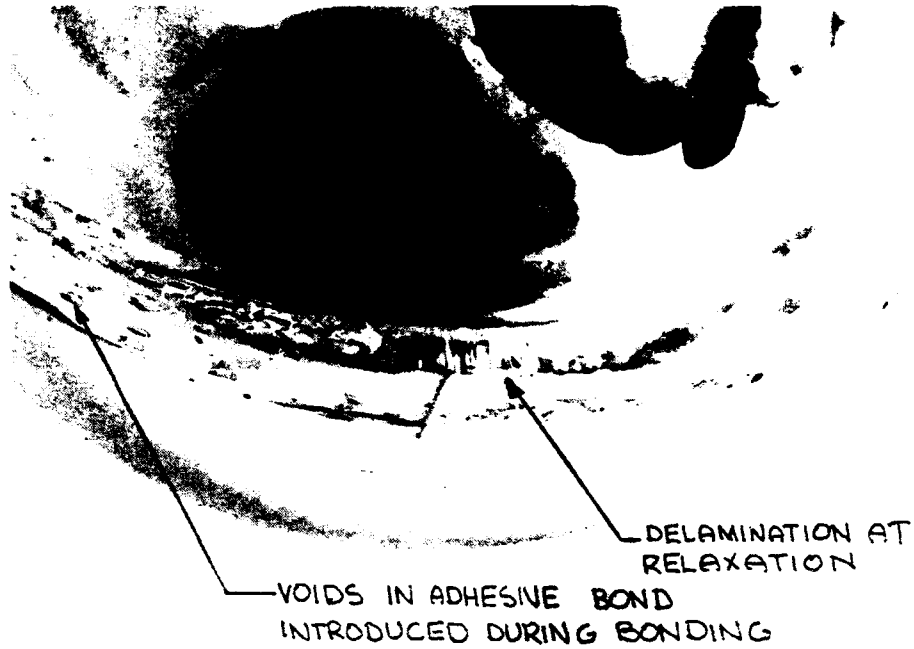
Figure 85. Equatorial joint on Model 6A after 312 hours of sustained pressure loading at 7,200 psi; note the partial delamination.
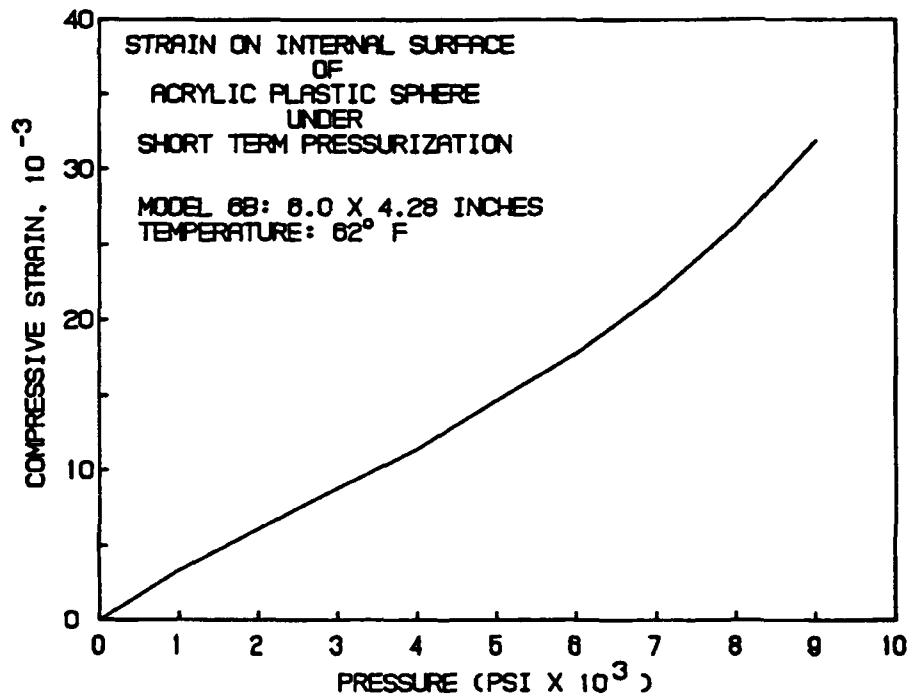
Figure 86. Strain on the interior surface of Model 6B during short-term pressurization to 9,000.
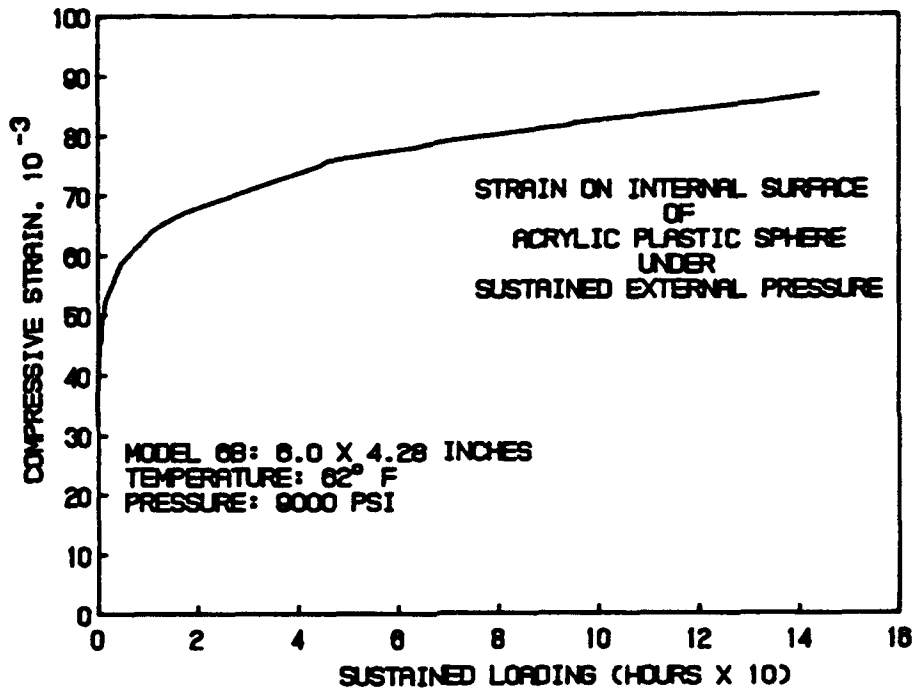
Figure 87. Strain on the interior surface of Model 6B during sustained pressure loading to 9,000 psi.
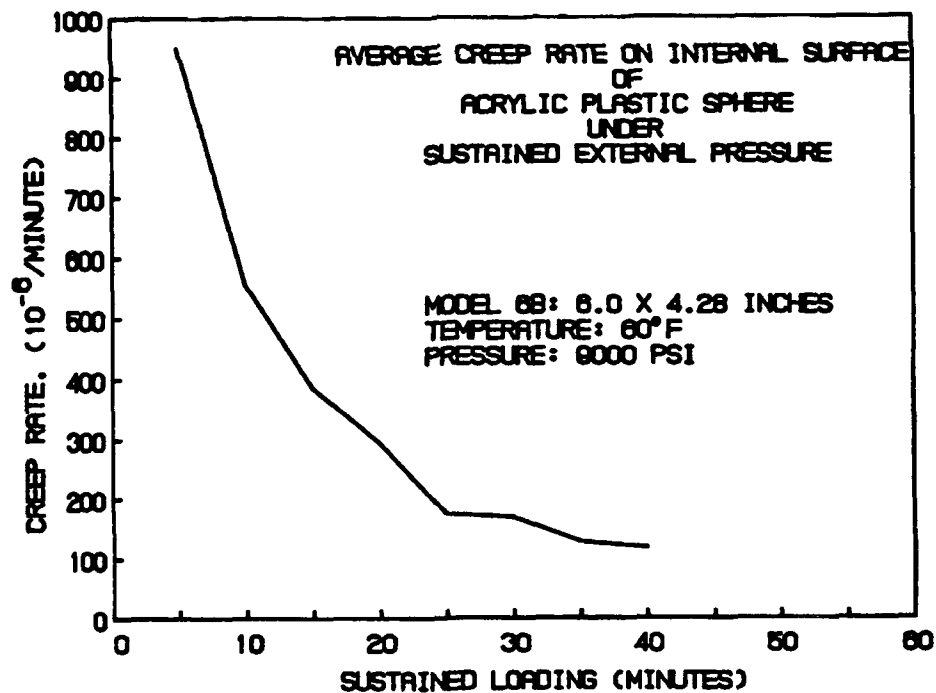
Figure 88. Creep rate on the interior surface of Model 6B during sustained pressure loading at 9,000 psi; 0 to 1 hour's duration interval.
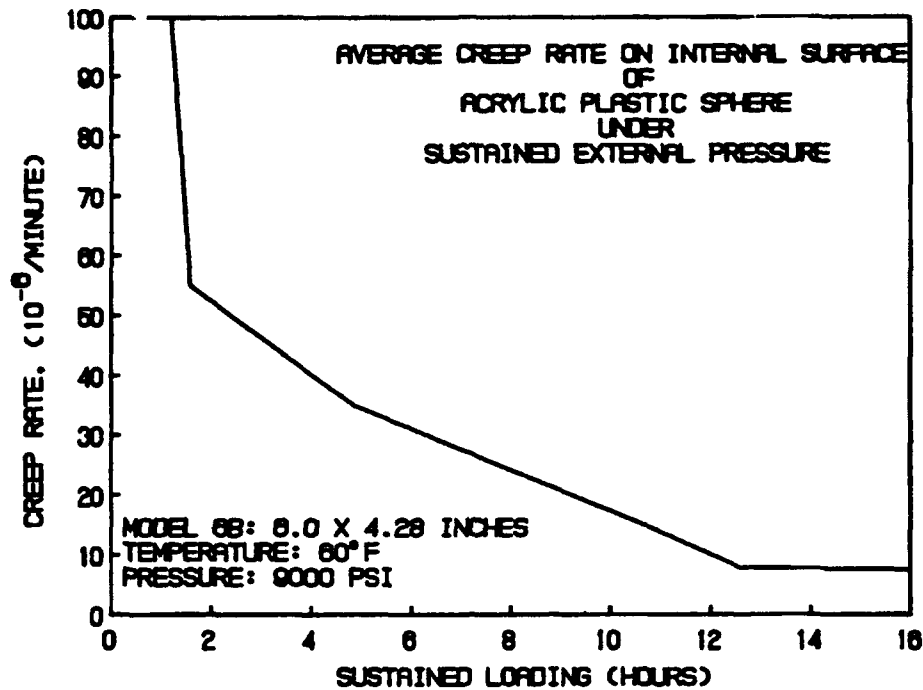
Figure 89. Creep rate on the interior surface of Model 6B during sustained pressure loading to 9,000 psi; 0 to 14 hour's duration interval.
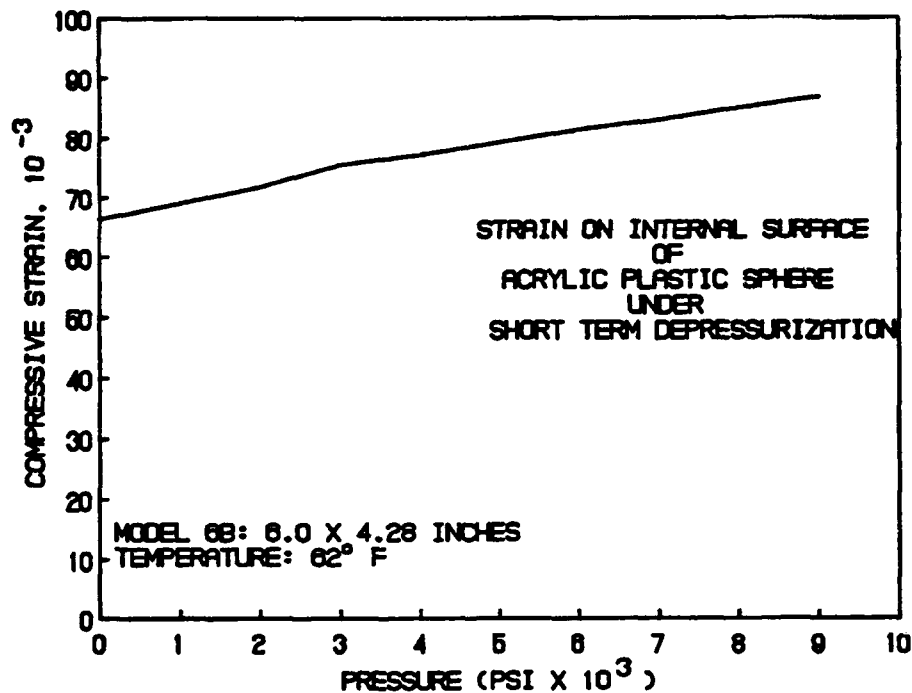
Figure 90. Strain on interior surface of Model 6B during depressurization after 144 hours of sustained pressure loading at 9,000 psi.
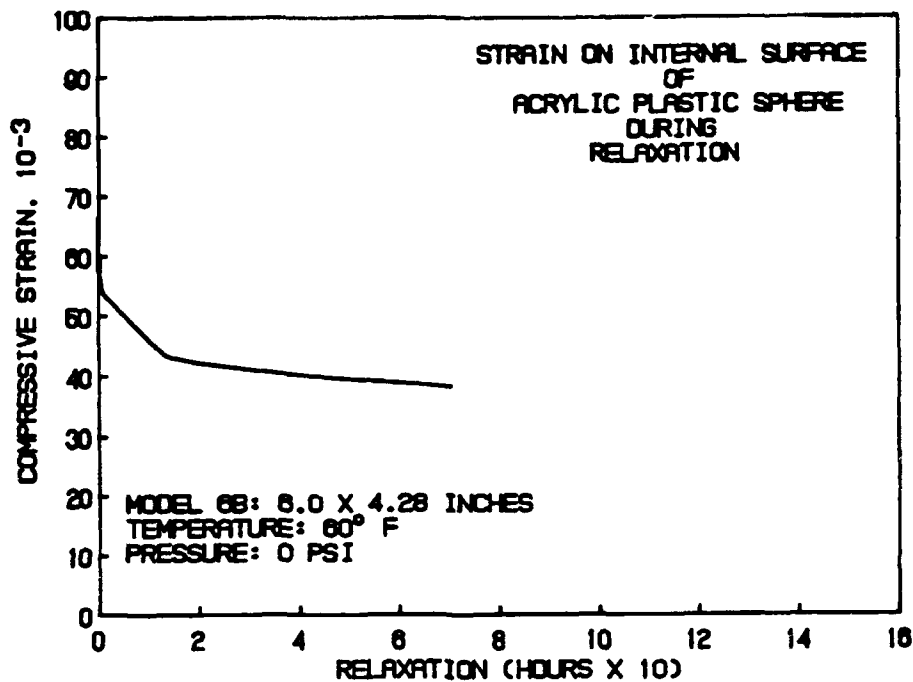
Figure 91. Strain on interior surface of Model 6B during relaxation after 144 hours of sustained pressure loading at 9,000 psi.
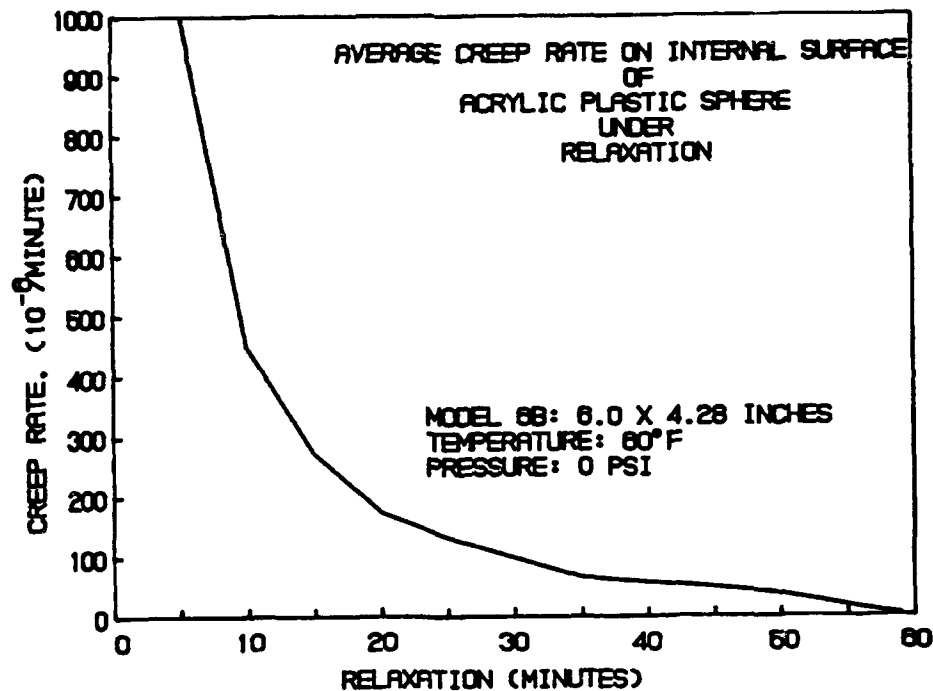
Figure 92. Creep rate on the interior surface of Model 6B during relaxation after 144 hours of sustained pressure loading at 9,000 psi; 0 to 1 hour's duration interval.
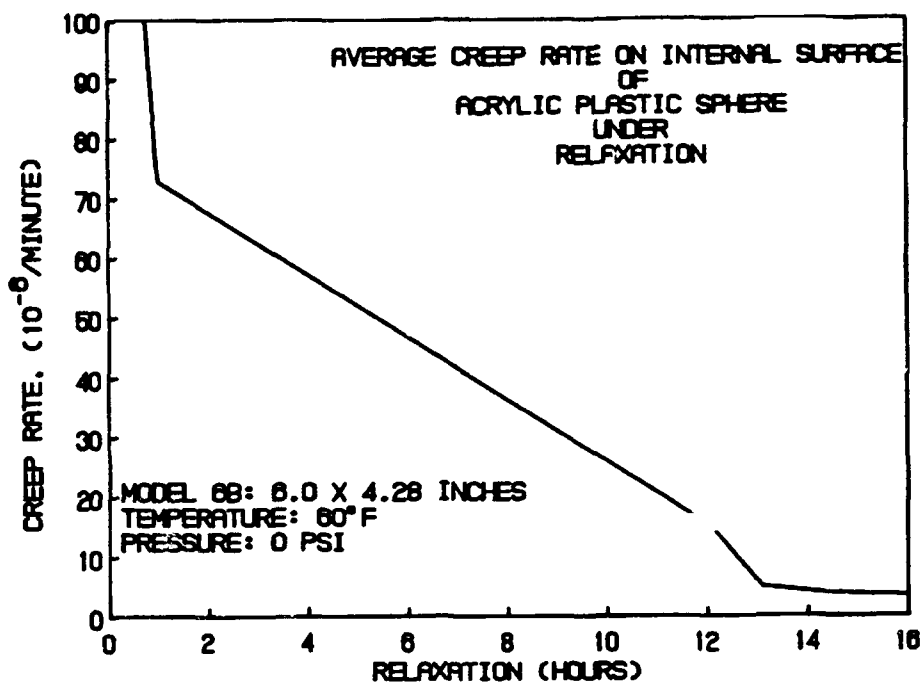
Figure 93. Creep rate on the interior surface of Model 6B during relaxation after 144 hours of sustained pressure loading at 9,000 psi; 0 to 16 hour's duration interval.

Figure 94. Model 6B after 144 hours of sustained pressure loading at 9,000 psi; note the delamination in the equatorial joint.

73
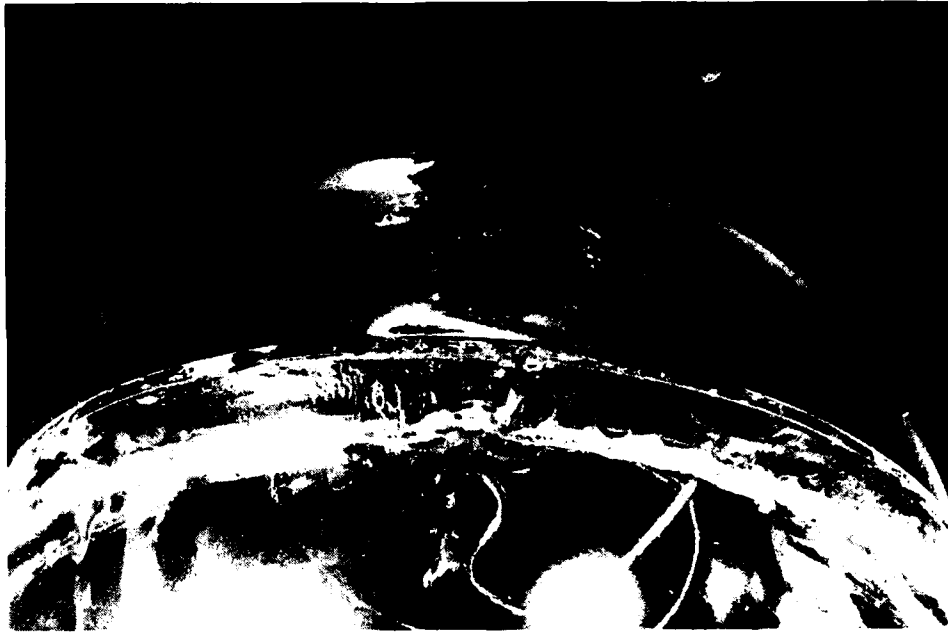
Figure 95. Detail of delaminated joint in Model 6B shown in figure 94.

6.0 IN R

1/8 IN

EQUATORIAL
JOINT

2.14 IN R
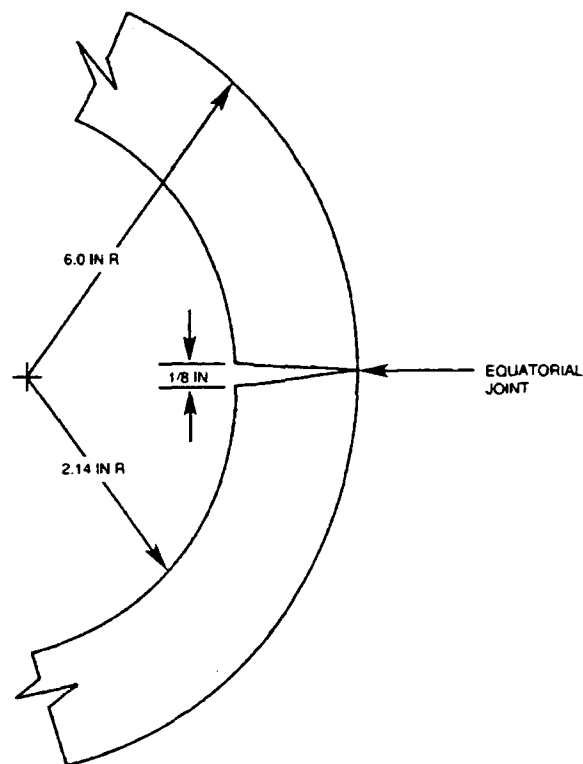
Model 6B.

Figure 96. Cross section of delaminated bond in
equatorial joint on Model 6B.
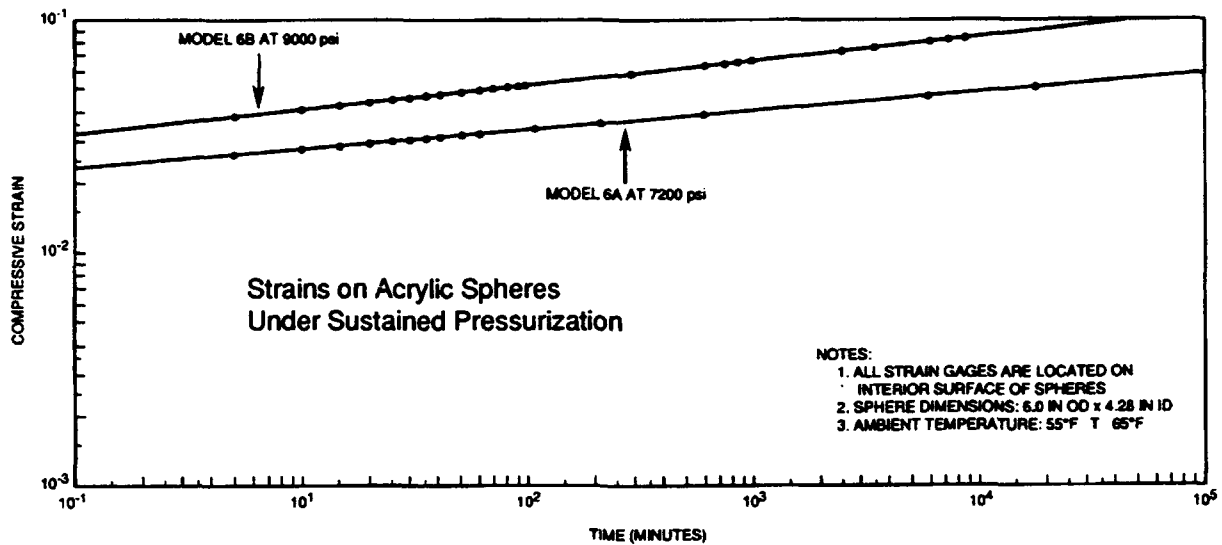
Figure 97. Summary of strain data generated by Models 6A and 6B during sustained pressure loading to 7,200 psi and 9,000 psi respectively.

Figure 98. Typical shearing cracks in the bearing surface of a hatch penetration in a 66-inch OD x 58-inch ID acrylic pressure hull resulting from repeated dives to a design depth of 3,000 feet. After refinishing of the bearing surface, the hull was placed back in operation. Similar cracks are to be expected in an acrylic spherical pressure hull with $t/D_i = 0.2$ after $\geq 1,000$ dives to its design depth of 8,000 feet.

Table 1. Specified values of physical properties for each lot.

Test Procedures	Physical Property	Minimum Values	
		U.S. Customary Unit	Metric Unit
ASTM D 256*	Izod notched impact strength	$\geqslant$ 0.25 ft-lb/in.-min	$\geqslant$ 13.3 J/m
ASTM D 542*	Refractive index	1.49 ± 0.01	1.49 ± 0.01
ASTM D 570*	Water absorption, 24 hr	$\leqslant$ 0.25%	$\leqslant$ 0.25%
ASTM D 621	Compressive deformation at 4000 psi (27.6 MPa), 122°F (50°C), 24 hr	$\leqslant$ 0.85%	$\leqslant$ 0.85%
ASTM D 638*	Tensile:		
	(a) ultimate strength	$\geqslant$ 9000 psi	$\geqslant$ 62 MPa
	(b) elongation at break	$\geqslant$ 2%	$\geqslant$ 2%
	(c) modulus	$\geqslant$ 400,000 psi	$\geqslant$ 2760 MPa
ASTM D 695*	Compressive:		
	(a) yield strength	$\geqslant$ 15,000 psi	$\geqslant$ 103 MPa
	(b) modulus of elasticity	$\geqslant$ 400,000 psi	$\geqslant$ 2760 MPa
ASTM D 732*	Shear ultimate strength	$\geqslant$ 8000 psi	$\geqslant$ 55 MPa
ASTM D 785*	Rockwell hardness	$\geqslant$ M scale 90	$\geqslant$ M scale 90
ASTM D 790*	Flexural ultimate strength	$\geqslant$ 14,000 psi	$\geqslant$ 97 MPa
ASTM D 792*	Specific gravity	1.19 ± 0.01	1.19 ± 0.01
ASTM E 308	Ultraviolet (290−330 nm) light transmittance	$\leqslant$ 5%	$\leqslant$ 5%
ASTM D 702	Clarity, visually rated	Must have readability	Must have readability
ASTM D 696	Coefficient of linear thermal expansion at	10^{-6} (in./in. °F)	10^{-6} (mm/mm °C)

°F	°C		
−40	−40	2.9	5.22
−20	−29	3.0	5.40
0	−18	3.2	5.76
+20	−7	3.4	6.12
+40	4	3.7	6.66
+60	16	4.0	7.20
+80	27	4.3	7.74
+100	38	4.7	8.46
+120	49	5.1	9.18
+140	60	5.4	9.72

Test Procedures	Physical Property	U.S. Customary Unit	Metric Unit
ASTM D 648	Deflection temperature of plastics under flexure at 264 psi (1.8 MPa)	$\geqslant$ 185°F	$\geqslant$ 85°C
PVHO-1 method, para. 2-3.8	Total residual monomer: (a) methyl methacrylate (b) ethyl acrylate	$\leqslant$ 1.6%	$\leqslant$ 1.6%

GENERAL NOTE:
Tests marked with an asterisk require testing of a minimum of two specimens. For others, test a minimum of one specimen. Where applicable, use the sampling procedures described in para. 2-3.7. For other tests, use the sampling procedures described in the appropriate ASTM test methods. Where two specimens are required in the test procedure, the average of the test values will be used to meet the requirements of the minimum physical properties of this Table.

Table 2. Specified values of physical properties for each casting.

Test Procedures	Physical Property	Specified Values	
		U.S. Customary Unit	Metric Unit
ASTM D 638*	Tensile: (a) ultimate strength (b) elongation at break (c) moduluss of elasticity	$\geq$9000 psi $\geq$2% $\geq$400,000 psi	$\geq$62 MPa $\geq$2% $\geq$2760 MPa
ASTM D 695*	Compressive: (a) yield strength (b) modulus of elasticity	$\geq$15,000 psi $\geq$400,000 psi	$\geq$103 MPa $\geq$2760 MPa
ASTM D 621*	Compressive deformation at 4000 psi (27.6 MPa) and 122°F (50°C), 24 hr	$\leq$1.0%	$\leq$1.0%
ASTM E 308	Ultraviolet transmittance (for 0.5 in (12.5 mm) thickness)	$\leq$5%	$\leq$5%
ASTM D 702	Visual clarity	Must pass readability test	Must pass readability test
PVHC-1	Total residual monomer: (a) methyl methacrylate (b) ethyl acrylate	 $\leq$1.6%	 $\leq$1.6%

GENERAL NOTE:
Tests marked with an asterick require testing of a minimum of two specimens. For others, test a minimum of one specimen. Where applicable, use the sampling procedures described in para. 2-3.7. Where two specimens are required in the test procedure, the average of the test values will be used to meet the requirements of the minimum physical properties of this table.

Table 3. Scale-model acrylic plastic spheres.

Specimen Description	Outside Diameter (inches)	Inside Diameter (inches)	t/D$_i$	Number of Penetrations	Bearing Gasket Materials	Hatch Materials
AA	18	12.85	0.2	1	Polycarbonate	Aluminum
BB	15	10.70	0.2	1	Polycarbonate	Aluminum
CC	15	10.70	0.2	5	Polycarbonate	Aluminum
					Epoxy	Aluminum
					Polyurethane	Aluminum
					Acrylic	Aluminum
					Cast Nylon	Aluminum
1	6	5.00	0.10	1	None	Acrylic
2	6	4.80	0.125	1	None	Acrylic
3	6	4.62	0.149	1	None	Acrylic
4	6	4.40	0.175	1	None	Acrylic
5	6	4.34	0.191	1	None	Acrylic
6, 6A, 6B	6	4.28	0.20	1	None	Acrylic
7	6	4.22	0.21	1	None	Acrylic
8	6	⋅14	0.225	1	None	Acrylic

NOTES: 1. All penetrations are conical, subtending a spherical included angle of 48 degrees, with the apex of the cone coinciding with the center of the sphere.

2. The outside of the bearing gaskets mates snugly with the conical surface of the penetrations. The inside of the bearing gaskets subtends a spherical conical angle of 44 degrees.

Table 4. Physical properties of bearing gasket materials.

Material	Tensile Strength PSI	Tensile Modulus PSI	Tensile Elongation Percent	Compressive Yield PSI	Compression Modulus PSI
Extryded Polycarbonate	7,160	3.2×10^5	2.6	12,800	3.7×10^5
Cast Polycarbonate	10,460	3.3×10^5	3.4	12,325	3.2×10^5
Cast Nylon	9,160	3.9×10^5	28	9,145	3.16×10^5
Cast Epoxy	10,460	2.8×10^5	2.0	14,410	3.5×10^5
Cast Polyrethane	7,300	3.23×10^5	12	9,490	3.06×10^5
Cast Acrylic	10,400	4.5×10^5	4.9	17,600	4.5×10^5

Material	Flexural Strength PSI	Flexural Modulus PSI	Compressive Deformation Percent*	Shear PSI	IZOD Notched ft lb/in
Extruded Polycarbonate	11,900	3.2×10^5	.12	10,400	.76
Cast Polycarbonate	13,930	3.24×10^5	.14	8,240	.9
Cast Nylon	12,580	3.89×10^5	1.25	5,500	.9
Cast Epoxy	16,520	3.62×10^5	.02	8,500	.73
Cast Polyurethane	13,610	5.14×10^5	.96	6,200	1.03
Cast Acrylic	15,900	4.5×10^5	.16	8,900	.4

Table 5. Strains on concave surface of Model AA during pressure cycling.

Pressure Cycle No.	At Beginning of Sustained Pressurization Period	At Conclusion of Sustained Pressurization Period	Creep During Sustained Pressurization Period	At Beginning of Relaxation Period	At Conclusion of Relaxation Period
0–1,000 psi	–3,200	–3,300	–100	–60	0
0–2,000 psi	–6,300	–6,800	–500	–290	–90
0–3,000 psi	–9,400	–10,300	–900	–400	–40
0–4,000 psi	–12,700	–14,600	–1,900	–500	–40
0–5,000 psi	–16,300	–19,500	–3,200	–650	+80
0–6,000 psi	–20,300	–25,400	–5,100	–700	+150

NOTES: 1. Model AA dimension: 18.0 inches outside diameter, 12.85 inches inside diameter
4.35 inches inside diameter of penetration
48° included spherical angle of penetration.

2. The typical pressure cycle consists of pressurizing at 650 psi/minute rate, 60 minutes of sustained pressurization, depressurizing at 650 psi/minute rate, and 60 minutes of relaxation at zero pressure in 65°F environment.

3. The hoop and meridional strains were the same at the pole of the sphere opposite from the penetration.

4. All strains are in microinches per inch.

5. The strain recorder was re-zeroed at conclusion of each pressure cycle.

Table 6. Strains on Models BB and CC during Cycle 1 short-term pressurization.

GAGES	PRESSURE (psi)						
	500	1000	1500	2000	2500	3000	3560
CC1**	-1698	-3350	-5030	-6750	-8560	-10380	-12660
CC2	-1685	-3240	-4810	-6390	-8050	-9630	-11590
CC3**	-2150	-3770	-5450	-7160	-8980	-10790	-12850
CC4	-1644	-3120	-4690	-6330	-8070	-9720	-11820
CC5**	-1193	-2550	-4160	-5960	-7960	-9820	-12180
CC6	-3720	-5490	-6870	-7960	-8860	-9890	-11040
CC7**	-1786	-3270	-4840	-6470	-8310	-10070	-12310
CC8	-1551	-3270	-5000	-6700	-8400	-10420	-12350
CC9**	-2000	-3080	-4140	-5250	-6780	-8390	-10290
CC10							
BB1	-1986	-3560	-5150	-6760	-8470	-10170	-12300
BB2**							
BB3							
BB4**	-1686	-3370	-5090	-6840	-8710	-10550	-12820
BB5	-1688	-3160	-4660	-6180	-7800	-9380	-11340
BB6**	-1689	-3410	-5150	-6920	-8800	-10660	-12790
BB7	-1034	-2100	-3290	-4660	-6170	-7560	-9080
BB8**	-1704	-3430	-5160	-6940	-8870	-10780	-12800
BB9	-1805	-3560	-5340	-7150	-9080	-10980	-12840
BB10**	-1768	-3480	-5210	-6960	-8840	-10690	-12820
RTD CC*	74						74
RTD BB*	74						74

* RTD = TEMP °F

** = HOOP STRAIN

STRAINS: MICROINCHES/INCH

Table 7. Strains on Models BB and CC during Cycle 1 sustained pressure loading.

GAGE	TIME (min)								
	5	10	20	35	55	110	140	170	240
	PRESSURE (psi)								
	3550	3560	3560	3500	3510	3470	3465	3461	3455
CC1**	-12850	-12890	-12900	-12910	-12920	-12930	-12930	-12930	-12940
CC2	-11790	-12070	-12260	-12380	-12490	-12730	-12780	-12800	-12830
CC3**	-12880	-12900	-12910	-12920	-12920	-12930	-12940	-12940	-12940
CC4	-12130	-12460	-12690	-12840	-12900	-12930	-12940	-12950	-12950
CC5**	-12570	-12890	-12930	-12950	-12950	-12970	-12980	-12980	-12980
CC6	-11040	-11120	-11080	-10990	-11910	-10720	-10680	-10650	-10620
CC7**	-12610	-12850	-12880	-12890	-12900	-12910	-12920	-12920	-12930
CC8	-12660	-12910	-12940	-12950	-12960	-12980	-12980	-12980	-12980
CC9**	-10520	-10760	-10920	-11060	-11160	-11380	-11430	-11450	-11480
CC10									
BB1	-12630	-12810	-12830	-12850	-12860	-12870	-12880	-12880	-12880
BB2**									
BB3									
BB4**	-12890	-12920	-12920	-12930	-12940	-12940	-12940	-12950	-12950
BB5	-11600	-11890	-12090	-12230	-12350	-12620	-12670	-12700	-12740
BB6**	-12800	-12840	-12850	-12860	-12870	-12870	-12880	-12880	-12880
BB7	-8970	-9040	-9050	-9020	-8980	-8910	-8890	-8880	-8880
BB8**	-12820	-12830	-12830	-12840	-12840	-12860	-12840	-12840	-12850
BB9	-12850	-12860	-12860	-12870	-12880	-12890	-12880	-12880	-12890
BB10**	-12850	-1286ι	-12860	-12870	-12870	-12890	-12870	-12870	-12890
RTD CC*									
RTD BB*									

* RTD = TEMP °F

** = HOOP STRAIN

STRAINS: MICROINCHES/INCH

TIME: MINUTES

79

Table 8. Strains on Models BB and CC during Cycle 1 short-term depressurization.

GAGES	PRESSURE (psi)						
	3014	2507	2004	1500	1000	500	35
CC1**	-12880	-11380	-9650	-7820	-5760	-3680	-1325
CC2	-11560	-9920	-8300	-6620	-4770	-2880	-875
CC3**	-12400	-11690	-10030	-8300	-6310	-4220	-1375
CC4	-12260	-10760	-9210	-7550	-5660	-3600	-1280
CC5**	-12960	-12430	-11120	-9580	-7560	-5020	-1415
CC6	-9320	-7550	-5930	-4460	-3380	-2790	-1427
CC7**	-12770	-11270	-9700	-8050	-6130	-3950	-1218
CC8	-12580	-10880	-9160	-7400	-5360	-3430	-1435
CC9**	-10590	-9490	-8330	-7090	-5710	-3990	-913
CC10	-929	-563	-283	-009	-373	-635	-100
BB1	-12640	-10950	-9250	-7500	-5550	-3590	-1302
BB2**							
BB3							
BB4**	-12880	-11180	-9370	-7500	-5380	-3220	-1086
BB5	-11470	-9914	-8340	-6710	-4920	-3110	-1118
BB6**	-12830	-11330	-9490	-7580	-5440	-3240	-1135
BB7	-7660	-6180	-4780	-3430	-2280	-1310	-525
BB8**	-12830	-11740	-9850	-7890	-5670	-3420	-1230
BB9	-12850	-11530	-9720	-7820	-5670	-3470	-1210
BB10**	-12850	-11510	-9680	-7760	-5590	-3370	-1120
RTD CC*							
RTD BB*							

* RTD = TEMP °F
** = HOOP STRAIN

STRAINS: MICROINCHES/INCH

Table 9. Strains on Models BB and CC during Cycle 1 relaxation.

GAGE	TIME (min)													
	5	10	25	45	85	115	135	145	160	175	190	220	235	245
	PRESSURE (psi)													
	33	33	27	25	25	25	31	31	31	31	30	30	31	31
CC1**	-834	-649	-476	-363	-277	-255	-237	-230	-220	-213	-207	-197	-192	-190
CC2	-522	-382	-251	-168	-106	-091	-079	-074	-068	-063	-059	-051	-048	-047
CC3**	-821	-618	-438	-323	-244	-225	-209	-201	-193	-187	-181	-169	-168	-163
CC4	-810	-633	-478	-375	-301	-283	-270	-264	-256	-247	-242	-235	-233	-231
CC5**	-943	-751	-567	-442	-343	-336	-314	-304	-291	-279	-268	-259	-250	-248
CC6	-1007	-826	-650	-535	-442	-406	-396	-391	-382	-375	-367	-357	-351	-349
CC7**	-802	-633	-472	-362	-279	-263	-246	-237	-226	-215	-205	-195	-191	-188
CC8	-914	-710	-520	-400	-314	-283	-266	-260	-247	-238	-230	-219	-212	-212
CC9**	-620	-492	-368	-283	-225	-222	-204	-196	-189	-183	-180	-175	-172	-171
CC10	-120	-117	-104	-092	-079	-068	-070	-070	-069	-068	-069	-075	-076	-077
BB1	-875	-682	-506	-391	-304	-283	-266	-258	-247	-238	-230	-218	-213	-209
BB2**														
BB3														
BB4**	-715	-562	-397	-296	-223	-206	-194	-188	-181	-176	-170	-162	-159	-157
BB5	-780	-633	-473	-368	-287	-268	-253	-245	-235	-227	-222	-214	-210	-208
BB6**	-774	-610	-440	-338	-255	-221	-226	-238	-233	-230	-226	-222	-217	-216
BB7	-340	-259	-169	-114	-070	-061	-052	-051	-045	-042	-039	-035	-032	-032
BB8**	-854	-684	-498	-386	-295	-278	-259	-251	-242	-233	-226	-215	-209	-207
BB9	-854	-692	-517	-411	-332	-312	-298	-292	-283	-277	-272	-262	-257	-256
BB10**	-789	-632	-461	-360	-280	-263	-250	-244	-235	-229	-222	-213	-207	-206
RTD CC*														
RTD BB*														

* RTD = TEMP °F
** = HOOP STRAIN

STRAINS: MICROINCHES/INCH
TIME: MINUTES

Table 10. Strains on Models BB and CC during Cycle 5 short-term pressurization.

GAGES	PRESSURE (psi)						
	500	1000	1522	2002	2508	3030	3575
CC1**	-1970	-3650	-5460	-7150	-9050	-10900	-12840
CC2	-1850	-3340	-4890	-6330	-7930	-9570	-11390
CC3**	-2240	-3780	-5450	-7060	-8860	10680	-12600
CC4	-1960	-3530	-5210	-6790	-8570	10320	-12270
CC5**	-2190	-3630	-5360	-6950	-8810	-10740	-12880
CC6	-2460	-3820	5290	-6540	-7540	-8250	-8400
CC7**	-2110	-3740	-5530	-7180	-9030	-10880	-12850
CC8	-1770	-3340	-5030	-6660	-8440	-10200	-12020
CC9**	-2440	-3980	-5750	-7330	-9120	-10900	-12690
CC10							
BB1	-2300	-3890	-5550	-7110	-8840	-10550	-12510
BB2**							
BB3							
BB4**	-1890	-3590	-5390	-7070	-8930	-10790	-12860
BB5	-2030	-3510	-5060	-6520	-8130	-9740	-11570
BB6**	-13240	-13240	-13240	-13240	8910	-10830	-12790
BB7	-750	-1402	-2240	-3190	-4610	-6070	-7700
BB8**	-1976	-3730	-5590	-7350	-9280	-11230	-12820
BB9	-2000	-3640	-5380	-7050	-8890	-10730	-12780
BB10**	-2040	-3800	-5620	-7320	-9190	-11080	-12850
RTD CC*	74						74
RTD BB*	74						74

* RTD = TEMP °F STRAINS: MICROINCHES/INCH
** = HOOP STRAIN

Table 11. Strains on Models BB and CC during Cycle 5 sustained pressure loading.

GAGE	TIME (min)											
	5	10	20	35	50	80	110	140	180	200	230	260
	PRESSURE (psi)											
	3550	3550	3550	3540	3545	3550	3540	3554	3553	3547	3544	3554
CC1**	-12900	-12910	-12920	-12920	-12930	-12930	-12940	-12940	-12940	-12950	-12940	-12950
CC2	-11750	-11990	-12170	-12300	-12510	-12700	-12790	-12860	-12870	-12890	-12890	-12900
CC3**	-12850	-12880	-12900	-12900	-12910	-12920	-12920	-12920	-12930	-12930	-12930	-12930
CC4	-12620	-12850	-12920	-12930	-12950	-12960	-12960	-12960	-12970	-12970	-12970	-12980
CC5**	-12940	-12960	-12970	-12970	-12980	-12990	-12990	-12990	-13000	-13000		-13000
CC6	-8450	-8480	-8540	-8560	-8660	-8720	-8720	-8780	-8780	-8750	-8730	-8760
CC7**	-12900	-12910	-12920	-12920	-12930	-12930	-12930	-12940	-12950	-12940	-12950	-12950
CC8	-12330	-12540	-12700	-12820	-12920	-12950	-12950	-12960	-12970	-12980	-12970	-12980
CC9**	-12800	-12820	-12830	-12840	-12850	-12850	-12850	-12860	-12870	-12870	-12870	-12870
CC10												
BB1	-12790	-12830	-12840	-12850	-12860	-12860	-12870	-12870	-12880	-12880	-12880	-12890
BB2**												
BB3												
BB4**	-12910	-12920	-12930	-12940	-12940	-12950	-12950	-12960	-12960	-12960	-12960	-12970
BB5	-11830	-12020	-12180	-12300	-12490	-12660	-12740	-12830	-12870	-12880	-12880	-12900
BB6**	-12820	-12830	-12840	-12840	-12850	-12850	-12850	-12850	-12870	-12870	-12870	-12870
BB7	-7820	-7940	-8020	-8070	-8170	-8260	-8280	-8350	-8390	-8400	-8410	-8450
BB8**	-12840	-12850	-12840	-12840	-12850	-12850	-12850	-12860	-12870	-12860	-12870	-12860
BB9	-12830	-12850	-12860	-12860	-12860	-12870	-12870	-12880	-12890	-12880	-12890	-12880
BB10**	-12860	-12870	-12870	-12870	-12870	-12880	-12880	-12880	-12890	-12890	-12890	-12880
RTD CC*	75	75	75	75	75	75	75	75	75	75	75	75
RTD BB*	74	74	74	74	74	74	74	74	74	74	74	74

* RTD = TEMP °F STRAINS: MICROINCHES/INCH
** = HOOP STRAIN TIME: MINUTES

Table 12. Strains on Models BB and CC during Cycle 5 short-term depressurization.

GAGES	PRESSURE (psi)						
	3005	2505	2005	1500	1000	500	42
CC1**	-12900	-11750	-10000	-8140	-6150	-4040	-1570
CC2	-11630	-10140	-8550	-6890	-5170	-3390	-1340
CC3**	-12750	-11290	-9710	-8040	-6300	-4450	-1550
CC4	-12670	-11280	-9750	-8030	-6180	-4090	-1630
CC5**	-12980	-12850	-11580	-9870	-7780	-5330	-1630
CC6	-7210	-5540	-3620	-1950	-1160	-1150	-1580
CC7**	-12900	-11920	-10360	-8600	-6620	-4390	-1510
CC8	-12060	-10550	-8930	-7210	-5540	-3570	-1730
CC9**	-12790	-11740	-10480	-9060	-7260	-4830	-1440
CC10							
BB1	-12770	-11250	-9570	-7790	-5960	-4060	-1690
BB2**							
BB3							
BB4**	-12890	-11340	-9560	-7660	-5670	-3580	-1390
BB5	-11610	-10150	-8590	-6970	-5290	-3550	-1540
BB6**	-12530	-10960	-8940				
BB7	-7000	-5640	-4240	-3060	-2180	-1490	-888
BB8**	-12830	-11940	-10080	-8070	-5980	-3830	-1606
BB9	-12750	-11120	-9400	-7520	-5580	-3560	-1401
BB10**	-12850	-11620	-9800	-7850	-5820	-3690	-1430
RTD CC*	74						74
RTD BB*	73						73

* RTD = TEMP °F
** = HOOP STRAIN

STRAINS: MICROINCHES/INCH

Table 13. Strains on Models BB and CC during Cycle 5 relaxation.

GAGE	TIME (min)								
	5	10	20	30	40	70	160	400	970
	PRESSURE (psi)								
	39	39	39	39	38	38	38	37	37
CC1**	-1240	-1020	-848	-748	-684	-627	-426	-339	-287
CC2	-1090	-900	-764	-682	-629	-582	-410	-329	-287
CC3**	-1210	-980	-813	-713	-652	-596	-400	-309	-258
CC4	-1320	-1110	-952	-859	-799	-742	-556	-476	-431
CC5**	-1300	-1080	-904	-801	-735	-670	-463	-377	-327
CC6	-1440	-1315	-1225	-1156	-1115	-1066	-883	-773	-701
CC7**	-1200	-990	-834	-736	-674	-613	-420	-331	-301
CC8	-1420	-1200	-1033	-930	-865	-805	-572	-467	-424
CC9**	-1160	-968	-839	-749	-695	-645	-476	-400	-364
CC10									
BB1	-1370	-1130	-977	-871	-808	-748	-529	-426	-371
BB2**									
BB3									
BB4**	-1130	-919	-782	-680	-625	-565	-390	-315	-272
BB5	-1300	-1090	-961	-863	-810	-749	-557	-470	-403
BB6**									
BB7	-759	-642	-574	-518	-487	-446	-326	-265	-234
BB8**	-1332	-1092	-944	-830	-770	-702	-494	-395	-332
BB9	-1152	-931	-805	-705	-654	-598	-423	-345	-299
BB10**	-1180	-957	-830	-727	-677	-613	-440	-364	-323
RTD CC*	74	74	74	74	74	74	75	74	74
RTD BB*	73	73	73	73	73	73	73	74	74

* RTD = TEMP °F
** = HOOP STRAIN

STRAINS: MICROINCHES/INCH
TIME: MINUTES

Table 14. Effect of pressure cycling on acrylic Models BB and CC.

MODEL DESCRIPTION	180 Cycles	435 Cycles	ACTION	1000 Cycles
Model BB	(4)			
Extr. Polycarbonate Insert	Single, deep, long circumferential crack. No extrusion	Extensive, deep cracks No extrusion	Replaced with a cast Nylon Insert	No cracks No extrusion
Penetration	Single short crack	Faint crazing		Very fine cracks
Model CC				
Cast Nylon Insert	No cracks No extrusion	No cracks No extrusion	Returned for further cycling	No cracks No extrusion
Penetration A	No cracks	No cracks		Frequency; 5–6 rows w/ 40% density Depth: 0.1 in Ave., 0.25 in Max.
Cast Polyurethane #10 Compound Insert	No cracks 0.05 in extrusion	Few fine cracks 0.150 in extrusion	Returned for further cycling	Many shallow cracks 0.3 in extrusion
Penetration E	No cracks	No cracks		No cracks
Cast Acrylic Insert	No cracks No extrusion	Slight cracking No extrusion	Replaced with a new acrylic insert	Many fine cracks No extrusion
Penetration C	No cracks	Slight cracking		Frequency: 4–5 rows w/ 25% density Depth: 0.1 in Ave., 0.25 in Max.
Cast Polycarbonate Insert	No cracks No extrusion	Extensive, deep cracks No extrusion	Replaced with polyurethane #9 Insert	Many fine cracks 0.16 in extrusion
Penetration B	No cracks	Few deep cracks		Frequency: 5–6 rows w/ 20% density Depth: 0.1 in Ave., 0.25 in Max.
Cast Epoxy Insert	Minor cracks No extrusion	Extensive, deep cracks No extrusion	Replaced with polycarbonate Insert #3	Extensive deep cracks No extrusion
Penetration D	Few shallow cracks	Few, deep cracks		Frequency: 4–5 rows w/ 30% density Depth: 0.5 in Ave., 1.25 in Max.

NOTES: 1. Ambient Temperature: 75°F   Sustained Pressure: 4 hrs
2. Cycling Schedule Max. Pressure: 3,560 psi   Relaxation: 4 hrs
     Press/Depress: 500 psi/min
3. Frequency: Approximate number of circumferentially oriented rows of cracks   Depth: Approximate depth of crack's penetration
     Density: Approximate cumulative length of all cracks in a single row
4. Acrylic sphere replaced with a new one because of equatorial bond separation.

Table 15. Effect of pressure cycling on acrylic Models SN01 through 08.

Model Number	t/D$_i$	Number of Cycles		
		120	435	1000
SN01	0.1	local buckling	——	——
SN02	0.125	OK	OK	OK
SN03	0.145	OK	OK	OK
SN04	0.175	OK	OK	OK
SN05	0.191	OK	OK	OK
SN06	0.200	OK	OK	OK
SN07	0.21	OK	OK	OK
SN08	0.225	OK	OK	OK

NOTES: 1. Ambient temperature: 75°F

2. Cycling
Max. Pressure: 3,560 psi
Sust. Pressure: 4 hrs
Relaxation: 4 hrs
Press/Depress. Rate: 500 psi/min

3. OK denotes no visible crazing or cracking

Table 16. Minimum physical properties of bearing gaskets.

ASTM–D–695	Compressive Yield	≥9,000 psi (62 MPa)
ASTM–D–695	Compressive Modulus	≥ 300,000 psi (2,069 MPa)
ASTM–D–638	Tensile Strength	≥ 6,000 psi (62 MPa)
ASTM–D–638	Tensile Modulus	≥ 300,000 psi (2,069 MPa)
ASTM–D–638	Tensile Elongation at Break > 10%	> 10%
ASTM–D–621*	Compressive Deformation under 4,000 psi at 75°F for 24 hours	$1 \leq \% \leq 2$
ASTM–D-732	Shear	≥ 4,000 psi (34.5 MPa)
ASTM–D–256	Izod Impact	≥ 1 ft lbs/in of notch

*This physical property is acceptable only for bearing gaskets in acrylic pressure hulls rated for ambient temperatures of ≤50°F. Still, acrylic pressure hulls rated for ≤50°F that operate extensively at ambient temperatures in the ≥75°F range at depths representing only 5 to 20 percent of their design depth must utilize bearing gaskets fabricated from a material meeting this compressive deformation requirement at 122°F test temperature.

Table 17. Strains on Model 6A during short-term
pressurization to 7,200 psi.

Pressure (psi)	Gages A	B	Average Strain	Temperature (C)
0	0	0	0	15.5
1000	−2905	−2845	−2875	15.5
2000	−5650	−5505	−5578	15.5
3000	−8833	−8609	−8721	15.5
4000	−11622	−11350	−11486	15.5
5000	−15042	−14689	−14866	15.5
6000	−18740	−18330	−18535	15.5
7000	−22490	−22000	−22245	15.6
7200	−23870	−23310	−23590	15.6

Sphere Dimensions: 6.0 x 4.28 inches
Location of gages: interior surface
Strains: microinches/inch

Table 18. Strains on Model 6A during sustained pressure bonding at 7,200 psi,
sheet 1.

Pressure (psi)	Gages A	B	Average Strain	Creep Rate	Time (minute)	Temperature (C)
7200	−23870	−23310	−23590		0	15.6
7200	−26550	−25780	−26165	−515	5	15.7
7200	−27870	−27040	−27455	−258	10	15.7
7200	−28690	−27830	−28260	−161	15	15.7
7200	−29750	−28860	−29305	−209	20	15.7
7200	−30270	−29350	−29810	−101	25	15.7
7200	−30920	−29990	−30455	−129	30	15.7
7200	−31260	−30310	−30785	−66	35	15.7
7200	−31520	−30590	−31055	−54	40	15.7
7200	−31780	−30820	−31300	−49	45	15.7
7200	−32160	−31030	−31595	−59	50	15.7
7200	−32160	−31180	−31670	−15	55	15.8
7200	−32330	−31340	−31835	−33	60	15.8
7200	−33120	−32130	−32625	−158	65	15.9
7200	−35080	−34040	−34560	−32	125	15.9
7200	−36900	−35700	−36300	−19	215	15.7
7200	−37600	−36360	−36980	−8	305	15.6
7200	−38800	−37581	−38191	−11	420	15.2
7200	−40130	−38680	−39405	−7	600	14.7
7200	−41730	−40120	−40925	−3	1080	14.0
7200	−43320	−41440	−42380	−2	1800	14.7
7200	−44640	−42490	−43565	−1	2595	13.8
7200	−44800	−42620	−43710	−0	2910	14.0
7200	−45640	−43310	−44475	−1	3480	14.4
7200	−46030	−43590	−44810	−1	4080	13.8
7200	−46110	−43620	−44865	−0	4335	14.1
7200	−47010	−44420	−45715	−1	4975	14.2
7200	−47330	−44610	−45970	−0	5520	13.8
7200	−48000	−45150	−46575	−1	6300	14.1
7200	−48500	−45580	−47040	−1	6900	13.9
7200	−48870	−45770	−47320	−0	7500	15.3
7200	−49180	−46060	−47620	−1	7740	15.0
7200	−49500	−46290	−47895	−0	8520	14.1
7500	−51130	−47600	−49365	−2	9240	14.9

Sphere Dimensions: 6.0 x 4.28 inches
Location of gages: interior surface
Strains: microinches/inch
Creep: microinches/inch/minute

Table 18. Strains on Model 6A during sustained pressure bonding at 7,200 psi, sheet 2.

Pressure (psi)	Gages A	B	Average Strain	Creep Rate	Time (minute)	Temperature (C)
7500	-51200	-47610	-49405	-0	9300	14.8
7400	-51330	-47600	-49465	-0	9900	14.4
7500	-51630	-47730	-49680	-0	10560	14.9
7500	-51780	-47830	-49805	-1	10680	14.8
7500	-52400	-48080	-50240	-0	11880	15.1
7500	-52560	-48200	-50380	-1	12000	14.8
7500	-52720	-48320	-50520	-1	12120	14.6
7400	-53160	-48430	-50795	-0	13440	14.8
7400	-53230	-48460	-50845	-1	13500	14.7
7400	-53800	-48660	-51230	-0	14910	15.1
7400	-53750	-48660	-51205	0	15030	15.0
7400	-54370	-48820	-51595	-0	16480	15.0
7300	-54900	-49000	-51950	-0	17760	15.1
7300	-54940	-49020	-51980	-0	17850	14.9
7300	-54940	-48890	-51915	0	18660	14.3

Sphere Dimensions: 6.0 x 4.28 inches
Location of gages: interior surface
Strains: microinches/inch
Creep: microinches/inch/minute

Table 19. Strains on Model 6A during short-term depressurization from sustained loading at 7,200 psi.

Pressure (psi)	Gages A	B	Average Strain	Temperature (C)
7300	-54940	-48950	-51945	14.3
7000	-54570	-48440	-51505	14.3
6000	-52470	-46770	-49620	14.3
5000	-50350	-44910	-47630	14.3
4000	-47930	-42790	-45360	14.3
3000	-45360	-40560	-42960	14.3
2000	-42750	-38310	-40530	14.3
1000	-39550	-35430	-37490	14.3
0	-36400	-32720	-34560	14.3

Sphere Dimensions: 6.0 x 4.28 inches
Location of gages: interior surface
Strains: microinches/inch

Table 20. Strains on Model 6A during relaxation at 0 psi pressure following sustained pressure loading at 7,200 psi.

Pressure (psi)	Gages A	Gages B	Average Strain	Creep Rate	Time (minute)	Temperature (C)
0	−36400	−32720	−34560	1732	0	14.3
0	−26680	−25120	−25900	610	5	14.4
0	−23430	−22270	−22850	350	10	14.4
0	−21680	−20520	−21100	243	15	14.4
0	−20430	−19340	−19885	184	20	14.4
0	−19480	−18450	−18965	148	25	14.4
0	−18710	−17740	−18225	124	30	14.4
0	−18060	−17150	−17605	106	35	14.4
0	−17510	−16640	−17075	86	40	14.4
0	−17060	−16230	−16645	90	45	14.4
0	−16590	−14500	−16195	76	50	14.4
0	−16200	−15430	−15815	72	55	14.4
0	−15820	−15090	−15455	48	60	14.4
0	−12880	−12400	−12640	33	120	14.4
0	−10800	−10513	−10657	17	180	14.4
0	−9770	−9520	−9645	15	240	14.4
0	−8810	−8720	−8765	6	300	14.4
0	−6600	−6750	−6675	2	680	14.5
0	−5215	−5590	−5403	1	1310	14.1
0	−4940	−5340	−5140	1	1490	14.4
0	−4740	−5160	−4950	1	1670	14.5
0	−4560	−5000	−4780	0	1910	14.7
0	−4490	−4950	−4720	0	2045	14.5
0	−4450	−4920	−4685	0	2120	14.4
0	−4235	−4754	−4495	1	2570	13.9
0	−3760	−4300	−4030	0	3470	14.7
0	−3320	−3920	−3620	0	4800	14.8
0	−3269	−3892	−3581	0	5455	14.1
0	−2921	−3594	−3258	0	6360	15.1
0	−2500	−3360	−2930	0	7730	15.2
0	−2405	−3410	−2908	0	8390	14.7
0	−2080	−3190	−2635	1	8690	15.3
0	−1800	−2950	−2375	0	9290	18.0
0	−1869	−3070	−2470	−0	9950	15.1

Sphere Dimensions: 6.0 x 4.28 inches
Location of gages: interior surface
Strains: microinches/inch
Creep: microinches/inch/minute

Table 21. Strains on Model 6B during short-term depressurization to 9,000 psi.

Pressure (psi)	Gages A	Gages B	Gages C	Average Strain	Temperature (C)
0	0	0	0	0	17.0
1000	−3339	−3190	−3410	−3313	17.0
2000	−6182	−6133	−6274	−6196	17.0
3000	−8802	−8735	−8895	−8811	17.0
4000	−11440	−11358	−11555	−11451	17.0
5000	−14650	−14561	−14808	−14673	17.0
6000	−17819	−17750	−18051	−17873	17.0
7000	−21552	−21910	−21847	−21770	17.0
8000	−26152	−26110	−26440	−26234	17.0
9000	−31870	−31640	−32180	−31897	17.0

Sphere Dimensions: 6.0 x 4.28 inches
Location of gages: interior surface
Strains: microinches/inch

Table 22. Strains on Model 6B during sustained pressure loading at 9,000 psi.

Pressure (psi)	Gages A	B	Gages C	Average Strain	Creep Rate	Time (minute)	Temperature (C)
9000	-36860	-36370	-36990	-36740	-949	5	17.0
9000	-39480	-39170	-39920	-39523	-557	10	16.7
9000	-41570	-41020	-41750	-41447	-385	15	16.7
9000	-43030	-42470	-43240	-42913	-293	20	16.6
9000	-43890	-43340	-44140	-43790	-175	25	16.6
9000	-44740	-44160	-44990	-44630	-168	30	16.6
9000	-45390	-44800	-45630	-45273	-129	35	16.5
9000	-45960	-45360	-46270	-45863	-118	40	16.6
9300	-47520	-46980	-47860	-47453	-318	45	16.5
9200	-48440	-47830	-48720	-48330	-175	50	16.3
9200	-50560	-49910	-50580	-50440	-106	70	16.3
9200	-50850	-50190	-51150	-50730	-58	75	16.3
9200	-51270	-50620	-51580	-51157	-85	80	16.3
9200	-51530	-50870	-51830	-51410	-51	85	16.2
9100	-51840	-51190	-52160	-51730	-64	90	16.2
9100	-52120	-51460	-52440	-52007	-55	95	16.2
9400	-58850	-58270	-59320	-58813	-35	290	15.6
9100	-64220	-63530	-64740	-64163	-14	660	14.8
9100	-64900	-64290	-65500	-64897	-8	755	14.8
9100	-65960	-65340	-66570	-65957	-8	890	14.9
9100	-66820	-66200	-67410	-66810	-7	1010	15.2
9100	-67270	-66660	-67900	-67277	-8	1070	15.3
9000	-74930	-74550	-75800	-75093	-5	2660	15.0
9000	-74540	-75330	-76590	-75853	-8	2750	14.9
9000	-77140	-76750	-77960	-77283	-2	3410	14.4
9000	-77620	-77350	-78550	-77840	-2	3740	14.5
8900	-78790	-78630	-79810	-79077	-2	4250	15.1
8900	-80110	-80100	-81210	-80473	-2	4955	14.4
8800	-81270	-81330	-82400	-81667	-2	5670	15.1
9000	-81510	-81630	-82660	-81933	-1	5675	15.1
9000	-81740	-81840	-82890	-82157	-3	5750	15.1
8900	-82720	-82930	-83920	-83190	-2	6380	14.4
9000	-85100	-85600	-86430	-85710	-2	8000	14.5
9000	-86130	-86760	-87530	-86807	-2	8640	15.1

Sphere Dimensions: 6.0 x 4.28 inches
Location of gages: interior surface
Strains: microinches/inch
Creep: microinches/inch/minute

Table 23. Strains on Model 6B during short-term depressurization from sustained pressure loading at 9,000 psi.

Pressure (psi)	Gages A	B	Gages C	Average Strain	Temperature (C)
9000	−86130	−86760	−87530	−86807	15.0
8000	−84360	−84990	−85790	−85047	15.0
7000	−82520	−83120	−83950	−83197	15.0
6000	−80800	−81360	−82240	−81467	14.9
5000	−78790	−79300	−80220	−79437	14.9
4000	−76740	−77180	−78170	−77363	14.9
3000	−74400	−76750	−75760	−75637	14.9
2000	−71320	−71550	−72590	−71820	14.9
1000	−68720	−68820	−69750	−69097	14.9
0	−66260	−66180	−67200	−66547	14.9

Sphere Dimensions: 6.0 x 4.28 inches
Location of gages: interior surface
Strains: microinches/inch

Table 24. Strains on Model 6B during relaxation at 0 psi pressure following sustained pressure loading at 9,000 psi.

Pressure (psi)	Gages A	B	Gages C	Average Strain	Creep Rate	Time (minute)	Temperature (C)
0	−66260	−66180	−67200	−66547		0	14.8
0	−61080	−61020	−62130	−61410	1027	5	14.8
0	−58880	−58730	−59890	−59167	449	10	14.8
0	−57530	−57370	−58500	−57800	273	15	14.8
0	−56650	−56470	−57660	−56927	175	20	14.8
0	−56010	−55800	−56980	−56263	133	25	14.8
0	−55340	−55160	−56320	−55607	66	35	14.8
0	−54900	−54700	−55850	−55150	91	40	14.8
0	−54400	−54200	−55350	−54650	100	45	14.0
0	−54040	−53810	−54940	−54263	77	50	14.8
0	−53840	−53630	−54740	−54070	39	55	14.8
0	−53480	−53260	−54380	−53707	73	60	14.8
0		−43360	−44260	−43810	15	725	14.0
0		−43050	−43930	−43490	5	785	14.1
0		−42730	−43610	−43170	4	860	14.1
0		−41800	−42620	−42210	3	1160	14.1
0		−40280	−40960	−40620	2	2075	13.9
0		−39490	−40020	−39755	1	2735	14.5
0		−38340	−38810	−38575	1	3935	14.5
0		−38140	−38600	−38370	1	4215	14.8

Sphere Dimensions: 6.0 x 4.28 inches
Location of gages: interior surface
Strains: microinches/inch
Creep: microinches/inch/minute

REPORT DOCUMENTATION PAGE

Form Approved
OMB No. 0704-0188

1. AGENCY USE ONLY (Leave blank)	2. REPORT DATE	3. REPORT TYPE AND DATES COVERED
	March 1993	Final

4. TITLE AND SUBTITLE

ACRYLIC PLASTIC SPHERICAL PRESSURE HULL FOR CONTINENTAL SHELF DEPTHS

5. FUNDING NUMBERS

PE: 0603713N
PROJ: S0397
ACC: DN302232

6. AUTHOR(S)

J. D. Stachiw, A. Clark, and C. B. Brenn

7. PERFORMING ORGANIZATION NAME(S) AND ADDRESS(ES)

Naval Command, Control and Ocean Surveillance Center (NCCOSC)
RDT&E Division
San Diego, CA 92152–5001

8. PERFORMING ORGANIZATION REPORT NUMBER

TR 1606

9. SPONSORING/MONITORING AGENCY NAME(S) AND ADDRESS(ES)

Naval Sea Systems Command
Washington, DC 20362

10. SPONSORING/MONITORING AGENCY REPORT NUMBER

11. SUPPLEMENTARY NOTES

12a. DISTRIBUTION/AVAILABILITY STATEMENT

Approved for public release; distribution is unlimited.

12b. DISTRIBUTION CODE

13. ABSTRACT (Maximum 200 words)

A spherical acrylic pressure hull of NEMO design has been designed for an operational depth of 8,000 feet. The design meets the requirements of the American Society of Mechanical Engineers (ASME) "Safety Standard for Pressure Vessels for Human Occupancy."

The performance of the spherical acrylic hull has been experimentally evaluated by pressure testing 13 scale-model acrylic spheres under short-term, long-term, and cyclic conditions. The test results have shown that the NEMO-type acrylic spherical hull with $t/D_i = 0.2$ thickness withstands >1,000 pressure cycles of 4 hour's duration to design depths of 8,000 feet at ambient temperatures $\leq 75°F$.

The acrylic hull withstood without catastrophic failure a 150-percent overpressurization (20,000 feet depth) of 150 hour's duration.

14. SUBJECT TERMS

acrylic plastic
external pressure housing
ocean engineering

15. NUMBER OF PAGES

104

16. PRICE CODE

17. SECURITY CLASSIFICATION OF REPORT	18. SECURITY CLASSIFICATION OF THIS PAGE	19. SECURITY CLASSIFICATION OF ABSTRACT	20. LIMITATION OF ABSTRACT
UNCLASSIFIED	UNCLASSIFIED	UNCLASSIFIED	SAME AS REPORT

21a. NAME OF RESPONSIBLE INDIVIDUAL	21b. TELEPHONE (include Area Code)	21c. OFFICE SYMBOL
J. D. Stachiw	(619) 553−1875	Code 5602

THE AUTHOR

DR. JERRY STACHIW is Staff Scientist for Marine Materials in the Ocean Engineering Division. He received his under-graduate engineering degree from Oklahoma State University in 1955 and graduate degree from Pennsylvania State University in 1961.

Since that time he has devoted his efforts at various U.S. Navy Laboratories to the solution of challenges posed by exploration, exploitation, and surveillance of hydrospace. The primary focus of his work has been the design and fabrication of pressure resistant structural components of diving systems for the whole range of ocean depths. Because of his numerous achievements in the field of ocean engineering, he is considered to be the leading expert in the structural application of plastics and brittle materials to external pressure housings.

Dr. Stachiw is the author of over 100 technical reports, articles, and papers on design and fabrication of pressure resistant viewports of acrylic plastic, glass, germanium, and zinc sulphide, as well as pressure housings made of wood, concrete, glass, acrylic plastic, and ceramics. His book on "Acrylic Plastic Viewports" is the standard reference on that subject.

For the contributions to the Navy's ocean engineering programs, the Navy honored him with the Military Oceanographer Award and the NCCOSC's RDT&E Division honored him with the Lauritsen-Bennett Award. The American Society of Mechanical Engineers recognized his contributions to the engineering profession by election to the grade of Life-Fellow, as well as the presentation of Centennial Medal, Dedicated Service Award and Pressure Technology Codes Outstanding Performance Certificate.

Dr. Stachiw is past-chairman of ASME Ocean Engineering Division and ASME Committee on Safety Standards for Pressure Vessels for Human Occupancy. He is a member of the Marine Technology Society, New York Academy of Science, Sigma Xi and Phi Kappa Honorary Society.